2005-05-05

Improving and Understanding Direct Methanol Fuel Cell (DMFC) Performance

Alexandre Hacquard
Worcester Polytechnic Institute

Improving and Understanding Direct Methanol Fuel Cell (DMFC) Performance

By

Alexandre Hacquard

A Thesis submitted to the faculty of

WORCESTER POLYTECHNIC INSTITUTE

In partial fulfillment of the requirement for the Degree of Master of Science
In
Chemical Engineering

May 2005

APPROVED

_____

Dr. Ravindra Datta, Professor, Major advisor

_____

Dr. David Dibiasio, Associate Professor, Department Head

Table of contents

List of figures

List of tables

List of symbols

A_S: Electrode surface

C_a: Anode double layer capacitance

C_c: Cathode double layer capacitance

C_{CH3OH}: Methanol concentration in the feed solution

$C^M{}_{H^+}$: Proton concentration in the membrane

C_t^*: Active catalytic sites concentration

$D^M{}_{H^+}$: Diffusion coefficient of protons in the membrane

F: Faraday's constant

k: Rate constant

K: Equilibrium

k_P: Hydraulic permeability of the membrane

$k\Phi$: electro kinetic permeability of the membrane

N_{CH3OH}: Methanol flux through the membrane

P_A: Anode pressure

P_C: Cathode pressure

Q: Feed flow rate

R: Perfect gases constant

T: Temperature of the cell

U^0: Standard cell voltage

V: Anode compartment volume

Greek letters

α: Charge transfer coefficient

γ: Roughness factor

η_A: Anode overpotential

η_C: Cathode overpotential

κ^M: Conductivity of the membrane

μ: Pore fluid viscosity in the membrane

Acknowledgments

First, I would like to thank my advisor Ravindra Datta for the opportunity to work in the Fuel Cell Center, his advice and guidance.

I would also like to acknowledge my lab-mates Nikhil Jalani and Saurabh Vilekar for their assistance, discussion and for sharing their experience. I also wish them gook luck for their PhD. Thanks to Ilie Fishtik and Caitlin Callaghan for their help on Reaction Network Theory.

Next, I thank the Chemical Engineering Department for giving me the opportunity to do a Master at Worcester Polytechnic Institute. I acknowledge the faculty of the department, its staff and students for making of my master a good time.

Finally, thanks to Sandy and Jo for their help on administrative problems and to Jack Ferraro and Douglas C. White for helping me to fix my experimental station.

Abstract

Direct methanol fuel cell (DMFC) is considered as a highly promising power source. It is based on polymer electrolytes membrane (PEM) fuel cell technology.

It posses a number of advantages such as a liquid fuel, quick refueling, low cost of methanol and the compact cell, design making it suitable for various potential applications including stationary and portable applications. DMFCs are also environmentally friendly. Although carbon dioxide is produced, there is no production of sulfur or nitrogen oxides.

The development of commercial DMFCs has nevertheless been hindered by some important issues. The most important are the low power density caused by the slow electrochemical methanol oxidation at the anode and methanol crossover through PEM, which is responsible for inhibiting the activity of the cathode catalyst as well.

With the eventual goal of improving the overall performance of the DMFC, this study has been concerned with an investigation of the issues and effect of various parameters on its performance.

First of all, the electrode preparation methodology and the effect of the catalyst were investigated. The most efficient membrane electrode assembly (MEA) was prepared with Pt/Ru black at anode and Pt black cathode on either side of a Nafion 117 membrane. Performance was however limited by current oscillations observed at low cell voltage and high current density attributed to carbon dioxide removal. Consequently, the effect of flow rate was investigated. Higher flow rates eliminated these oscillations.

Then attention was focused on the management of the two-phase flow that occurs in the diffusion layer of the electrode as well as in the anode bipolar plate flow channels. Removal of carbon dioxide formed during methanol oxidation was thus found to be an important issue in DMFC. There is a competition between methanol diffusion to the catalyst layer and CO_2 removal in the opposite direction. The two fluxes needed to be balanced in order to optimize performance. To accomplish this, the ratio of hydrophilic and hydrophobic pores respectively formed in the catalytic layer by Nafion and PTFE (Teflon) was altered. It also had an effect on crossover. The effect of a barrier layer was

investigated to reduce crossover. Finally, zirconia and silica nano-composite membranes were tested instead of Nafion and found to reduce crossover.

Developing a good understanding of what happens on the catalyst surface is important to develop a strategy on how improve DMFC performance. Thus is why a dynamic model based on a simplified mechanism for methanol electro-oxidation reaction was developed. It shows, amongst other insights, how the intermediate species coverage evolves with time. The mechanism was however too simple to provide an idea of which poisoning species are formed on the catalyst surface. A more exhaustive mechanism is thus being developed using Reaction Route analysis.

I. Literature review

1. The promise of fuel cells

Fuels cells do not store electricity but produce it directly from fuel. They simply need to be fed with fuel and oxygen to work. That is why they have undeniable advantages over regular batteries such as increased operating time, reduced weight and ease of recharging.

Besides, most of the world's energy comes from burning fossil fuels in low efficiency processes. The wide application range of fuel cells could also provide an alternative to these processes both for stationary and transportation applications.

The state of the art fuel cells are based on proton exchange membranes (PEM). The PEM fuel cells are the most promising fuel cells and show excellent performance when fed with hydrogen. However, production, storage and use of hydrogen are still a key limitation. Further, its performance is severely affected by poisoning species in hydrogen.

2. The promises of direct methanol Fuel Cell

a. Advantages

Methanol releases six protons and electrons per molecule during its oxidation. Its high energy density makes from methanol a suitable fuel for fuel cells [1]. DMFC works at low and intermediate temperatures (up to 150ºC) and are fed with a dilute aqueous solution of methanol in water.

Cells operation in gas phase also gives good performance. Actually, the higher temperature enhances kinetics and methanol crossover is lowered with a gas phase feed. However, need for vaporization may be a limitation for some applications.

b. Environmental concerns

Fuel Cells are considered as environmentally friendly as they do not produce toxic byproducts. However, they are not emission-free. They still produce carbon dioxide

which is a green house gas. This is also true for hydrogen which produces CO_2 indirectly during reforming step in the water-gas shift reaction.

Methanol and other alcohols also produce some other byproducts like aldehydes, ketones and carboxylic acids but in very low concentrations. If produced from biomass, the CO_2 formed during cell operation would nevertheless be balanced by CO_2 consumed in photosynthesis. Consequently, this form of energy would contribute no more to green house effect and will be renewable. Further, the higher efficiency of fuel cells makes that less CO_2 / kW is produced as compared to conventional processes.

c. Potential applications

There are essentially three main types of applications for fuel cells. Fuel cells are well known for being an alternative to the internal combustion engines but are also considered for portable and stationary applications.

- Stationary applications:

Fuel cells are able to produce electricity directly from fuel with a good efficiency. For stationary applications, they would replace the combustion-based electric-generating methods where energy losses occur in the thermal engine as well as in the electric generator. They can be applied to residential, commercial and industrial sectors for electricity as well as for heat production [2].

As DMFC do not need any reforming of methanol, there are no losses in the reformer. Besides the medium/low operating temperature make them suitable for residential-grade water heating.

- Transportation:

Although modern cars emit a lower amount of toxic gases than their predecessors, transportation is still a great source of pollution. Replacing a significant fraction by fuel cells would have a substantial effect on the environment.

Methanol fuel cells have been carefully investigated for transportation applications. The main advantage is that storage and tank refilling is easy for liquid methanol [3]. Besides, they do not need any reformer or humidification system that would consume a lot of the

available space in a car. Actually, their design is compact even if some water is needed to dilute methanol.

- Portable applications and micro-fuel cells:

The most important feature for a portable or micro fuel cell is a compact design. For a minimized size and weight, the cell has to work at ambient temperature. The low operating temperature of PEM fuel cell is a great advantage for portable applications. Actually, it is the only fuel cell able to work at ambient temperature [4]. For reasons similar to transportation application, it appears clearly that DMFC are more suitable than hydrogen fuel cells.

Fuel cells are still a developing technology and need improvement in both technological performance and cost.

3. Direct Methanol Fuel Cell principle

a. Generalities

Basically, the direct methanol fuel cell is a proton exchange membrane fuel cell that is fed with an aqueous solution of methanol.

The two catalytic electrodes where the methanol oxidation (anode) and the oxygen reduction (cathode) occur are separated by a membrane which conducts protons from anode to cathode, while other compounds diffusion is blocked. The combination of electrodes and membranes is called membrane electrode assembly (MEA). Each electrode is made of a gas diffusion layer and a catalytic layer (Figure 1).

The state of the art in membranes is Nafion. It was created by addition of sulfonic acid groups into the bulk polymer matrix of Teflon. These sites have strong ionic properties and act as proton exchange sites.

Aqueous methanol is fed at the anode side. It diffuses through the diffusion layer to the catalytic layer where it is electrochemically oxidized into mainly carbon dioxide protons and electrons.

Protons formed during this reaction diffuse through the Nafion membrane to the cathode catalytic layer. They participate in oxygen reduction to form water at cathode side. Oxygen may be pure but can also come form air.

Electrons are collected by graphite bipolar plates which are the two poles of the cell. The structure of the cell is described in Figure 1.

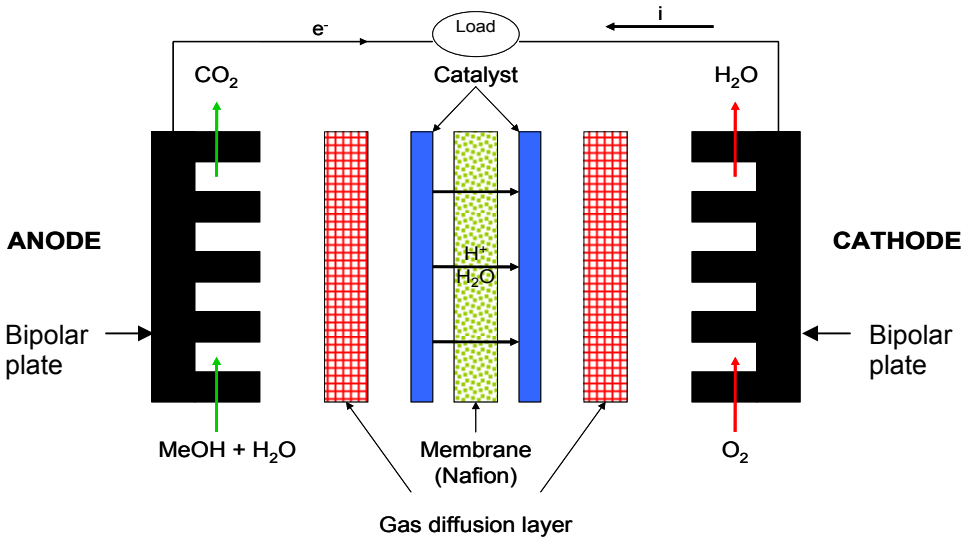

Figure 1: DMFC principle scheme

b. Reactions

Anode reaction:	$CH_3OH + 7H_2O \leftrightarrows CO_2 + 6H_3O^+ + 6e^-$	E^0=0.02V
Cathode reaction:	$^3/_2O_2 + 6H_3O^+ + 6e^- \leftrightarrows 9H_2O$	E^0=1.23V
Overall reaction:	$CH_3OH + ^3/_2O_2 \leftrightarrows CO_2 + 2H_2O$	E^0=1.21V

At anode, the methanol is oxidized into carbon dioxide and six protons (as hydronium ions) plus six electrons. The six protons formed react at the cathode with oxygen to form water.

The overall reaction looks like a combustion reaction and is thus sometimes referred to as cold combustion. Actually the cell is a mean to control this reaction and use it to produce current directly.

The standard cell voltage for a DMFC at 25ºC is 1.21V. However, this potential is never obtained in reality. The open circuit potential is usually about 0.6 to 0.8V in the best case.

4. Issues in DMFC

a. Slow electro-oxidation kinetics

Various surface intermediates are formed during methanol electro-oxidation. Methanol is mainly decomposed to CO which is then further oxidized to CO_2. Other CO-like species are also formed: COH_{ads}, HCO_{ads}, $HCOO_{ads}$ [11]. Principle by-products are formaldehyde and formic acid. Some of these intermediates are not readily oxidizable and remain strongly adsorbed to the catalyst surface. Consequently, they prevent fresh methanol molecules from adsorbing and undergoing further reaction. Thus electro-oxidation of intermediates is the rate limiting step.

This poisoning of the catalyst surface seriously slows down the oxidation reaction. Besides, a small percentage of the intermediates desorbs before being oxidized to CO_2 and hence reduce fuel efficiency but undergoing in complete oxidation.

Thus, a very important challenge is to develop new electrocatalysts that inhibit the poisoning and increase the rate of the reaction. At the same time, they should have a better activity toward carbon dioxide formation.

b. Methanol Crossover

- Description:

In PEM fuel cells, one of the objectives of the membrane is to stop fuel and oxygen to reach the electrode on the other side and undergo non-electrochemical oxidation.

However, in DMFC, the fuel diffuses through Nafion membrane. Due to the hydroxyl group and its hydrophilic properties, methanol interacts with the ion exchange sites and is dragged by hydronium ions in addition to diffusion as a result of concentration gradient between anode and cathode.

Methanol that crosses over reacts directly with oxygen at the cathode (Figure 2). Electrons are brought directly from the anode to the cathode along with methanol resulting in an internal short circuiting and consequently a loss of current (Figure 3). Besides, the cathode catalyst, which is pure platinum, is fouled by methanol oxidations intermediates similar to anode.

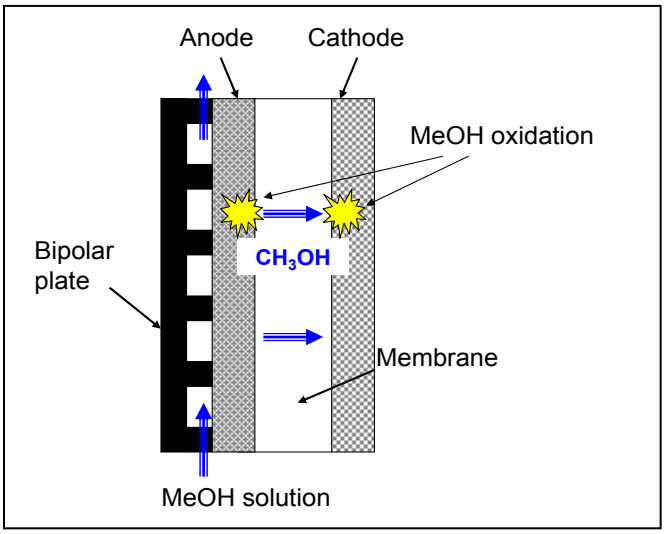

Figure 2: Methanol crossover phenomenon

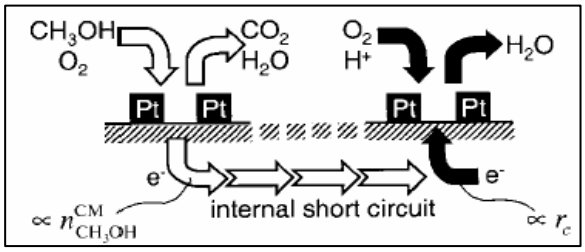

Phys. Chem. Chem. Phys., 2001, **3**, 347-355

Figure 3: Internal short circuit created by crossover

- Simple solutions to prevent crossover:

Crossover is enhanced by the concentration and pressure gradient between anode and cathode. It can be easily limited by using a low methanol concentration in the anode feed solution and by increasing cathode pressure in a certain measure. A compromise should be found for the concentration. It should be small enough to reduce crossover as much as possible but also supply the anode catalytic layer with enough methanol to produce an acceptable current density.

This phenomenon is also promoted by high temperature (Figure 4).

- Experimental data for methanol crossover are shown below:

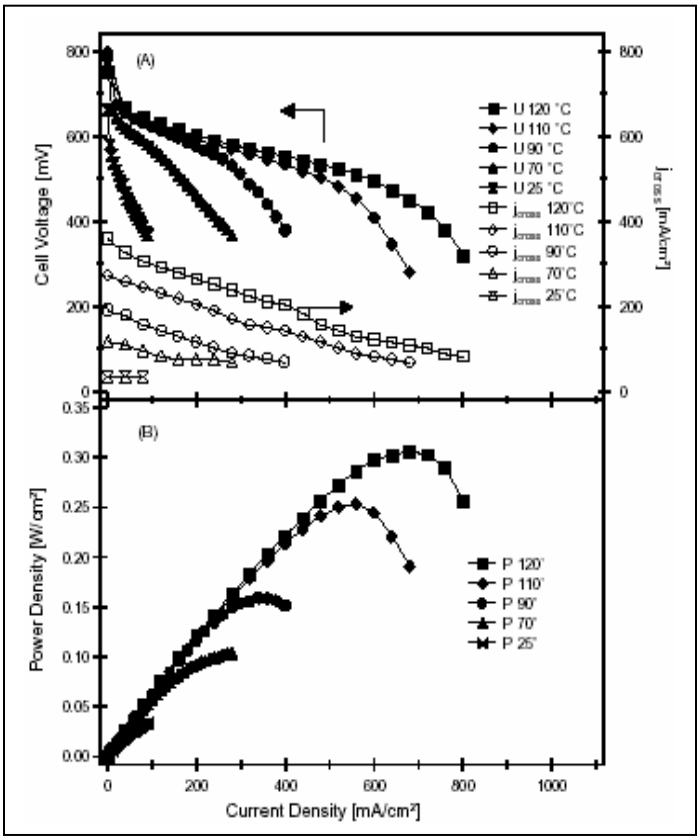

Journal of Power Sources, Volume 127, Issues 1-2, 10 March 2004, Pages 172-180
V. Gogel , T. Frey , Zhu Yongsheng , K. A. Friedrich , L. Jörissen

Figure 4: Crossover currant losses compared to total current density

These experimental results were obtained by Gogel et al [5] for the following operating conditions:

- Anode and Cathode flow rates are respectively 4ccm (1M) and 4000sccm;
- Anode and Cathode catalyst loadings are respectively 5.4mg/cm^2 Pt/Ru and 6.3mg/cm^2 Pt black;
- Anode and Cathode outlet pressures are respectively 2.5 and 4 bar respectively;
- The membrane is Nafion 105.

Methanol crossover (j_{cross}) was deduced from the outlet flow rate of CO_2 at the cathode.

The small thickness of the electrode promotes methanol crossover. Besides the cell is operated under harsh conditions which gives high performance. The data showed here are not comparable to those which will be presented later on in the experimental part as our operating conditions are quite different. However, it gives an idea of how crossover changes with temperature and how an issue it can be.

It can be seen that despite the pressure difference of 1.5 bars between anode and cathode j_{cross} is substantial. Current losses due to crossover are close to 50% at 120ºC and close to 10% at ambient temperature.

c. Gas management on anode side

Most of the carbon dioxide formed during methanol oxidation is in the gas phase and has to be removed via the feed channel.

CO_2 is formed in the anode catalytic layer and diffuses to the top of the gas diffusion layer. There, CO_2 bubbles form at the outlet of the pores. Their size depends on the size of the pores and the wettability of the electrode backing. After they reach a certain size, these bubbles are released into the methanol solution [6]. There is thus a two phase flow inside the feed channels and this is not without consequences on cell performance (Figure 5). The high concentration of bubbles makes them coalesce and form slugs. This results in a reduction of the methanol diffusion area. Consequently, the supply of methanol may not be sufficient to maintain a desired current density. The current density becomes limited by methanol diffusion.

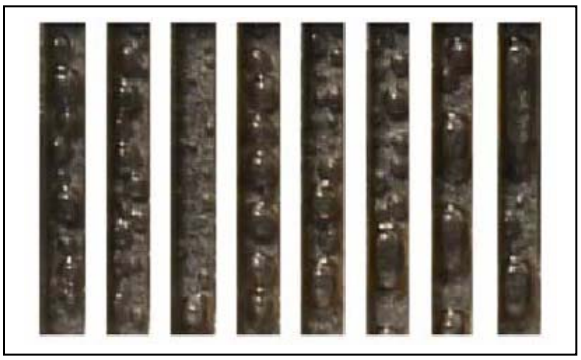

Journal of Power Sources, Volume 106, Issues 1-2, 1 April 2002, Pages 364-369

Figure 5: CO_2 bubbles formation and coalescence in the anode feed channel

This phenomenon is especially an issue at high current densities where a large amount of carbon dioxide is formed.

Two techniques are considered to take care of this problem. They certainly have to be developed and used simultaneously. First, the patterns of the feed channels can be changed to help a quick removal of CO_2. Second, Lu and Wang [6] investigated the structure of the diffusion layer itself and formation of bubbles on the top.

According to them, small and homogeneously spread pores would create small diameter bubbles rather than slugs. This may generate a bubbly flow rather than a slug flow.

5. Electrode structure

The gas diffusion layer of an electrode is usually carbon cloth. Carbon paper has also been used but has shown a higher resistance to methanol diffusion [7]. Besides CO_2 bubbles formation management was not as good as with carbon cloth.

a. Catalysts

The catalytic layer is made from a catalytic powder applied to the diffusion layer or directly on the membrane. Catalyst for anode and cathode are different.

- Anode catalyst:

It has been proven that an adsorbed hydroxyl group is needed in rate determining steps of methanol oxidation [1]. This group comes from water dissociation on the catalyst surface which occurs only at high electrode potential (0.6V) on Pt. That makes methanol oxidation difficult on a pure Pt catalyst.

However, water discharging occurs at much lower potential on ruthenium (0.2V). That is why a bimetallic catalyst containing both platinum and Ruthenium is commonly used at anode.

The chemisorption process of methanol is significantly favored on Pt sites. Consequently, the steps concerned by the hydroxyl groups can only occur on adjacent Pt

and Ru sites. This should be taken in count during the catalyst preparation [7]. An optimized contact area between both catalysts is desired.

- Cathode catalyst:

Pure platinum is almost universally used as a cathode catalyst. The catalytic powders used for DMFC are either metal black or supported catalyst on carbon particles at various loadings. Both of them are widely used.

b. Catalyst structure

The catalytic layer contains catalyst particles but also Nafion particles [6]. Nafion is added to the catalyst to help proton removal (Figure 6). A good continuity of the Nafion network is needed for effective transport of protons to the membrane. This reduces electric resistance of the catalytic layer. However, a too high Nafion loading would covers the catalyst particles and reduces the active area.

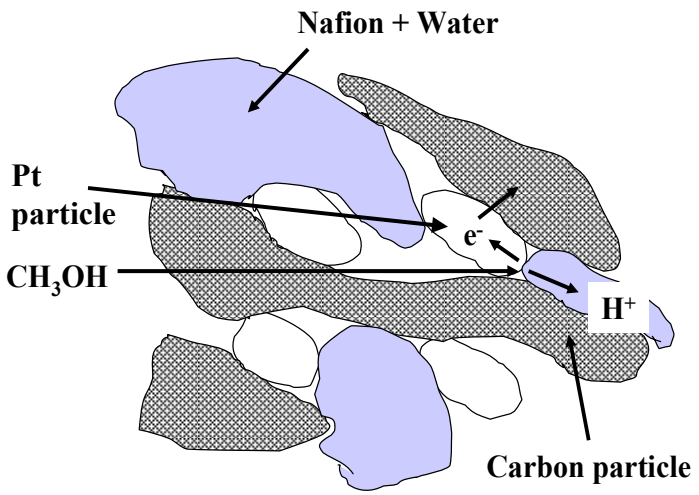

Figure 6: Catalyst structure

6. Electrodes and MEA preparation

Electrodes are prepared by applying a catalytic ink to an electrode backing used as a gas diffusion layer.

a. Catalytic ink preparation

There are various techniques for electrodes preparation. However, most of them involve the use of catalytic ink. This ink contains catalyst particles in suspension in a mixture of an organic solvent and water.

To increase the catalytic area, a smaller particle size is preferable. That is why catalyst particles are milled. Three techniques can be utilized [8]:

- Magnetic stirring;
- Mixing in a sonic bath;
- Ball milling.

As discussed previously, the catalytic layer needs to contain a certain amount of Nafion. Nafion solution is added to reach a desired percentage of the weight of catalyst.

b. Application to the diffusion backing

The most common technique is ink spraying. It can be done directly on the electrode backing (usually carbon cloth) or on the membrane. A third option consists in applying it to a Teflon sheet and then transferring it onto the membrane by hot-pressing [9]. In case of application on the diffusion backing, droplets of ink can also be spread on its surface.

Once electrodes are made, solvent is evaporated in an oven at a temperature between 80 and 120ºC.Other techniques such as dry spraying or screen printing exist. However, they are still developing techniques.

c. MEA preparation

During cell operation, formed protons need to be transferred as quickly as possible to the cathode. This implies a good continuity between Nafion contained in the catalytic layer and the membrane. To achieve that, the electrodes and the membrane are pressed together high temperature.

The techniques used are either hot-rolling, or more frequently, hot-pressing.

7. The fuel cell station

- Bipolar plates:

As discussed above, the Membrane Electrode Assembly is the heart of the fuel cell. However, it can not be used alone. Bipolar plates are used as current collector as well as a fuel provider. On their surface a channel network is machined. Methanol is fed to the part of the electrode in contact with the channel, while electrons are transferred from the electrode to the bipolar plate where they are in direct contact.

There are different patterns for the channel. The two more famous are (Figure 7) the parallel fluid flow (PFF) and the single serpentine flow Field [10].

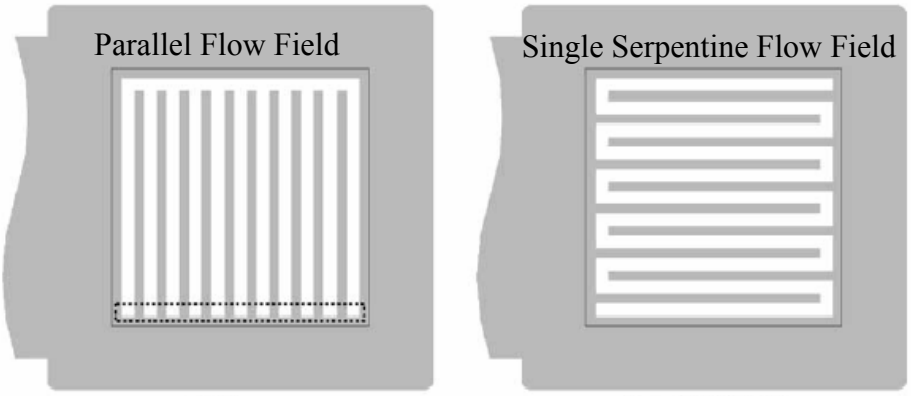

Journal of Power Sources, Volume 106, Issues 1-2, 1 April 2002, Pages 364-369

Figure 7: Flow patterns for bipolar plates

Other patterns have also been investigated like Pin Flow (Figure 8). Pin flow seems to be promising for DMFC.

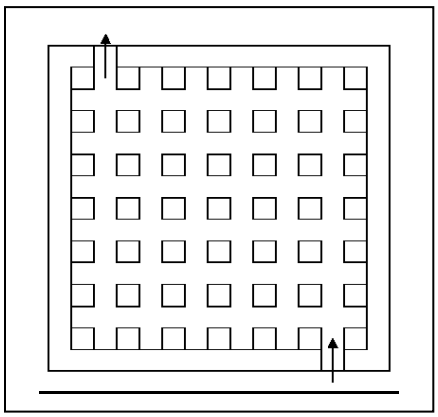

Figure 8: Pin Flow pattern

- Complete stack:

Teflon gaskets of appropriate thickness are used on each side of the membrane. They have to be as thick as the electrodes to prevent leaks but not too thick so as to keep good electrical contact between the electrodes and the bipolar plates (Figure 9).

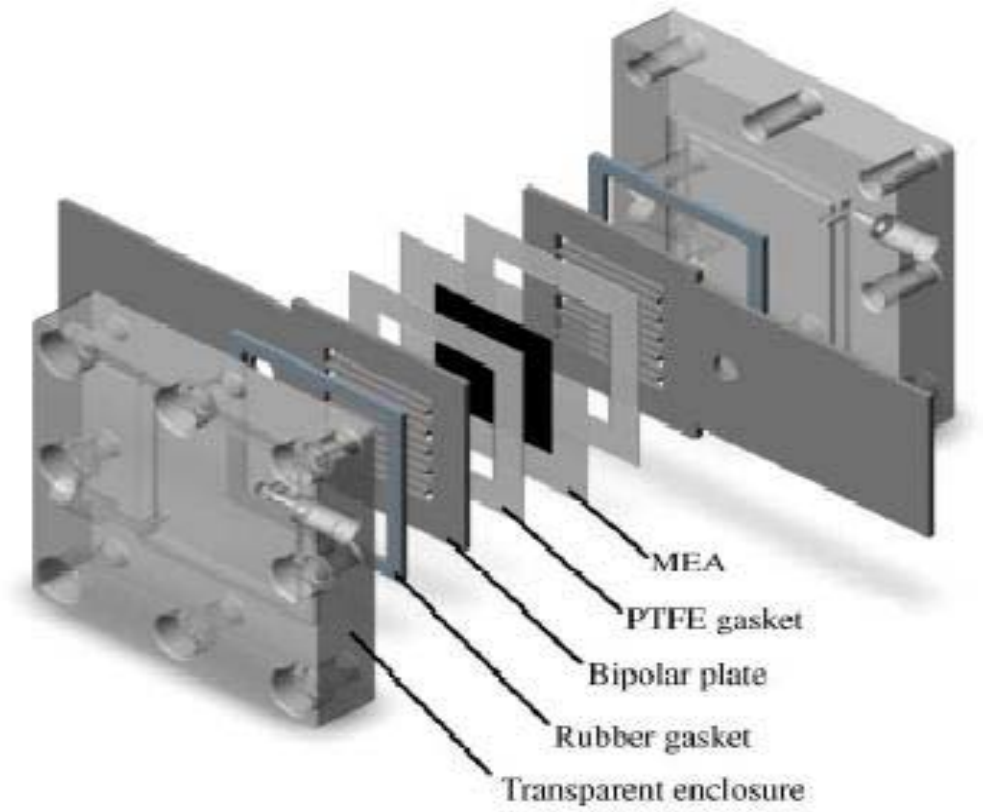

Journal of Power Sources, Volume 134, Issue 1, 12 July 2004

Figure 9: Fuel Cell Stack

On the other sides of the bipolar plates rubber gasket are used to insulate them from enclosures. Those enclosures are bolted to hold everything together.

III. Experimental methods

1. Membrane pretreatment

Nafion membranes 117 from Electrochem were treated by consecutive boiling:

- ½ hour in deionized water to soak them;
- ½ hour in 5 %vol hydrogen peroxide to oxidize impurities;
- ½ hour in deionized water;
- 1 hour in 0.5mol/L sulfuric acid;
- ½ hour in deionized water.

2. Membrane Electrode Assembly (MEA) preparation

The catalytic ink was prepared by mixing the amount of catalyst (from Alfa Aesar) needed for one electrode with 5mL of deionized water and 5mL of methanol. Then 5% Nafion solution (1100EW from DUPONT [ρ=2.01g/cm^3]) is added. The weight of Nafion is 10% of the weight of catalyst. The ink was sonicated for 3 hours.

WARNING: Ethanol and isopropanol are the most frequent organic solvent used in catalytic ink preparation for DMFC. They can **react violently** with catalysts (especially Pt and Pt/Ru black) and start a **combustion reaction**.
To prevent any risk, when the ink is prepared, the catalyst should be first mixed with water and completely soaked before alcohol addition. Besides the desired amount of alcohol needs to be poured into a beaker before being added to the ink.

The ink was sprayed on 5cm^2 carbon cloth pieces (1.75g/cc, Teflon treated from Electrochem).

MEAs were prepared by hot-pressing electrodes on each side of the Nafion membrane for 2 min 30 at 275 F under 2 tons.

This operating mode has initially been developed for hydrogen fuel cells.

3. Experiments and experimental conditions

The DMFC was operated in a station designed for both hydrogen and methanol PEM fuel cell. The difference lies in the anode feeding system. For DMFC, a syringe pump (ISCO 1000D) replaces the hydrogen bottle and the humidifier (Figure 10). Humidifiers are used to maintain a certain humidity in the feed stream which keeps the water content of the membrane constant. Heating tapes prevent water condensation in the feeding pipes. Besides, there are two pressure controllers on the oxygen feeding stream. The first one which pressurizes the humidifier is used in addition to the heating tapes as a mean to control oxygen humidity. The second one located at the outlet of the cell control the cathode pressure.

Either current or potential can be fixed with a controller and acquisition software (PCVE) is used to record both current and potential as a function of time.

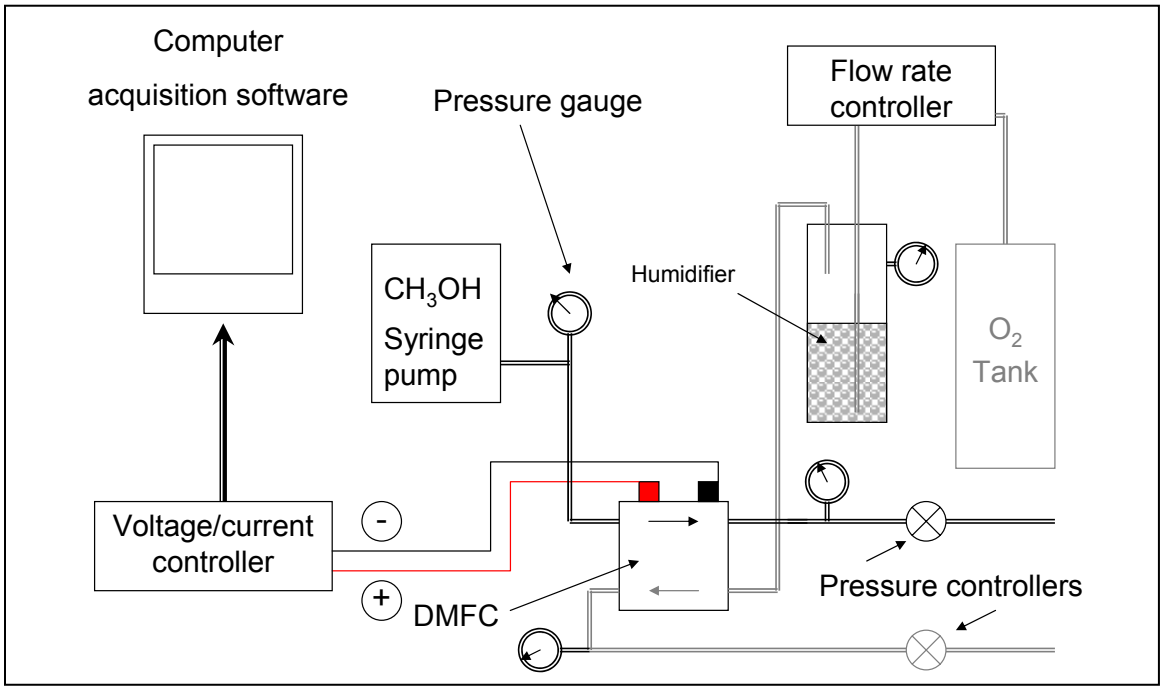

Figure 10: Fuel Cell Stack

Experiments consist in obtaining a polarization curve for the tested membrane at various experimental conditions.

The MEA first needs to be activated. The cell containing the MEA is operated at 80ºC and under a fixed voltage 0.3V for 6 hours or until the current profile becomes flat.

During experiments, the cell voltage is kept constant while current is measured as a function of time. Thus the steady state can be visualized for each applied potential. The cell voltage is switched manually from 0.5V to 0.1V with a step of 0.1V.

Anode and cathode are respectively fed continuously with a solution of methanol in water via a syringe pump and pure oxygen.

Open circuit potential is also measured by switching from a non-zero current to no current.

The cell was operated at 60ºC or 80ºC. The anode and cathode flow rate were respectively 1ccm of 1M methanol solution and 75sccm of pure oxygen. The cathode side humidifier temperature was kept at ambient temperature.

Anode and cathode were left at atmospheric pressure.

These experimental conditions remained the same in the following experiments except when specified otherwise.

IV. Experimental results

The following experiments were aimed at improving the overall performance of the DMFC. Various parameters were successively investigated. The three main area of investigation were: effect of the catalyst, Nafion and Teflon loading in the catalytic layer, and the effect of nano-composite membranes. Conclusions drawn during the course of this study were utilized to reorient it, if warranted.

1. Effect of catalyst layer

a. Performance of commercial electrodes

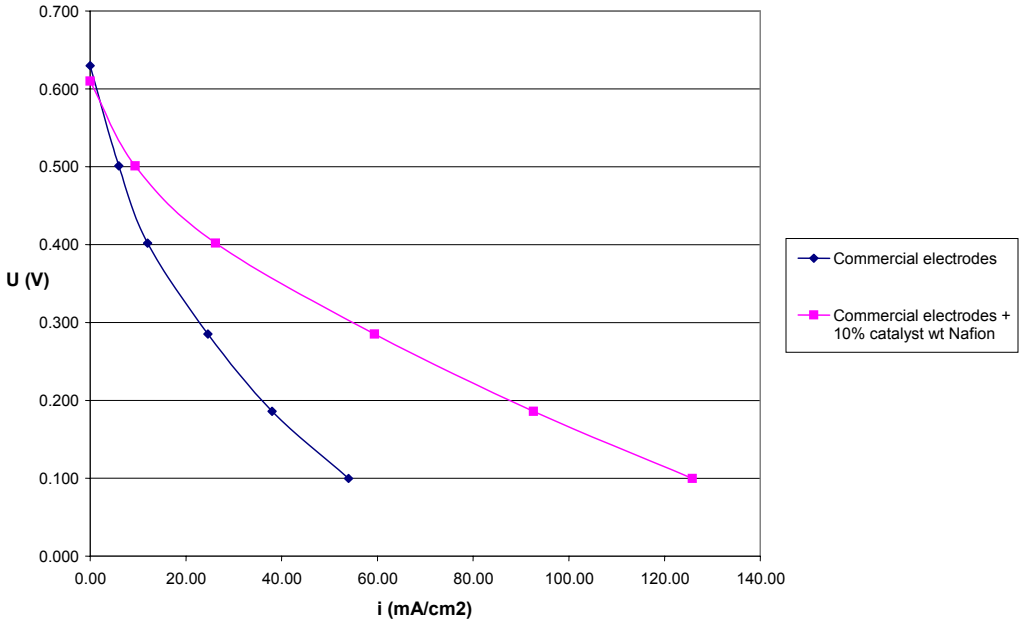

Figure 11: Performance of commercial electrodes

(T = 80ºC, Anode flow rate = 1ccm, Cathode O_2 flow rate = 75sccm, $T_{humidifier}$ = 25ºC)

DMFCs use different catalyst for anode-side and cathode-side electrodes. Commercial DMFC electrodes (E-Tek) contain 4mg/cm^2 Pt/Ru black for the anode and 4mg/cm^2 Pt black for the cathode. Using "black"catalysts allows high catalyst loading in thin layers.

Commercial electrodes performance was quite low (Figure 11) compared to Sundmacher et al [11] results. They did their experiments at similar conditions and with a similar MEA. Despite their goal was to compare their model to experiments and not to get high performance our MEA was far from giving acceptable performance. For example they obtained current densities of 25 and 110 mA/cm^2 at respectively 0.5V and 0.35V whereas we obtained current densities of 10 and 25 mA/cm^2 at respectively 0.5V and 0.35V. Nevertheless, results couldn't be compared at lower cell voltage because they used different methanol concentration.

Fuel cell electrodes contain Nafion to help proton conduction. A way to improve their performance could be to spray a Nafion solution on them. A solution was thus prepared by mixing 0.25ml of 5% in weight (wt%) Nafion solution with 10ml of ethanol. It corresponds to 10% of the weight of catalyst considering 20% of losses during spraying.

After treatment with this solution performance increase (Figure 11) but was still half of what was desired.

b. Home-made electrodes

With the goal of improving DMFC performance we began by trying to optimize the MEA preparation [12]. Membranes remained the same (commercial Nafion117 from Electrochem) but electrodes were prepared in the lab using Pt/Ru and Pt black with an atomic ratio of 1. The Pt/Ru black catalyst will remain the same in this study.

For both electrodes the catalytic ink was prepared by mixing 24mg of catalyst with 20ml of water and 20ml of ethanol and sonicated for 24h in order to ground and disperse the catalyst particle agglomerates. 0.25ml of 5wt% Nafion solution was added 1h before utilization. Then this ink was sprayed on a 5cm^2 piece of Teflon treated carbon cloth and the electrode dried for 1h at 80º C.

20% losses were considered during the preparation including spraying. To deposit roughly of 4mg/cm^2 of catalyst, 24mg were used instead of 20mg.

Home-made catalyst gave slightly better performance (Figure 12). However the gain is not significant. The catalyst layer appeared non-uniform on the carbon cloth surface. It

appeared that the catalytic ink has penetrated too far into the carbon cloth instead of forming a layer on its surface.

To address this problem, a more concentrated and thus viscous ink was prepared. The amount of solvent was reduced to 10ml for both water and ethanol. A nice layer was thus formed on the carbon cloth surface and performance appeared to be better (Figure 12).

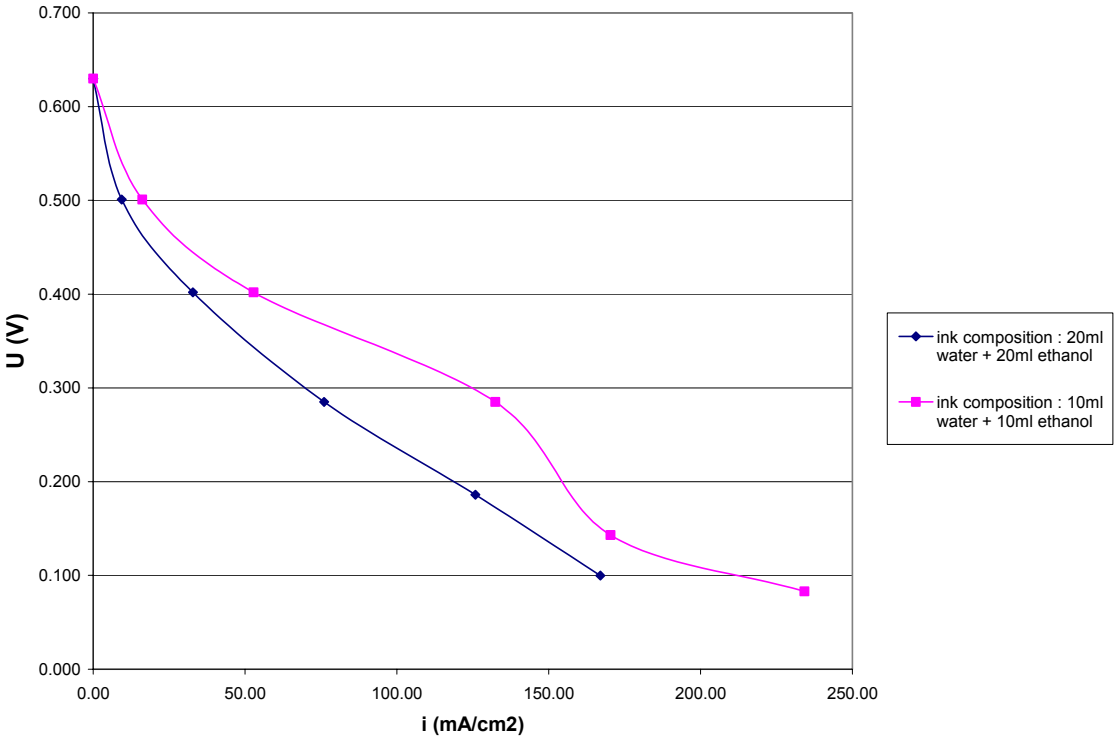

Figure 12: Performance of hand-made electrodes

(T = 80ºC, Anode flow rate = 1ccm, Cathode O_2 flow rate = 75sccm, $T_{humidifier}$ = 25ºC)

The new polarization curve shows nonetheless a sharp drop in performance at low potential. Actually at these cell voltages irregular current oscillations (figure 13) occur and an average value of current was thus plotted. These oscillations were found to disappear when the anode feed flow rate was increased to 5ccm (figure 14).

- Origin of oscillations:

As oscillations seemed to be linked to the flow rate, it was assumed that mass transport was involved in this phenomena, rather than being due to surface chemistry.

At low cell voltages and high current densities, a lot of gaseous carbon dioxide is synthesized. It, thus, occupies a much larger volume than the methanol solution in the feed channel [13]. Consequently, if too much carbon dioxide is produced, the solution is no longer in contact with the diffusion backing and is not effectively supplied to the catalytic layer thus resulting in a drop of current. In other words, the current is limited by mass transport.

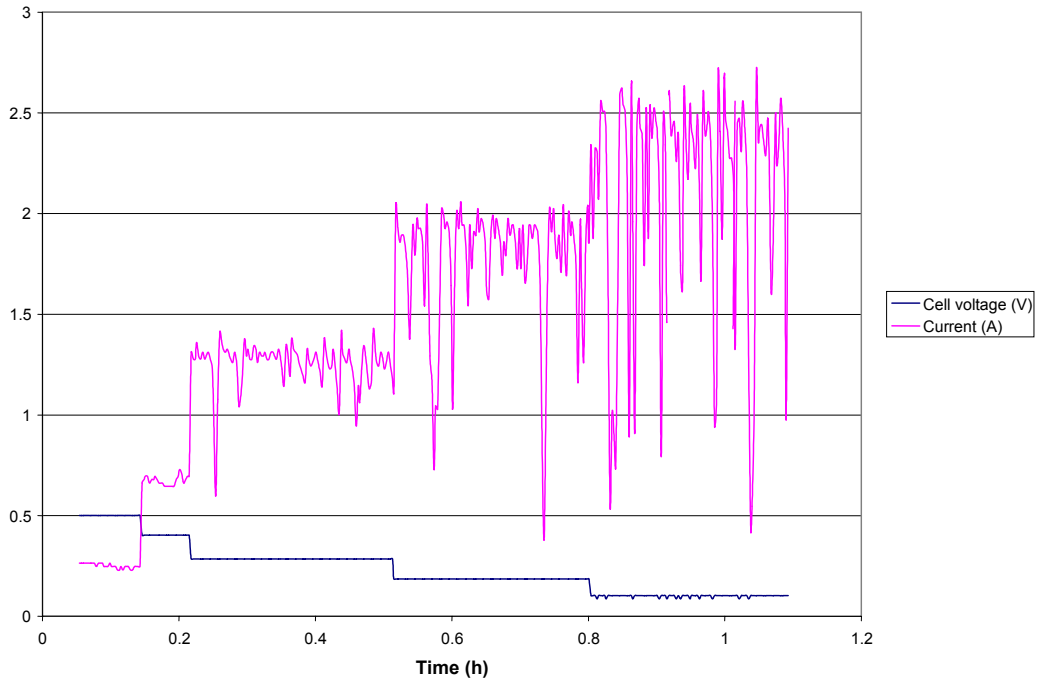

Figure 13: Current oscillations at fixed potential and anode feed flow rate of 1ccm (T = 80ºC, Anode catalyst: 4mg/cm^2 Pt/Ru black, Cathode catalyst: 4mg/cm^2 black, Cathode O_2 flow rate = 75sccm, $T_{humidifier}$ = 25ºC)

According to this hypothesis, the erratic oscillations are related to limited anode catalytic layer methanol concentration. When the cell voltage is switched to a value around 0.3V or less, methanol supply to catalyst layer becomes limited and its concentration in the catalytic layer declines. Crossover declines at the same time. Thus, less CO_2 is formed due to low current. Then it is removed from the feed channel and methanol again reaches the catalytic layer and the cell can again produce a high current. As the current starts to rise and more CO_2 is produced, fresh methanol is again unable to reach the cathode.

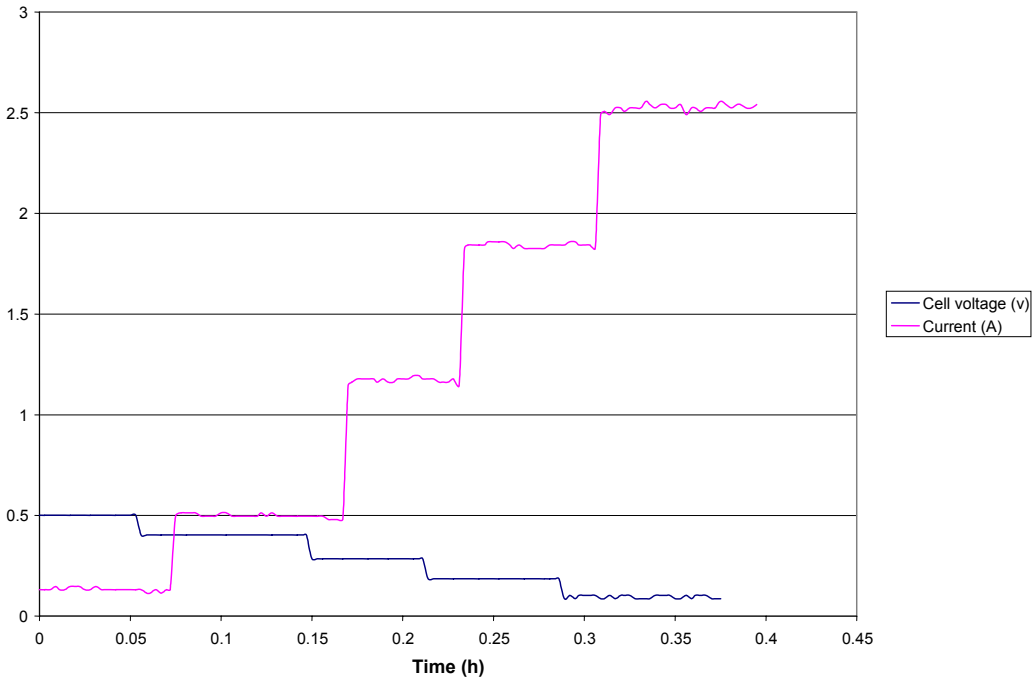

Figure 14: Current oscillations at fixed potential and anode feed flow rate of 5ccm

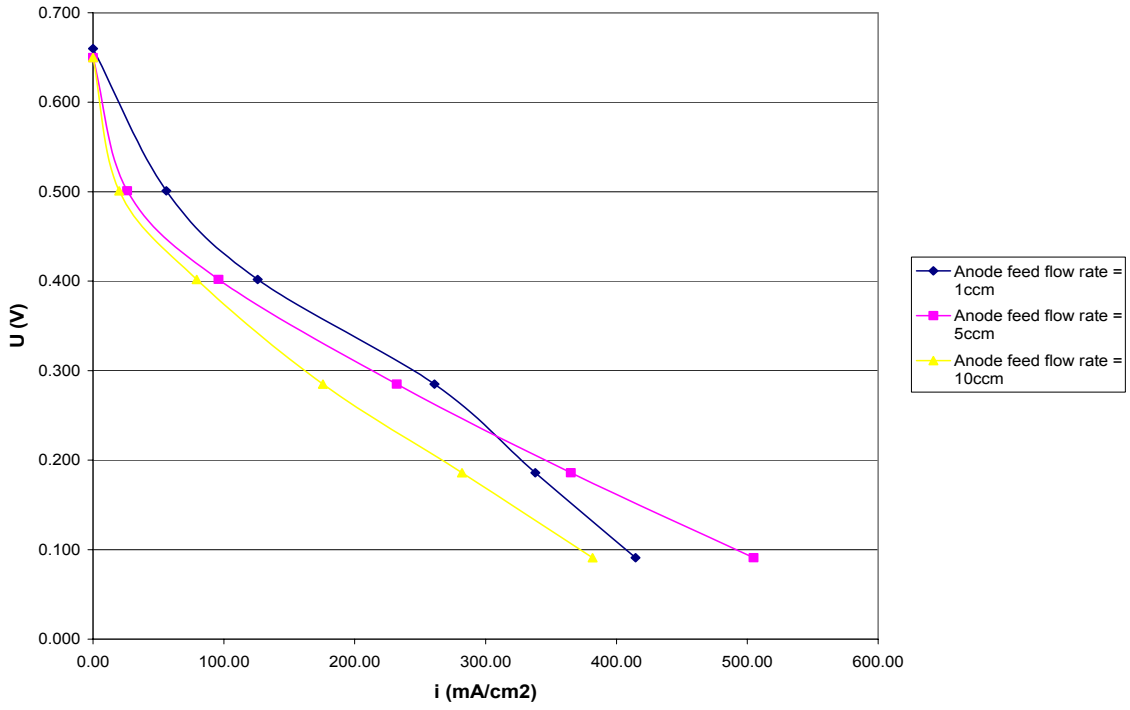

Figure 15: Effect of flow rate on cell performance

(T = 80ºC, Anode catalyst: 4mg/cm^2 Pt/Ru black, Cathode catalyst: 4mg/cm^2 black, Cathode flow rate = 75sccm, $T_{humidifier}$ = 25ºC [for both figures])

If the anode feed flow rate is increased, CO_2 is removed more rapidly. There is no longer competition between carbon dioxide removal and methanol supply. That is why oscillations disappear at higher flow rates (Figure 14).

However there is a penalty for higher flow rates. It can be seen that at higher cell voltage that performance is lower for a 5ccm flow rate (Figure 15). Methanol transfer increases with the flow rate it increases methanol crossover as well. In this range of potential it increases methanol crossover and decreases slightly performance by inhibiting the performance of the cathode. It also explains why flow rate can not be increased too much. As seen in Figure 15, 10ccm flow rate gives even lower performances.

c. Catalyst supported on carbon

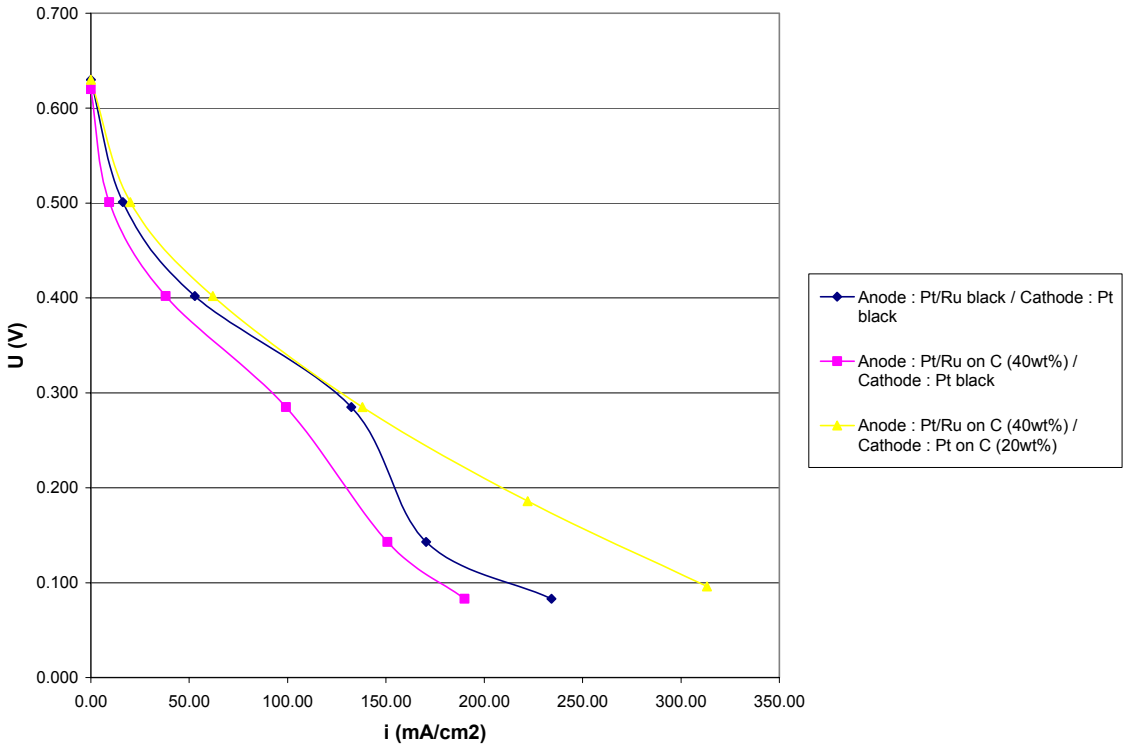

Figure 16: Performance of supported catalysts

(T = 80ºC, Anode flow rate = 1ccm, Cathode O_2 flow rate = 75sccm, $T_{humidifier}$ = 25ºC)

According to literature [1], optimal activity for a platinum catalyst is obtained when it is supported on carbon with high loading (40 to 60wt%). This allows a high active surface

as well as a high catalyst loading, although the catalyst layer thickness increases.

This idea was applied to both the anode and cathode catalyst layer. Pt/Ru black was replaced by 60mg of 40wt% Pt/Ru supported on carbon (equivalent to 24mg of Pt/Ru black [atomic ratio equal to 1]) at the anode and Pt black by 120mg of 20wt% Pt/C (equivalent to 24mg of Pt/Ru black) at the cathode so that the catalyst loading remained 4mg/cm^2. The Nafion loading, in this case, is expressed as a percentage of the overall weight of carbon powder plus catalyst. It remained 10wt%.

Better performance were obtained with Pt/Ru black than with supported Pt/Ru on carbon (Figure 16). However interesting changes concerned supported platinum on carbon at the cathode at low cell voltages.

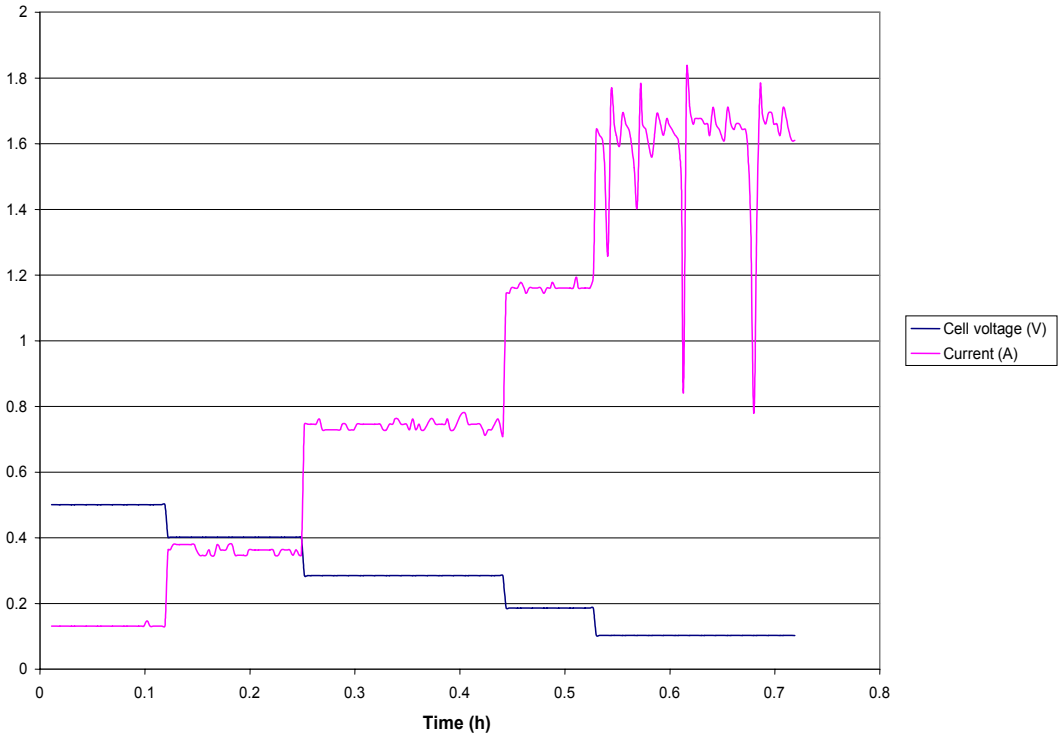

Figure 17. a: Current oscillations at fixed potential for an anode flow rate of 1ccm (T = 80ºC, Anode catalyst: 4mg/cm^2 Pt/Ru black, Cathode catalyst: 1mg/cm^2 20wt% Pt/C, Cathode O_2 flow rate = 75sccm, $T_{humidifier}$ = 25ºC)

At low cell voltages, Figure 16 shows that there is no performance drop for a supported platinum cathode. At the same time, the current density vs. time (Figure 17. a)

plot shows that the amplitude of the erratic oscillations was reduced compared to a platinum black cathode.

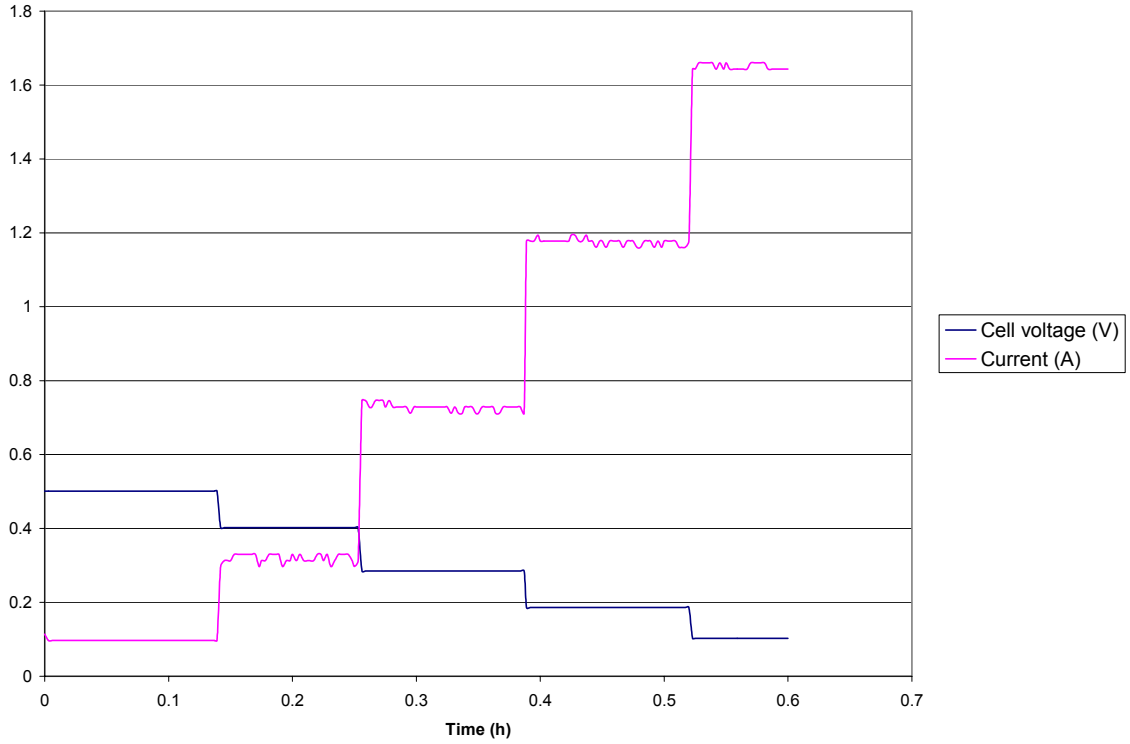

Figure 17. b: Current oscillations at fixed potential for an anode flow rate of 5ccm (T = 80ºC, Anode catalyst: 4mg/cm^2 Pt/Ru black, Cathode catalyst: 1mg/cm^2 20wt% Pt/C, Cathode O_2 flow rate = 75sccm, $T_{humidifier}$ = 25ºC)

The oscillations again disappear when the flow rate is increased (Figure 17. b). The lower amplitude of oscillation can be imputed to the lower performance.

They can be explained, both for supported Pt and Pt/Ru, by the higher catalyst layer thickness.

d. Effect of Pt black at Cathode (non-supported platinum)

As after some experience, better electrodes were prepared in an efficient manner. Pt black was tested again at cathode side showed better performance than Pt on C (Figure 18).

Earlier, an experiment showed that increasing anode flow rate to 5ccm almost suppressed the oscillations. These oscillations were limiting the performance so it seemed

possible to obtain higher current densities at low potential. However, it can easily be seen that with a Pt black cathode performance is found to be higher for a 1ccm flow rate at higher cell voltage and lower current densities. In this range less carbon dioxide is formed and thus more methanol diffuses to the anode catalytic layer. However, since less methanol is consumed crossover is promoted.

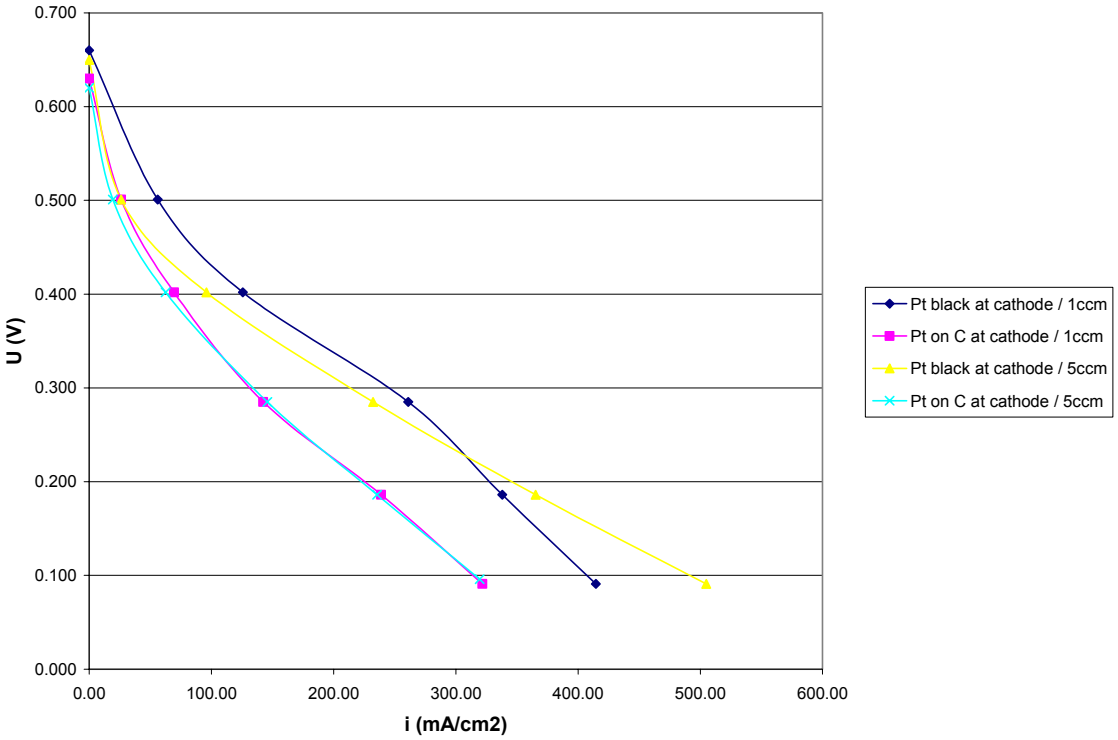

Figure 18: Effect of flow rate on a Pt/Ru black and Pt black MEA
(Anode catalyst: 4mg/cm^2 Pt/Ru black, Cathode O_2 flow rate = 75sccm, T = 80ºC, $T_{humidifier}$ = 25ºC)

Figure 18 shows that for the supported platinum cathode, the flow rate had almost no influence. The thicker catalytic layer may have limited methanol crossover.

e. Pt/Ru catalyst on both sides of the membrane

As methanol crossover is an issue in DMFC and Pt/Ru is a promising catalyst for methanol oxidation it was also tested at the cathode side.

It was hypothesized to help to oxidize methanol coming from the anode and prevent poisoning. Performance is lower at both temperatures (figure 19). Platinum ruthenium black is, thus, not a good catalyst for oxygen reduction. A pure platinum catalyst is better.

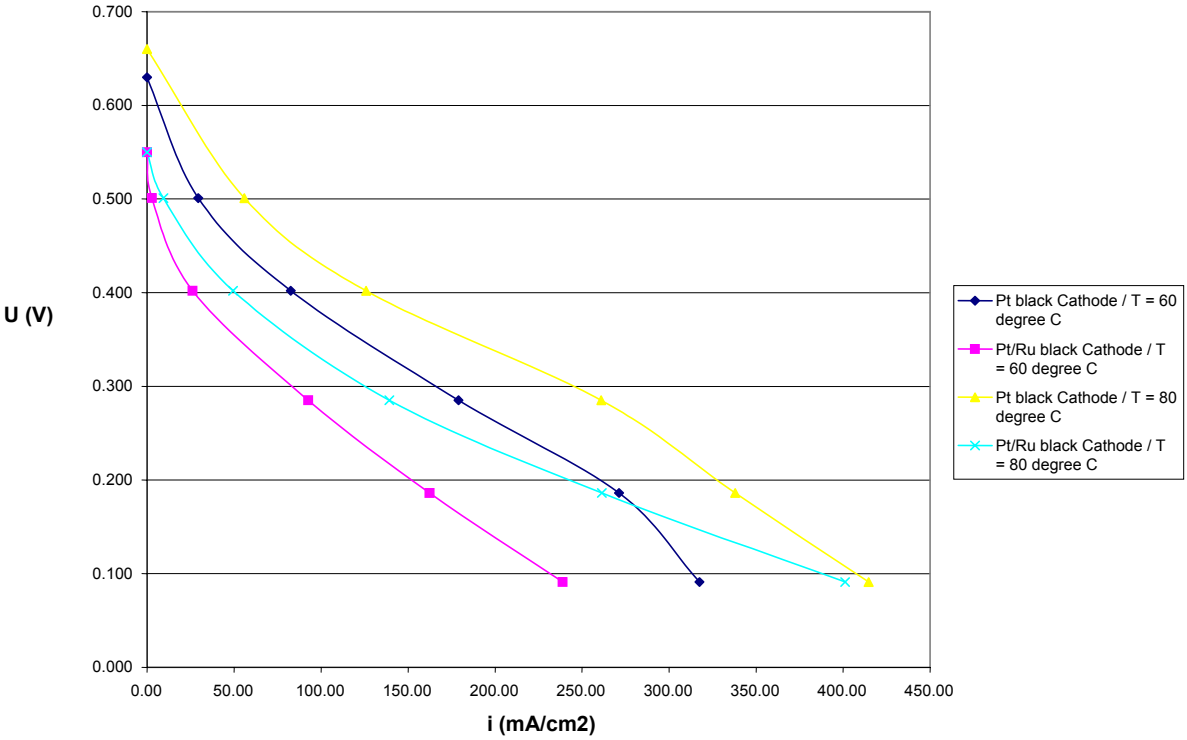

Figure 19: Effect of temperature on an MEA made with Pt/Ru black on anode and cathode

(Anode catalyst: 4mg/cm^2 Pt/Ru black, Cathode catalyst: 4mg/cm^2 Pt/Ru black, Anode flow rate = 1ccm, Cathode O_2 flow rate = 75ccm, $T_{humidifier}$ = 25ºC)

f. Segregated methanol decomposition and hydrogen oxidation on bilayer electrodes

Janssan et al [14] have described bilayer anodes for an improved removal of poisoning species coming from fuel reformation.

Two different inks which were successively applied on the same electrode backing.

- Electrode preparation:

Both a bilayer anode and a bilayer cathode were prepared as follows:

Anode: The electrode backing was first sprayed with an ink made of 12mg of Pt/Ru black in 5ml of water and 5ml of ethanol. Then it was sprayed with 12mg of Pt black in 5ml of water and ethanol.

Cathode: The electrode backing was first sprayed with an ink made of 12mg of Pt/Ru black in 5ml of water and 5ml of ethanol, then with 60mg of 20wt% Pt/C in 5ml of water and ethanol.

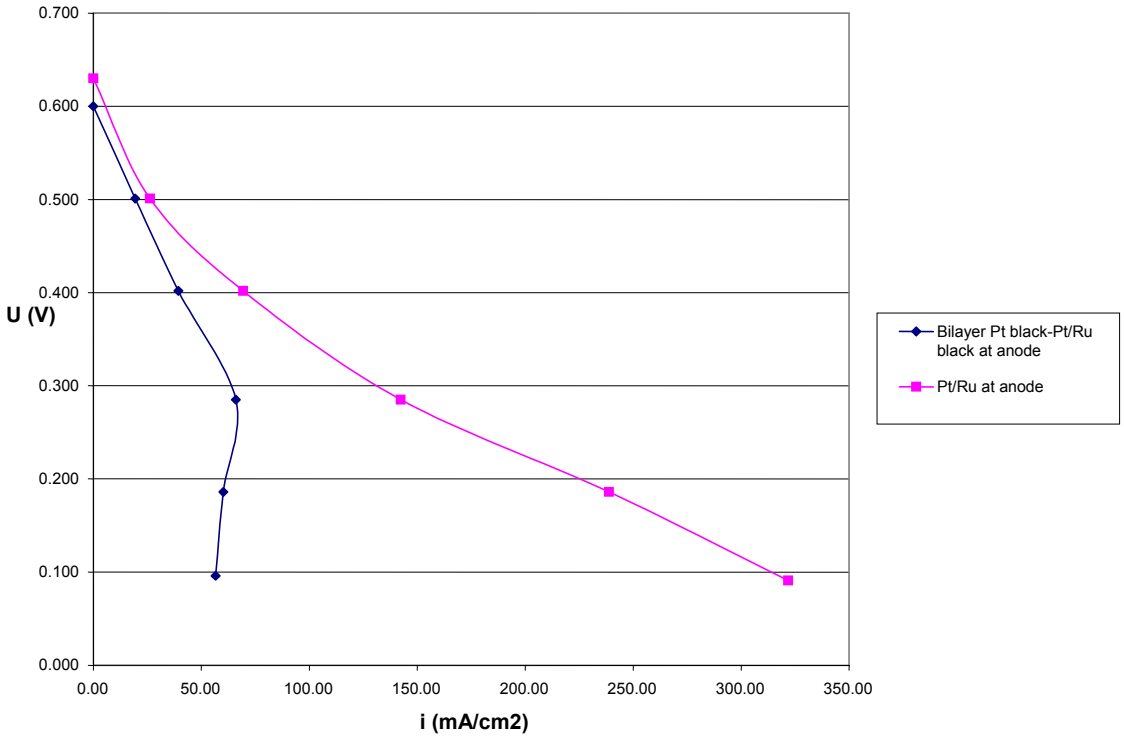

Figure 20: Bilayer Pt black-Pt/Ru black at anode

(T = 80ºC, Bilayer Anode, Cathode catalyst: 1mg/cm^2 Pt on C, Anode flow rate = 1ccm, Cathode O_2 flow rate = 75sccm, $T_{humidifier}$ = 25ºC)

This bilayer anode gave a very poor performance (Figure 20). It was supposed to separate methanol decomposition (Pt/Ru) layer and adsorbed hydrogen oxidation (Pt layer).

The amount of Pt/Ru was likely not sufficient to adsorb and decompose all the methanol molecules. Consequently the platinum layer was also poisoned and rendered ineffective. Thus basically, only half of the catalyst remained active.

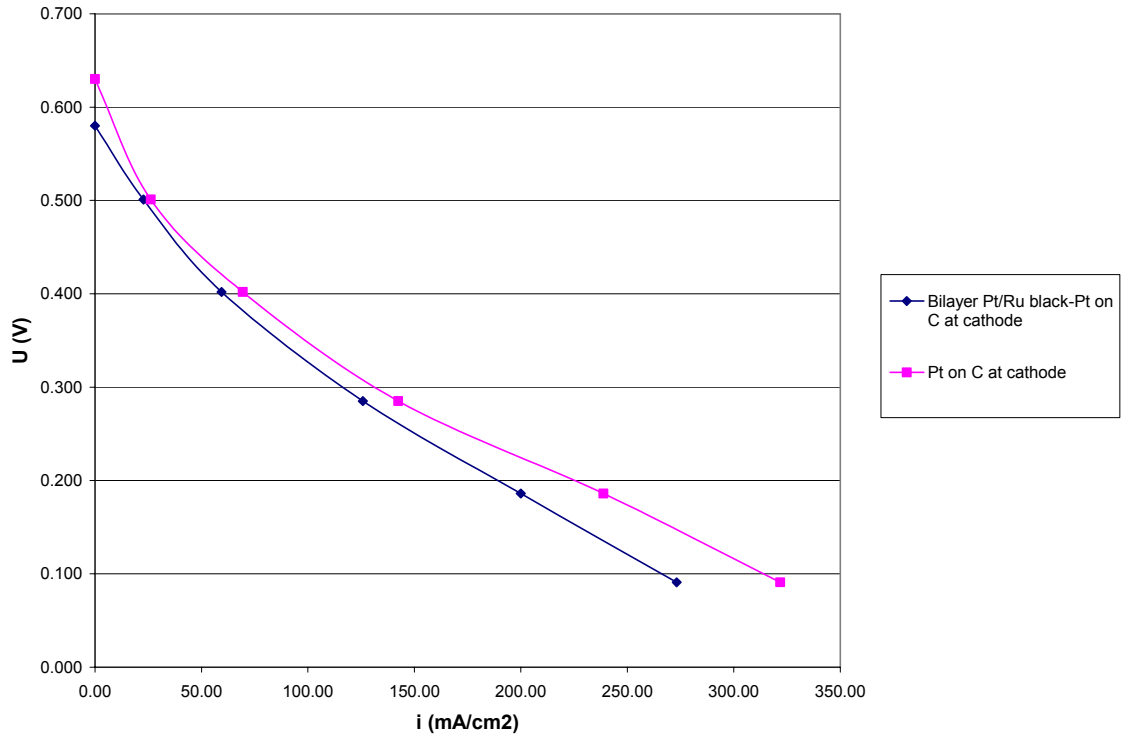

Figure 21: Bilayer Pt/Ru black-Pt on C at anode

(T = 80ºC, Anode catalyst: 4mg/cm^2 Pt/Ru black, Cathode Bilayer, Anode flow rate = 1ccm, Cathode O_2 flow rate = 75sccm, $T_{humidifier}$ = 25ºC)

Performance was found to be lower for the bilayer cathode (Figure 21). It may be due to a reduced amount of Pt catalyst. However, one must be careful when adding more supported platinum. More catalyst results in a thicker catalytic layer and lowers protons mass transfer.

2. Effects of temperature, humidification and flow rate on Pt/Ru black and Pt/C Membrane Electrode Assembly

After some experience, good reproducibility was obtained in the preparation of MEAs. Electrodes using Pt supported on C were used at the cathode as they helped to prevent oscillations.

Their behavior was investigated while varying such parameters as temperature, anode feed flow rate (Figure 22) and cathode humidification (Figure 23) were changed.

As expected, temperature increases performance. The increase in flow rate has the same effect at 60ºC. However when temperature is increased the effect of flow Rate becomes smaller. Actually at 80ºC there is no effect of flow rate.

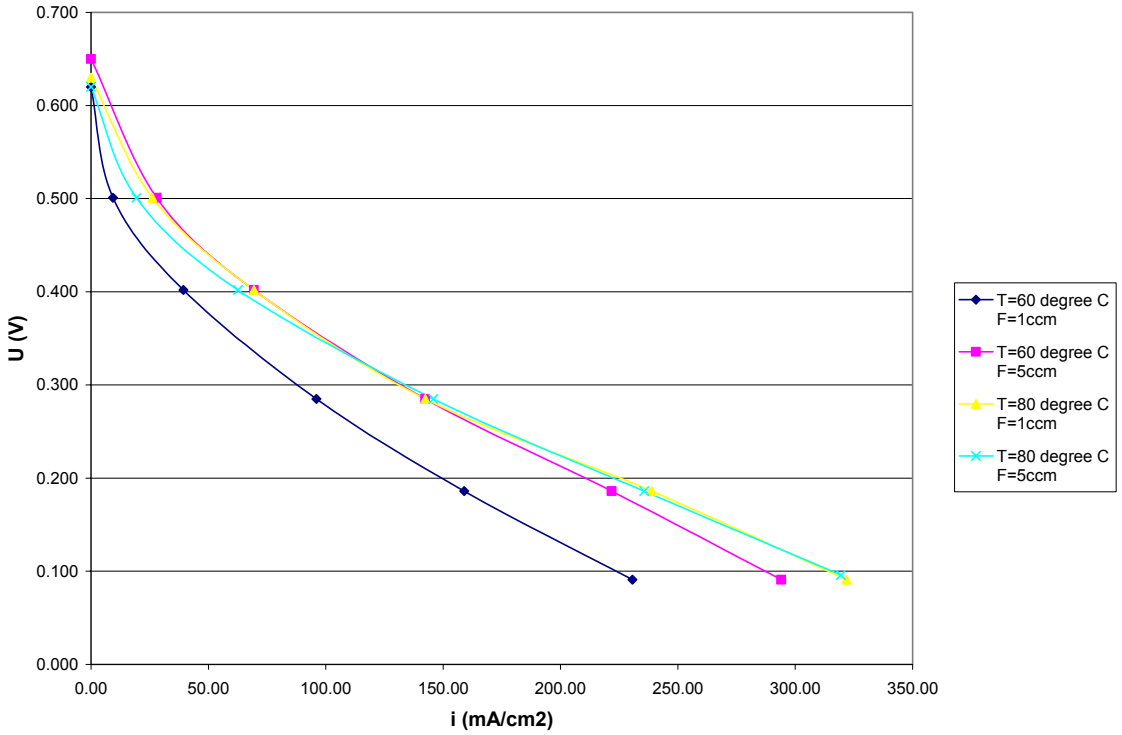

Figure 22: Effect of temperature and flow rate
(Anode catalyst: 4mg/cm^2 Pt/Ru black, Cathode catalyst: 1mg/cm^2 20wt% Pt/C, Cathode O_2 flow rate = 75ccm, $T_{humidifier}$ = 25ºC)

At 60ºC, an improvement in methanol transfer due to flow rate shows an improvement in performance. However, when temperature is increased, methanol crossover is also increased [15]. At 80ºC, the beneficial effect of a higher flow rate is, thus, annihilated by a higher crossover, resulting in no overall improvement.

Humidification was found to have little effect (Figure 23). It is due to water flooding from anode side to cathode side. It seems that humidification is not an issue in DMFC with a liquid feed.

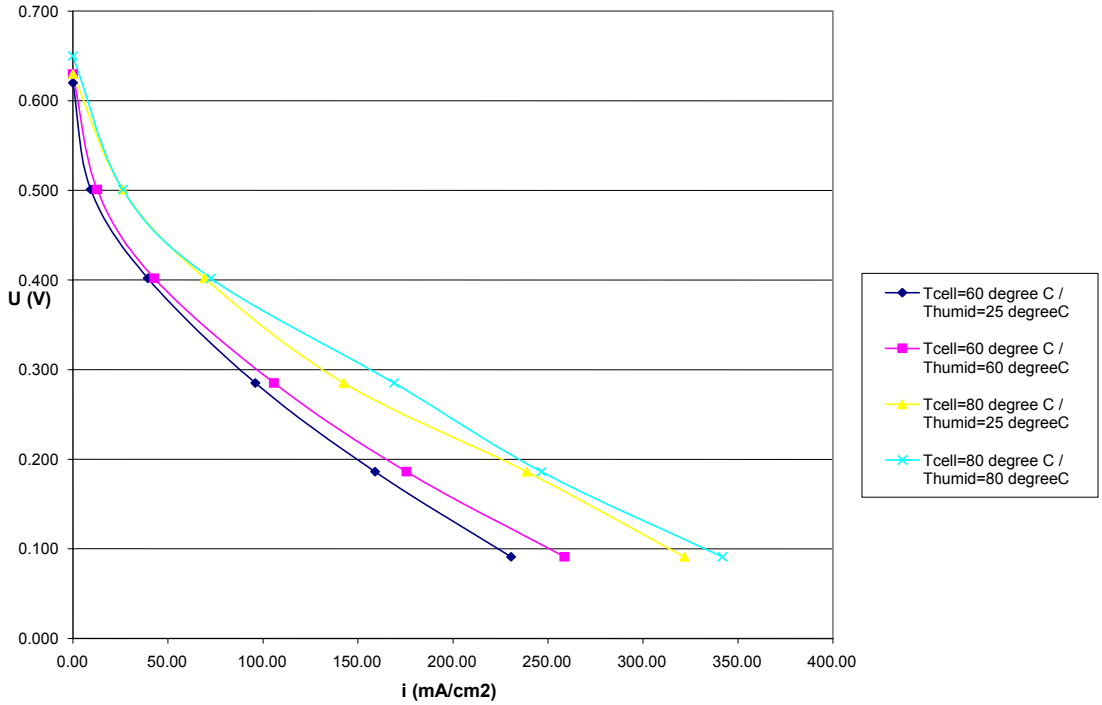

Figure 23: Effect of cathode humidification

(Anode catalyst: 4mg/cm^2 Pt/Ru black, Cathode catalyst: 1mg/cm^2 20wt% Pt/C, Cathode O_2 flow rate = 75ccm, Anode flow rate = 1ccm, $T_{humidifier}$ = 25ºC)

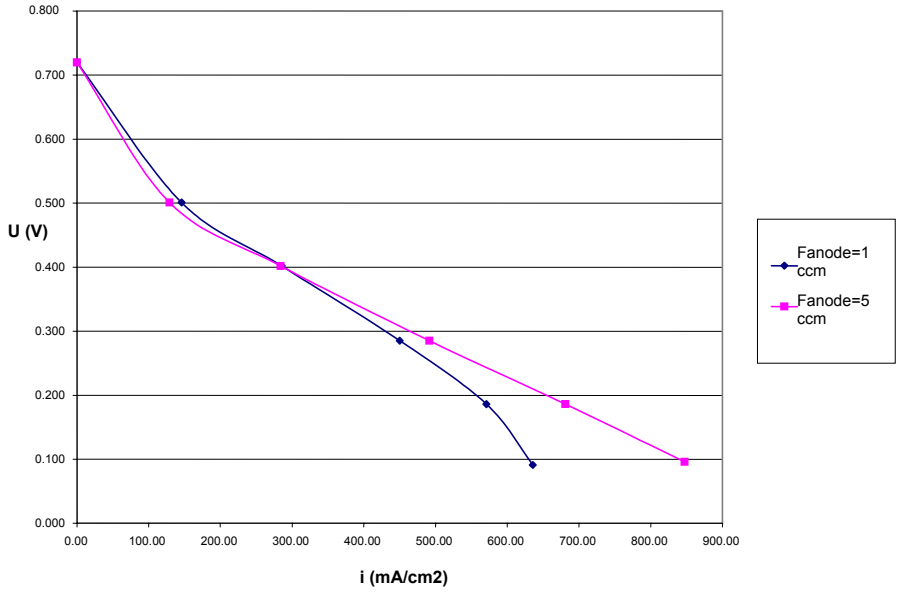

Figure 24: Polarization curves at 110ºC for anode flow rates of 1ccm and 5ccm

(T = 80ºC, Anode catalyst: 4mg/cm^2 Pt/Ru black, Cathode catalyst: 4mg/cm^2 Pt black, Cathode O_2 flow rate = 75ccm, $T_{humidifier}$ = 25ºC, $P_A = P_C$ = 1atm gage)

High performance could be obtained at 110ºC (Figure 24). To keep the methanol solution liquid, however, the anode compartment was pressurized at one atmosphere gage pressure. Cathode pressure was also kept at 1 the same pressure to keep the zero pressure difference between each side of the membrane, to reduce methanol crossover due to pressure difference between anode and cathode. However, pressurized fuel cells will not likely be suitable for small size portable applications such as laptops and cell-phones.

3. Effect of Nafion and PTFE content in the catalytic layer

a. Effect of Nafion

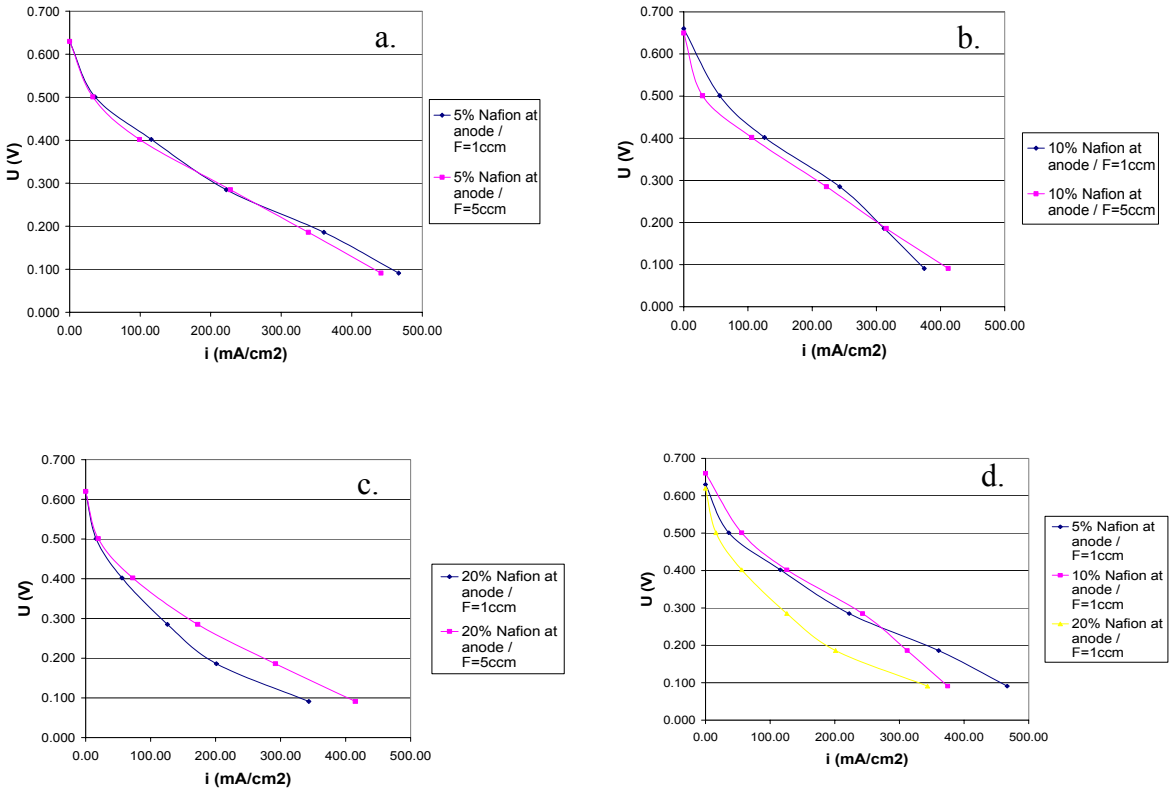

Figure 25: Effect of Nafion content at anode

(T = 80ºC, Anode catalyst: 4mg/cm^2 Pt/Ru black, Cathode catalyst: 1mg/cm^2 20%wt Pt/C, Cathode O_2 flow rate = 75sccm, $T_{humidifier}$ = 25ºC)

Nafion contained in electrodes helps to conduct protons to the membrane. A content of 10%wt was used previously according to [11]. That is why both a higher and lower Nafion content were tested, respectively 5wt% and 20wt%.

20wt% of Nafion at anode appears not to be a good option (Figure 25. d). 5 and 10wt% loading gave similar performance at high and medium voltage. However, at low cell voltage, the current drop was lower with a 5wt% Nafion loading.

Nafion creates hydrophilic paths in the catalytic layer, whereas carbon dioxide needs hydrophobic paths to diffuse through it. As seen above, CO_2 removal is an issue at low potentials and high current densities where a lot of CO_2 is formed. The decrease in Nafion loading could help its removal by decreasing porosity and thus increase methanol supply. An improved supply would result in higher performance, if it does not simultaneously increase methanol crossover.

It seems that the lower Nafion content could really enhance performance since when Nafion loading is increased (figures 25. a, b, and c) the effect of flow rate becomes more important. It means that for an increased loading the drop in CO_2 diffusion should be compensated by a higher flow rate.

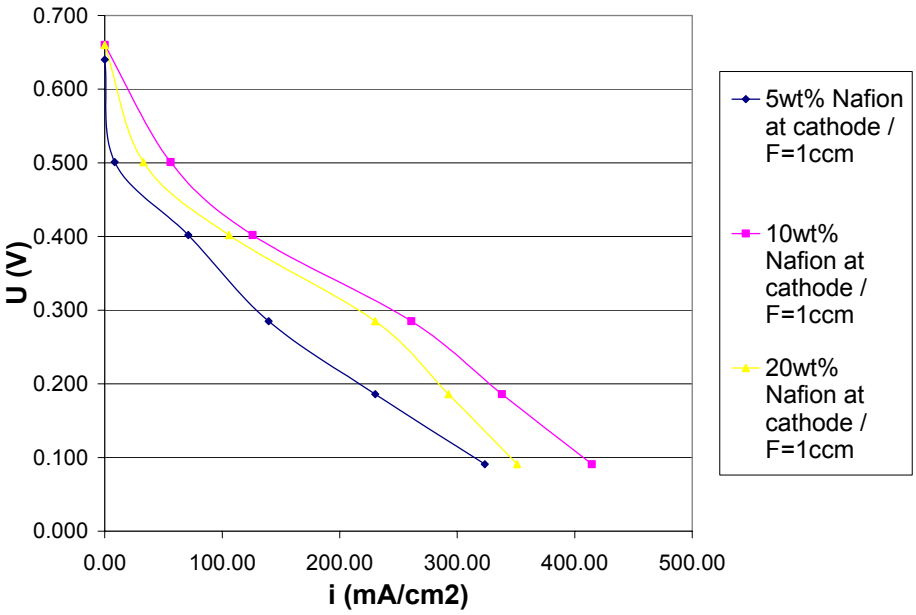

Figure 26: Effect of Nafion content at Cathode

(Anode catalyst: 4mg/cm^2 Pt/Ru black, Cathode catalyst: 4mg/cm^2 Pt black, Cathode O_2 flow rate = 75sccm, $T_{humidifier}$ = 25ºC)

A 10wt % Nafion loading at the cathode was the best choice (figure 26). 20wt% Nafion gave also good performance. However, 5wt% seemed to be a too low loading to properly carry protons to the active catalytic sites where they react. On the contrary, a too high Nafion loading certainly prevents oxygen which needs hydrophobic pores to diffuse easily to the catalytic layer.

b. Effect of PTFE

PTFE (Teflon) is used in hydrogen fuel cells in order to create hydrophobic paths to help gas diffusion through porous media. Thus, it was added to the cathode to help oxygen transfer to the catalytic layer. 5wt% is the amount that is usually used in hydrogen fuel cells.

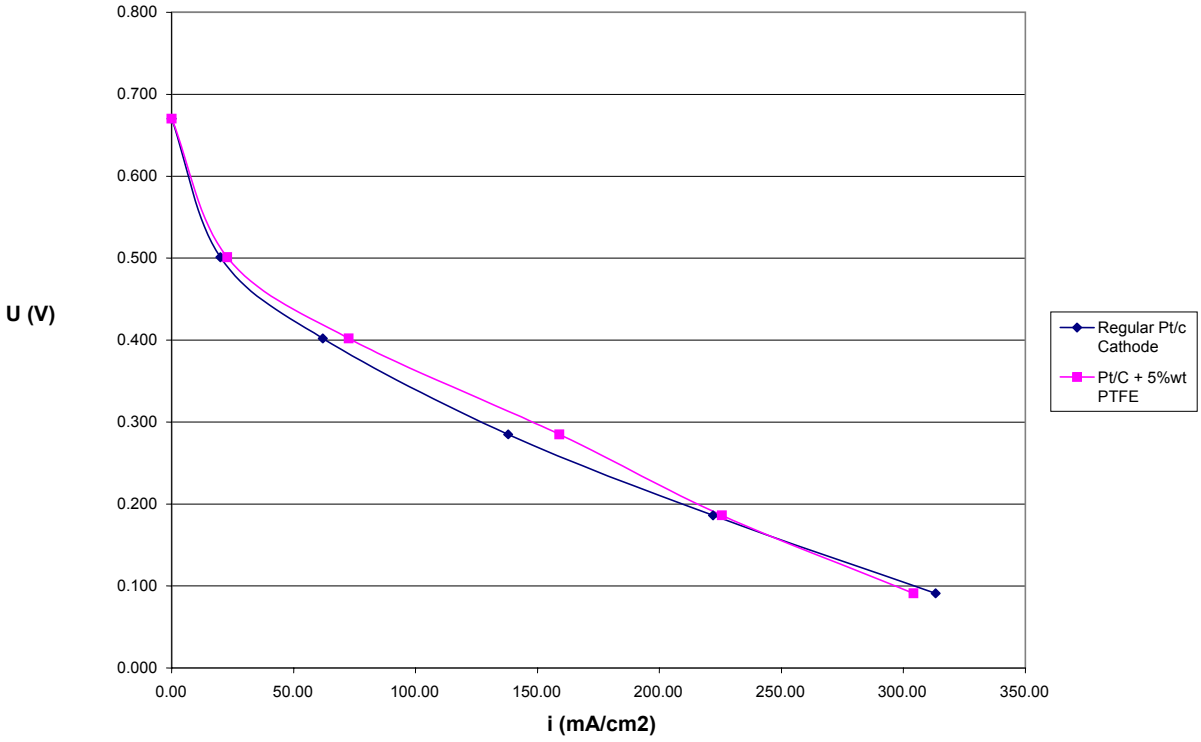

Figure 27: Effect of PTFE at the cathode

(T = 80 degree C, Anode catalyst: 4mg/cm^2 Pt/Ru black, Cathode: 1mg/cm^2 Pt/C, Anode flow rate = 1ccm, Cathode O_2 flow rate = 75sccm, $T_{humidifier}$ = 25ºC)

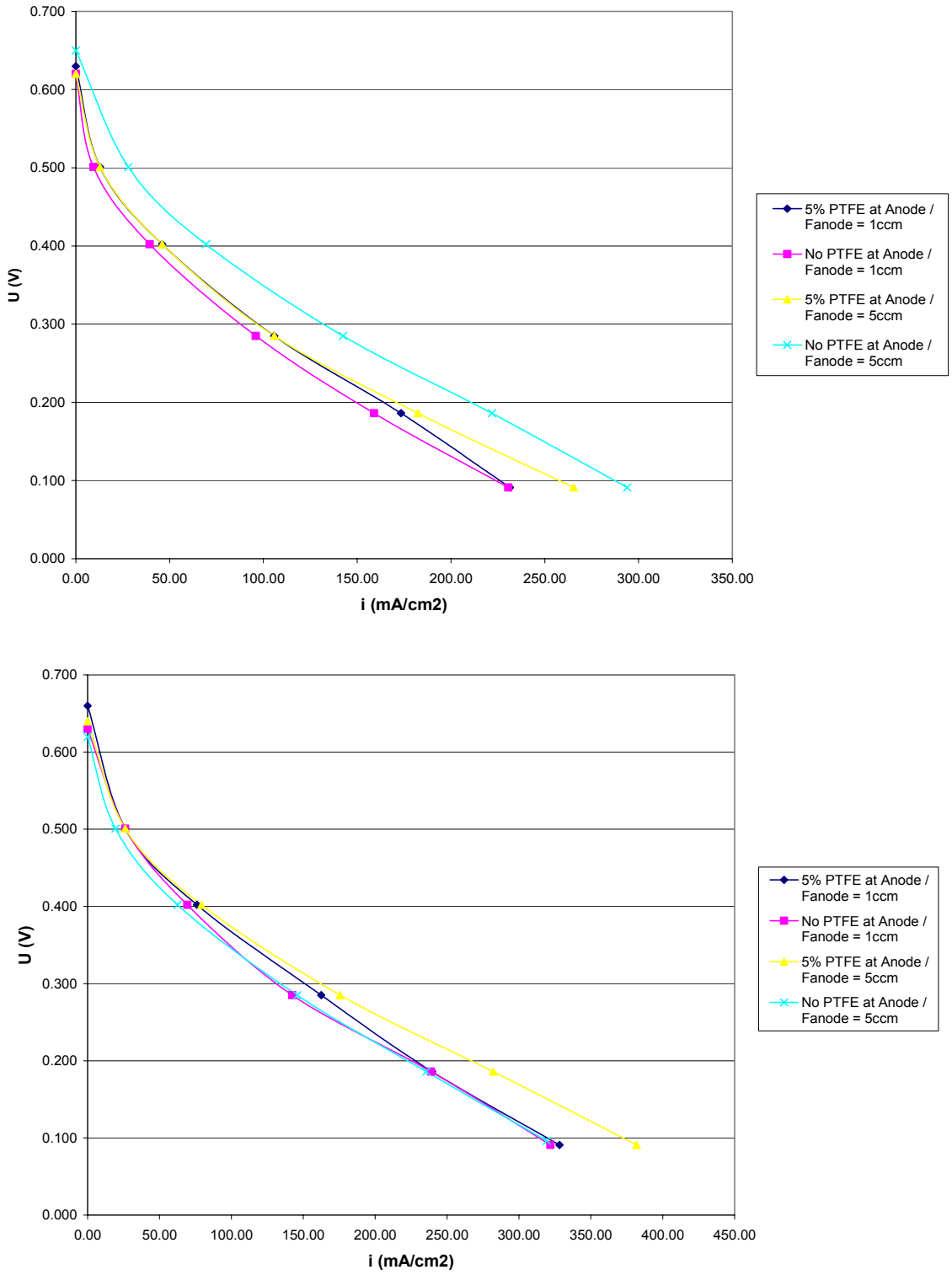

Figure 28: Effect of 5wt% of PTFE and flow rate at the Anode at T = 60ºCand T = 80ºC (Anode catalyst: 4mg/cm^2 Pt/Ru black, Cathode: 1mg/cm^2 Pt/C, Anode flow rate = 1ccm, Cathode O_2 flow rate = 75sccm, $T_{humidifier}$ = 25ºC [for both figures])

Thus, 5, 10 and 20wt% PTFE electrodes were tested. For cathode side, only the 5wt% electrode was investigated. Nafion loading remained 10wt% for each electrode.

Addition of PTFE does not have a great effect on the cell performance (Figure 27). Oxygen diffusion to the catalytic layer seems not to be a key issue for pure oxygen use on cathode.

Nordlund et al [16] also suggested that adding PTFE to the anode may make the morphology more favorable for carbon dioxide to evolve as a gas by creating the necessary pores. Thus PTFE may help carbon dioxide diffusion through the anode catalytic layer. The improved removal should also provide a better methanol supply to the catalyst.

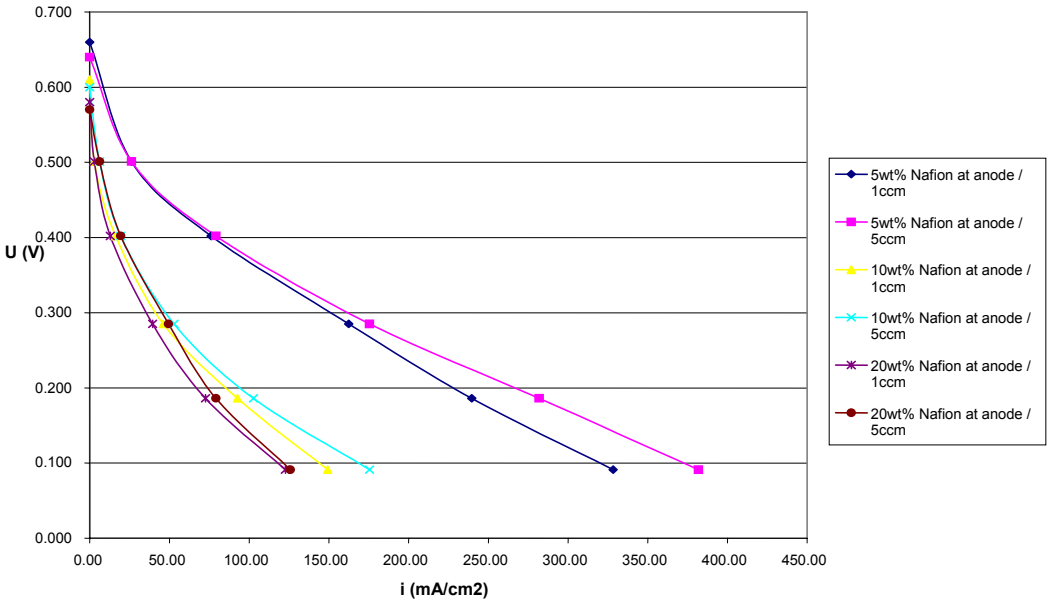

Figure 29: Effect of various PTFE content at the Anode (T=80ºC)
(Anode catalyst: 4mg/cm^2 Pt/Ru black, Cathode: 1mg/cm^2 Pt/C, Cathode O_2 flow rate = 75sccm, $T_{humidifier}$ = 25ºC)

For 5% PTFE at 60ºC, flow rate had no influence on performance except at very low cell voltage. So we could assume that methanol transfer to the anode was no longer a problem (Figure 28). However, better performance was obtained without PTFE but at a feed flow rate of 5ccm. At 80ºC, performance is slightly higher using 5% PTFE and the

difference becomes significant at low cell voltage for a feed flow rate of 5ccm (Figure 28). Kinetics is improved by temperature. Consequently, at 80ºC, more methanol is needed at the catalytic layer. PTFE and higher flow rate both have a beneficial effect.

For the anode, performances decreased with the PTFE loading (figure 29). The high concentration of hydrophobic pores apparently blocked methanol diffusion to the anode catalytic layer.

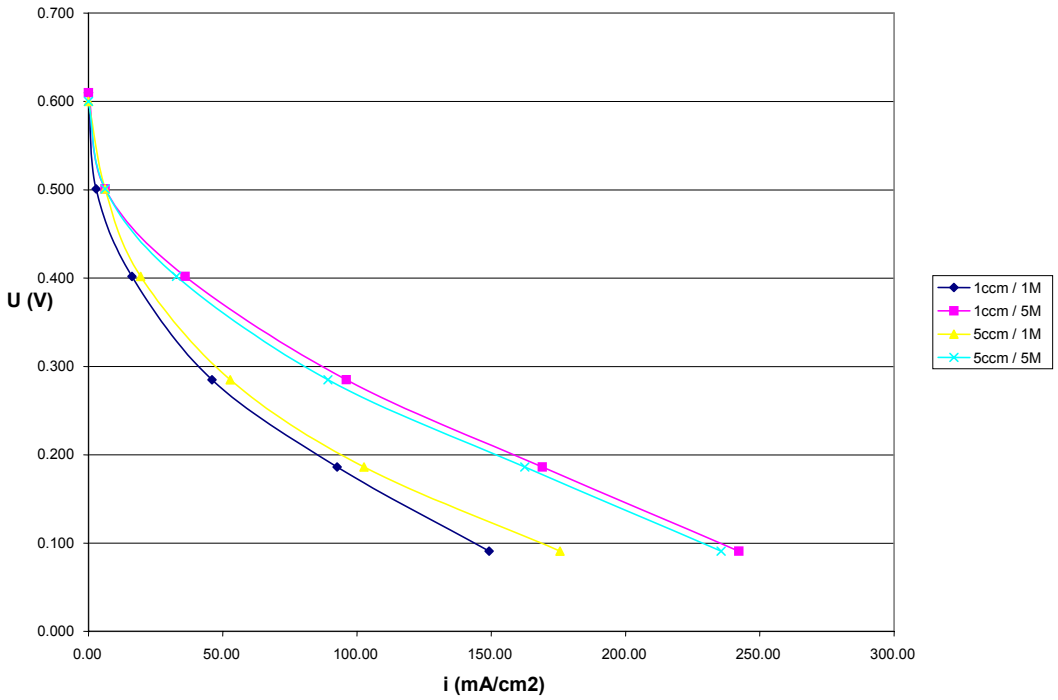

Figure 30: Effect of methanol concentration on a 20wt% PTFE at the Anode (T=80ºC) (Anode catalyst: 4mg/cm^2 Pt/Ru black, Cathode: 1mg/cm^2 Pt/C, Cathode O_2 flow rate = 75sccm, $T_{humidifier}$ = 25ºC)

Based on the idea that PTFE reduces methanol diffusion to the catalytic layer, a 20wt% PTFE anode was tested with both a 1 and 5 molar solution (figure 30). The 5 mol/L solution was able to compensate for the low methanol diffusion and give better results. However performance is still lower than that observed without PTFE. This result is interesting as it shows that good performance can be kept even when the cell is fed with a high methanol concentration with the use of PTFE treated anode.

4. Operation at higher methanol concentration with barrier layer

Operating the cell with a 1mol/L solution is not acceptable for transportation and portable applications, as too much water needs to be carried. However, performance drops quickly when concentration increases beyond this because of crossover.

This phenomenon can be limited using PTFE to increase electrode resistance to methanol diffusion. It might keep a constant anode catalytic layer concentration whatever the concentration of the feed stream is. This is possible to achieve if resistance and concentration gradient are well balanced. The goal is to get the same performance as when a regular Pt/Ru-Pt black MEA is fed with a 1mol/L solution of methanol. The polarization curve obtained for this MEA will be used a reference during the study.

Three ways to create a PTFE barrier come immediately to mind. The first and easier one is to spray directly PTFE solution on the top of an electrode. It may be more efficient than adding PTFE directly to the catalytic layer.

a. Effect of a PTFE solution sprayed on the top of the anode

0.2mL of PTFE solution was diluted in 1mL of ethanol before being sprayed on the 4mg/cm^2 Pt/Ru black electrode. The amount of PTFE was set at 10% of the weight of catalyst. The cathode catalyst was 4mg/cm^2 Pt black. Performance was extremely low and did not improve with higher methanol concentration. PTFE seems to have almost completely covered the carbon cloth surface and blocked methanol.

b. Effect of a PTFE solution sprayed between the electrode backing and the anode catalytic layer

The same solution as in the previous experiment was used.

Performance was slightly increased using PTFE with a 5mol/L solution (Figure 31). It is nevertheless far from what was hoped. The PTFE resistance is too high for a 5mol/L solution. It might have been expected that higher concentration may improve performance. However, with the 10wt % PTFE resistance layer the optimal feed concentration was 5mol/L. Beyond, performance dropped again.

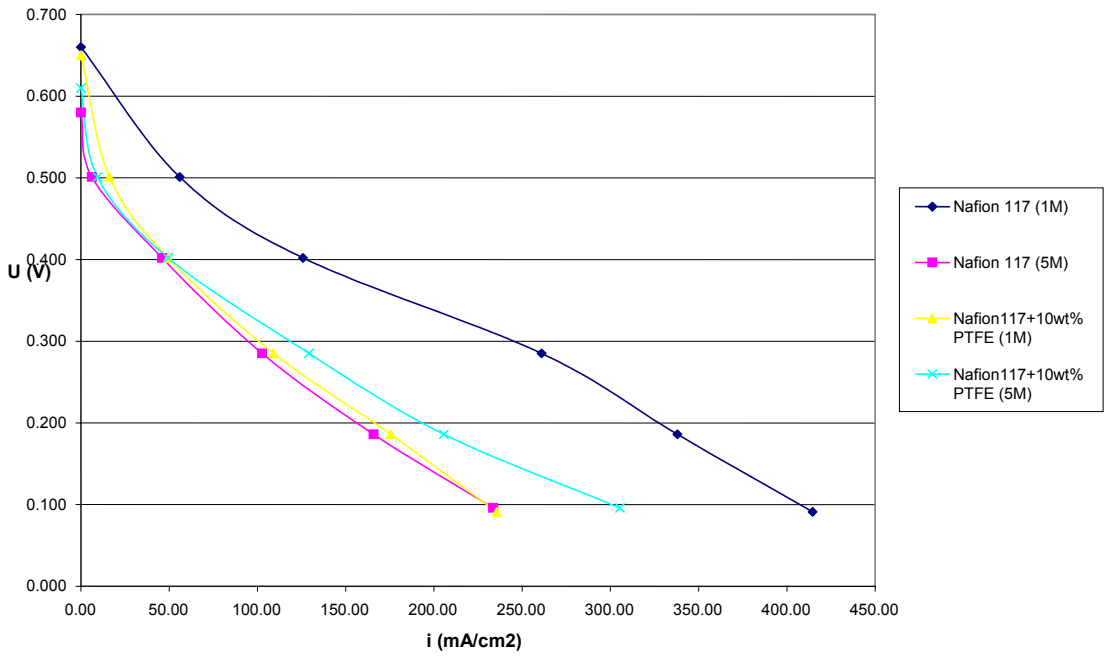

Figure 31: 10wt% PTFE resistance barrier at the Anode

(T = 80ºC, Anode catalyst: 4mg/cm^2 Pt/Ru black, Cathode: 4mg/cm^2 Pt black, Anode flow rate = 1ccm, Cathode O_2 flow rate = 75sccm, $T_{humidifier}$ = 25ºC)

c. Effect of a supported Pt/Ru resistance layer between the electrode backing and the catalytic layer

Having a fine control on methanol diffusion seems to be difficult when using a pure PTFE barrier. An option in creating a resistance layer is spraying a mixture of carbon powder and PTFE before the catalytic ink to create a resistance barrier. The thickness and PTFE loading of this layer are easier to control.

However, a 40% supported Pt/Ru on carbon was used instead of carbon powder because it was already available in the lab. Some methanol will adsorb on its surface and foul it. However, it should not affect the performance since the catalytic layer is still there for of the oxidation reaction. This layer has only to act as a barrier.

The resistance layer was designed to have half the thickness of the catalytic layer. Thus, 12mg of powder were sprayed of the 5cm^2 electrode. The PTFE content of the ink was adjusted at 10% of the weight of the supported Pt/Ru powder.

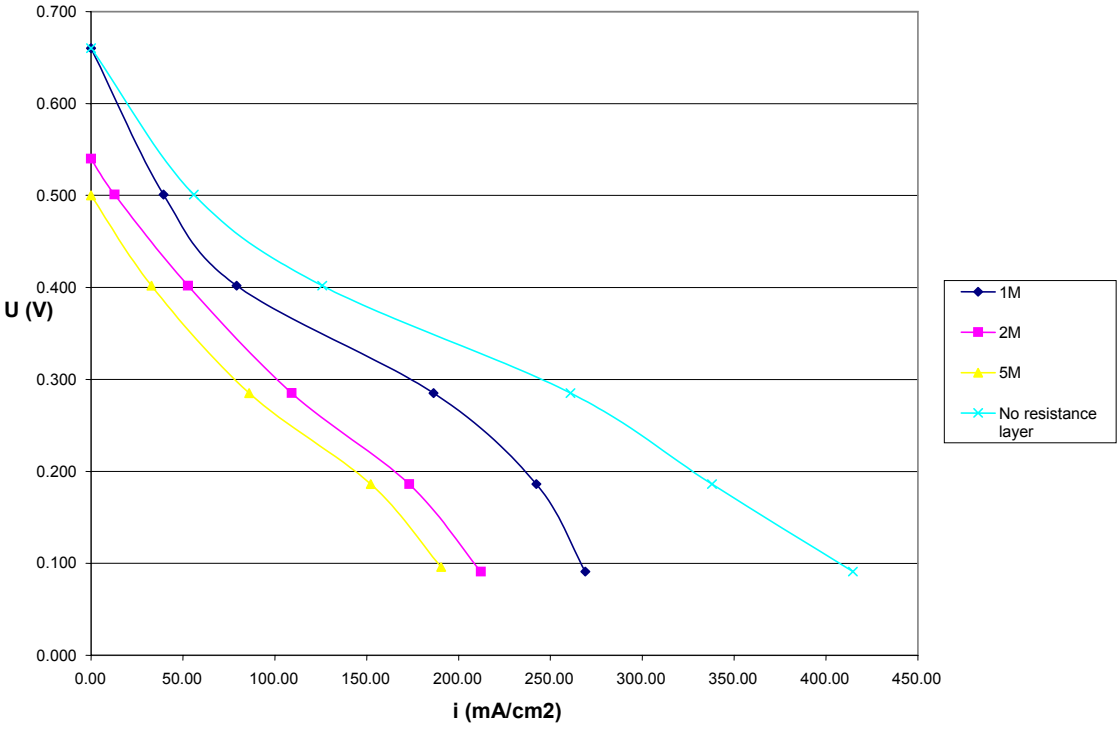

Figure 32: 10wt% PTFE resistance layer at the Anode

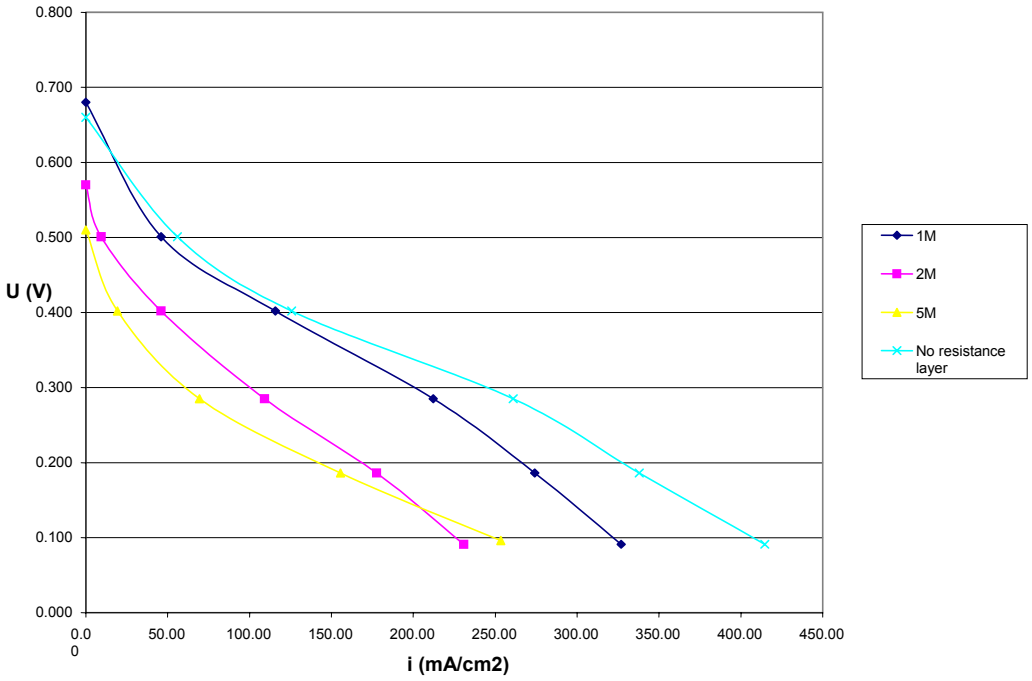

Figure 33: 20wt% PTFE resistance layer at the Anode

(T = 80ºC, Anode catalyst: 4mg/cm^2 Pt/Ru black, Cathode: 4mg/cm^2 Pt black, Anode flow rate = 1ccm, Cathode O_2 flow rate = 75sccm, $T_{humidifier}$ = 25ºC [for both figures])

Performance decreased with increasing concentration, however (Figure 32). Besides, it can be seen that the limiting current is decreased. Resistance is too low to operate at higher methanol concentration. However, it is still too high at 1mol/L to reach expected performance.

When PTFE loading is increased, performance is still decreased (Figure 33). However, higher current densities are obtained at low cell voltage for a 5mol/L concentration than for 2mol/L. It shows that, in this range of cell voltage where more methanol is consumed, a high concentration is needed to balance diffusion resistance. It also shows that diffusion does not have the same concentration dependence in all the cell voltage range.

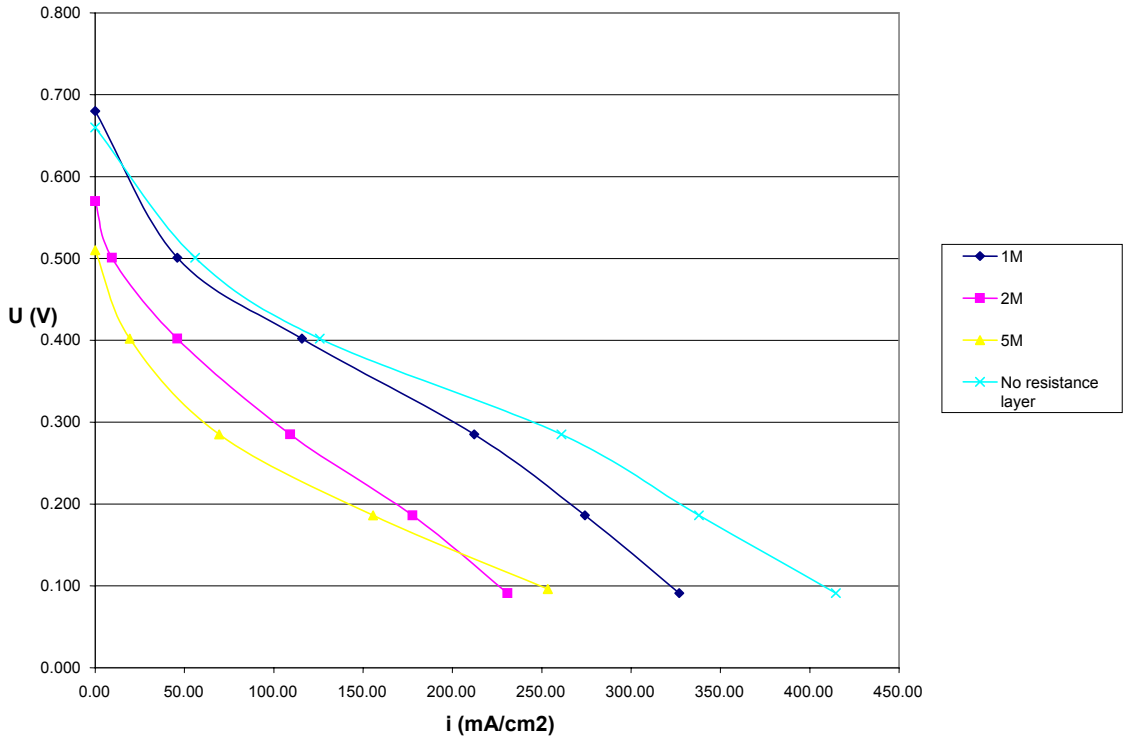

Figure 34: 10wt% PTFE / 10wt% NAFION resistance layer at the Anode
(T = 80ºC, Anode catalyst: 4mg/cm^2 Pt/Ru black, Cathode: 4mg/cm^2 Pt black, Anode flow rate = 1ccm, Cathode O_2 flow rate = 75sccm, $T_{humidifier}$ = 25ºC)

When Nafion is added to the resistance layer, performance is still decreased compared to regular electrodes but to a smaller extent (Figure 34). The polarization curve at 5mol/L is now below the 2mol/L one except at 0.1V. Adding Nafion promotes

methanol diffusion in the resistance layer and the high concentration has no longer a beneficial effect.

In all experiments including a resistance layer done with supported catalyst, performance was decreased when the flow rate was increased from 1ccm to 5ccm. Only in one case this phenomena was not observed. It was with the 10wt% PTFE/10wt% NAFION resistance layer at 5mol/L (Figure 35).

The explanation that can be given may be the following. At a high feed flow rate CO_2 concentration becomes less important in the feed channel. Consequently, more carbon dioxide can diffuse through the resistance layer and this flux may reduce block methanol. When PTFE is added this is not true anymore since methanol diffuses through specific hydrophilic pores. Its diffusion can thus be increased by the flow rate.

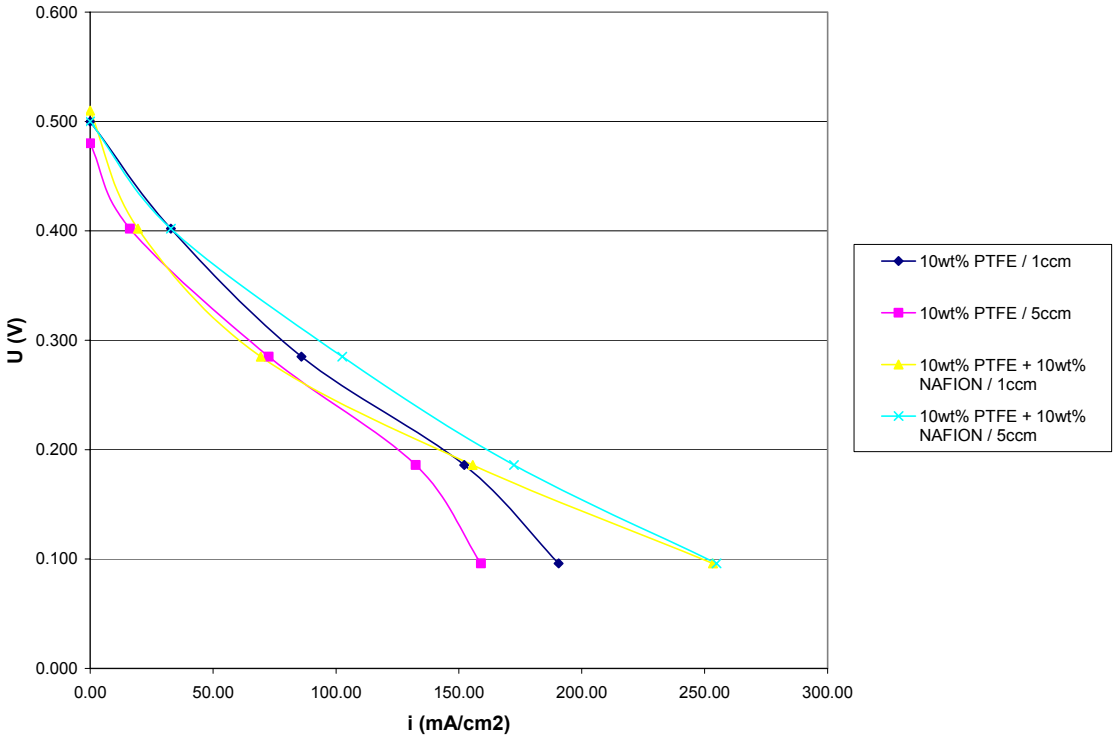

Figure 35: Effect of flow rate on the 10wt% PTFE and the 10wt% PTFE / 10wt% NAFION resistance layers at C_{MeOH} = 5M
(T = 80ºC, Anode catalyst: 4mg/cm^2 Pt/Ru black, Cathode: 4mg/cm^2 Pt black, Cathode O_2 flow rate = 75sccm, $T_{humidifier}$ = 25ºC)

d. Effect of the location of the supported catalyst on carbon resistance layer on cell performance

On the contrary to the study on PTFE loading, there is no need to find a compromise between methanol supply and CO_2 removal with a resistance layer. It can actually be placed directly in contact with the membrane either at anode side or at cathode side.

The 10wt% PTFE plus 10wt% Nafion was used again to prevent a high limitation of protons transfer.

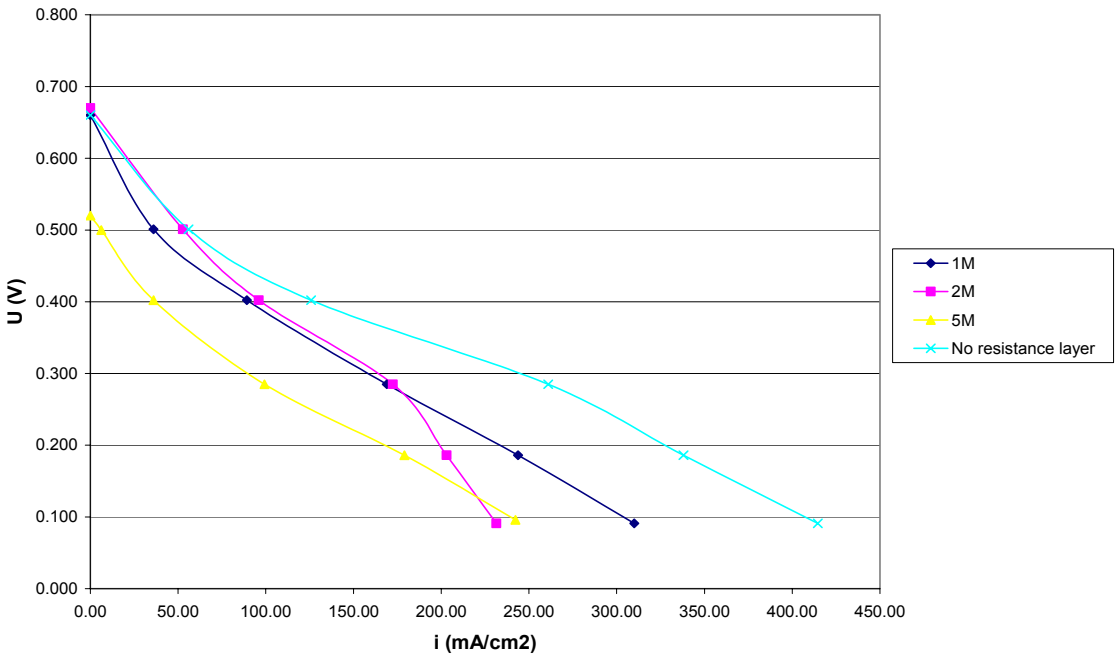

Figure 36: 10wt% PTFE / 10wt% NAFION resistance layer located between the anode catalytic layer and the membrane

(T = 80ºC, Anode catalyst: 4mg/cm^2 Pt/Ru black, Cathode: 4mg/cm^2 Pt black, Cathode O_2 flow rate = 75sccm, $T_{humidifier}$ = 25ºC)

When the resistance layer was located between the anode catalytic layer and the membrane, it was possible to get higher performance with a 2mol/L solution at high cell voltages (Figure 36). Between the open circuit cell voltage and 0.5V 1mol/L and 2mol/L solutions gave similar performance. On the contrary, performance dropped at low cell

voltages. The higher methanol concentration certainly promoted carbon dioxide formation because it disappeared when the feed flow rate was switched to 5ccm.When the resistance layer was located between the membrane and the cathode catalytic layer, performance was dramatically low (Figure 37). This location seems to seriously limit the transfer of protons to the cathode catalytic layer.

The double layer anode with a resistance barrier is definitely more suitable than the double layer cathode. The concept using higher methanol concentration with a resistance layer has not been proven to be very effective in this study. However, the idea is still interesting, and may reduce the amount of water that needs to be carried with the methanol fuel cell. It has however showed that performance could be improved in high cell voltage range which is the most interesting for practical applications.

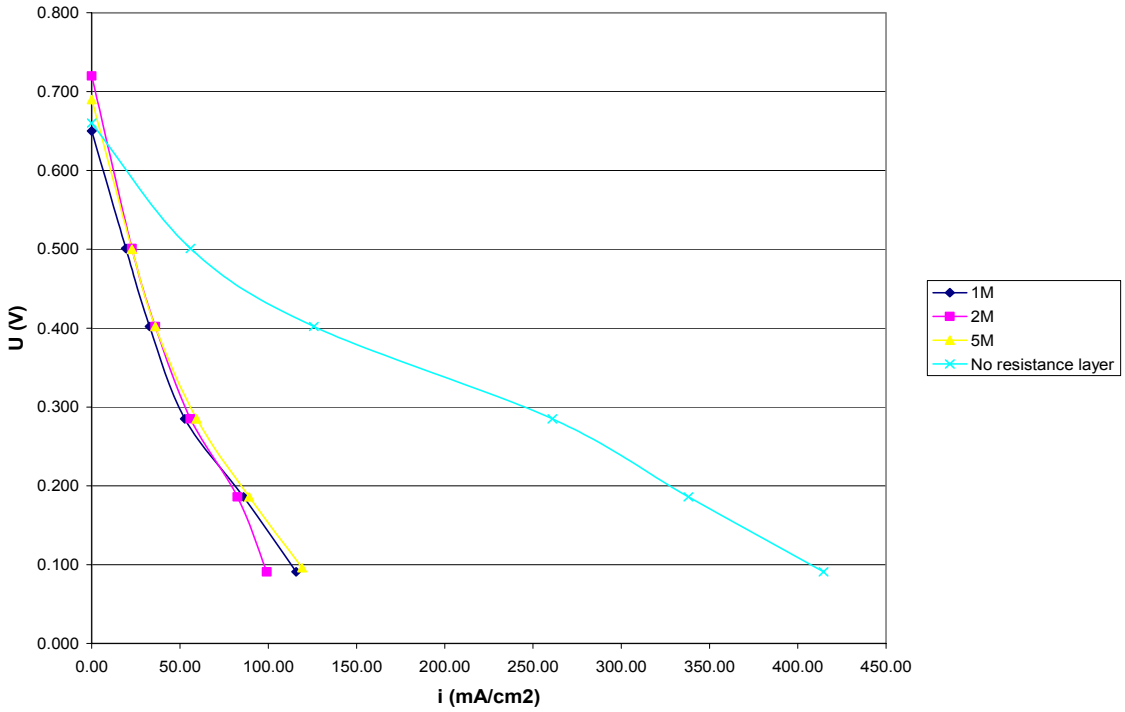

Figure 37: 10wt% PTFE / 10wt% NAFION resistance layer located between the membrane and the anode catalytic layer

(T = 80ºC, Anode catalyst: 4mg/cm^2 Pt/Ru black, Cathode: 4mg/cm^2 Pt black, Cathode O_2 flow rate = 75sccm, $T_{humidifier}$ = 25ºC)

Best performance was obtained when the resistance layer was located between the catalytic layer and the membrane on anode side. It is reasonable to think that it will remain true if the PTFE and Nafion loading as well as the layer thickness are changed. However, they certainly need to be refined to improve the previous results.

Besides, since the resistance to diffusion seems to vary with the cell voltage, the previous parameters may need to be adapted to a specific operating range.

5. Nano-composite membranes and methanol crossover

Membranes have a great effect on DMFC performance, especially their behavior toward methanol crossover. A compromise needs to be found between membrane proton conductivity and methanol diffusion.

Nano-composite membranes have shown low methanol permeability [18, 19] but have also a higher resistance to protons transfer. Consequently, thinner membranes with lower electrical resistance may be used to minimize crossover.

Different types and thickness of Nano-composite membranes were tested. MEAs were prepared with 117 and 112 membranes and 4mg/cm^2 Pt/Ru black and 1mg/cm^2 20wt% Pt/C electrodes. The anode feed flow rate was set at 5ccm to prevent oscillations. The methanol concentration was kept at 1mol/L unless the effect of concentration itself was tested.

The membranes contained roughly of 5wt% zirconia.

a. 117 membranes

Polarization curves were plotted for both Nafion and Nano-composite 117 membranes at 60ºC and 80ºC.

At an anode feed flow rate of 5ccm the Nano-composite membrane performance was close to that for Nafion (Figures 38 and 39) for both 60ºC and 80ºC. It even dropped at high current densities.

However, it could have been expected that at higher flow rate, the positive effect of higher methanol diffusion to the anode catalytic layer wouldn't be suppressed by crossover. This assumption was not valid as it lowered performance.

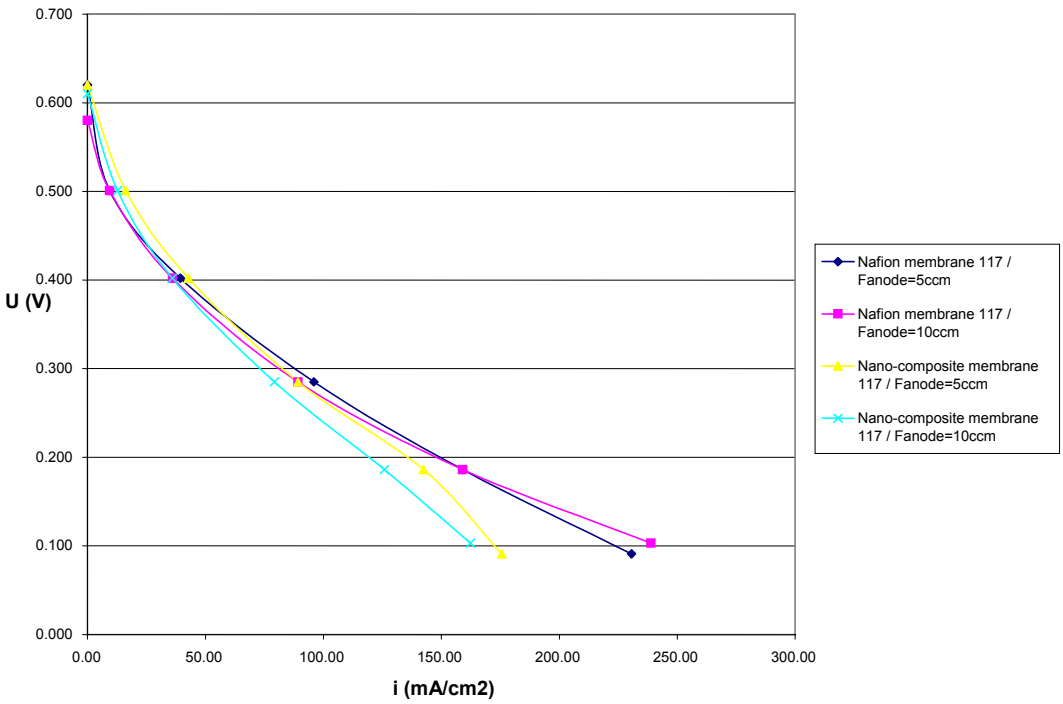

Figure 38: Effect of 117 a Nano-composite membrane on the cell performance at 60ºC

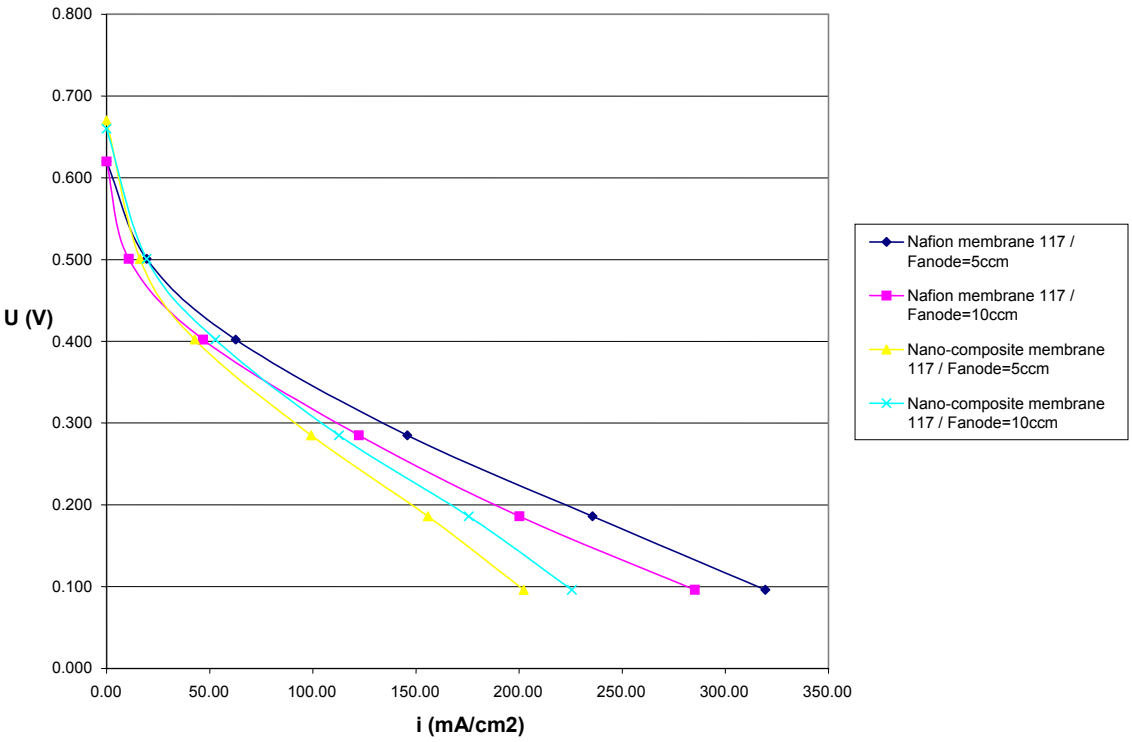

Figure 39: Effect of 117 a Nano-composite membrane on the cell performance at 80ºC (Anode catalyst: 4mg/cm^2 Pt/Ru black, Cathode catalyst: 1mg/cm^2 20wt% Pt/C, Cathode O_2 flow rate = 75sccm, $T_{humidifier}$ = 25ºC[for both figures])

The same behavior was observed at higher methanol concentration (5M) (Figure 40). It seems that even if methanol crossover is reduced with 117 Nano-composite membranes, proton conductivity becomes too low to increase performance.

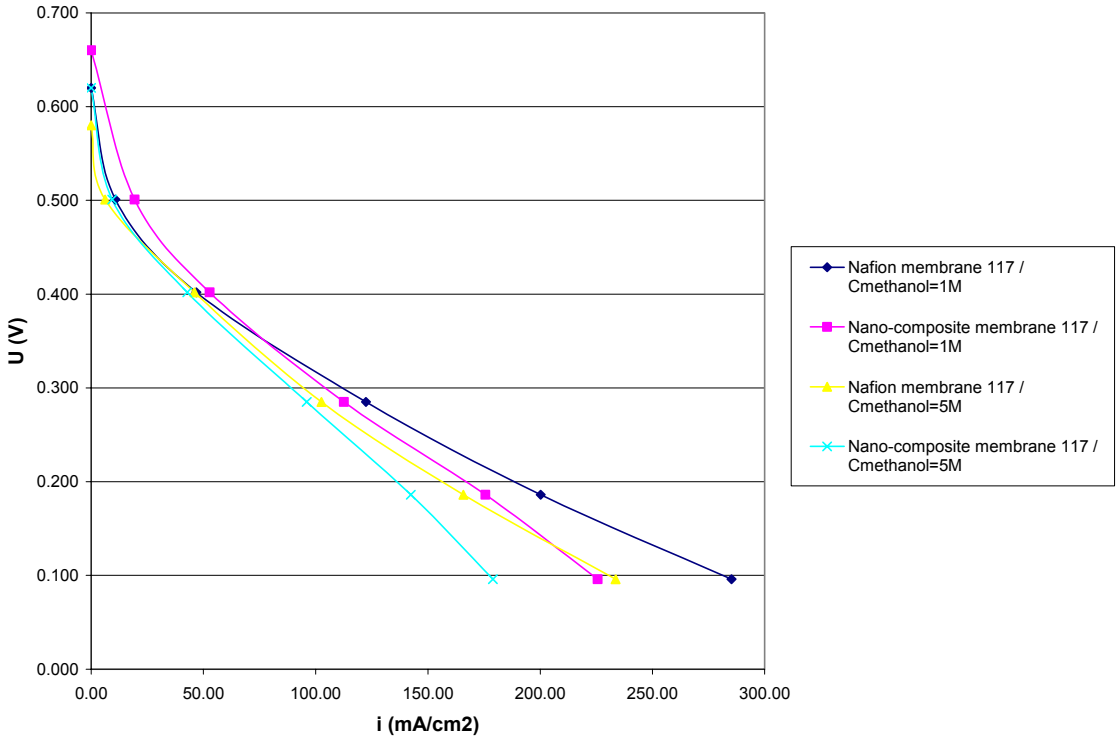

Figure 40: Effect of methanol concentration on a 117 Nano-composite membrane at 80ºC

(Anode catalyst: 4mg/cm^2 Pt/Ru black, Cathode catalyst: 1mg/cm^2 20wt% Pt/C, Anode flow rate 5ccm, Cathode flow rate = 75sccm, $T_{humidifier}$ = 25ºC)

b. 112 membranes

Different Nano-composite membranes were tested. A zirconia, two mixed zirconia-silica and a silica membrane. The amount of silica was 2wt% for the first mixed membrane (Zr/Si1) and for the silica nano-composite membrane. It was slightly increased for the second mixed membrane (Zr/Si2).

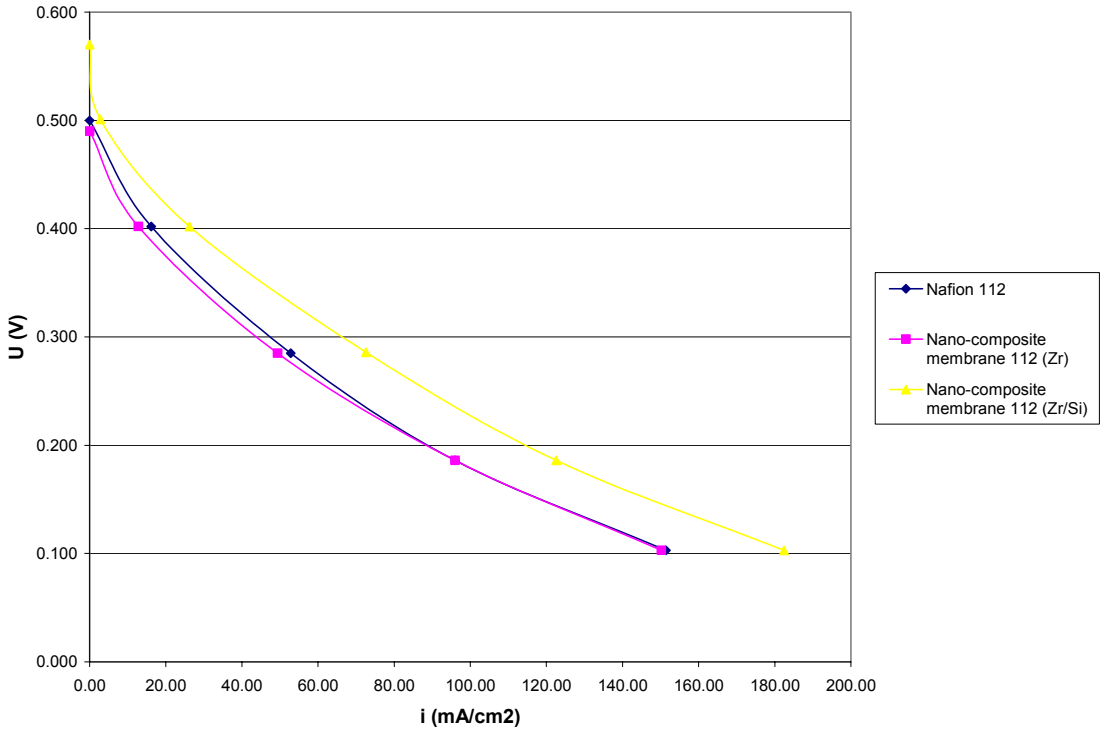

Figure 41: Effect of 112 Nano-composite membranes on the cell performance at 60ºC

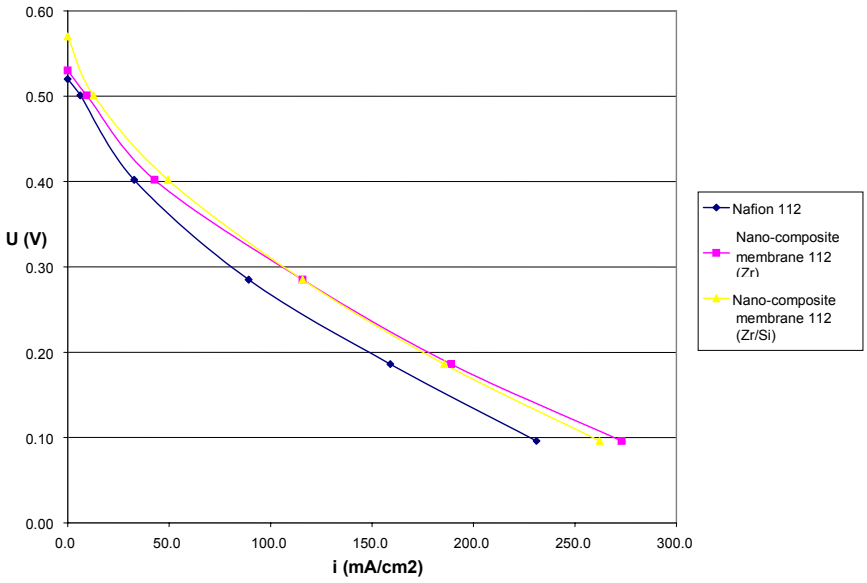

Figure 42: Effect of 112 Nano-composite membranes at 80ºC

(Anode catalyst: 4mg/cm^2 Pt/Ru black, Cathode catalyst: 1mg/cm^2 20wt% Pt/C, Cathode O_2 flow rate = 75sccm, $T_{humidifier}$ = 25ºC[for both Figures])

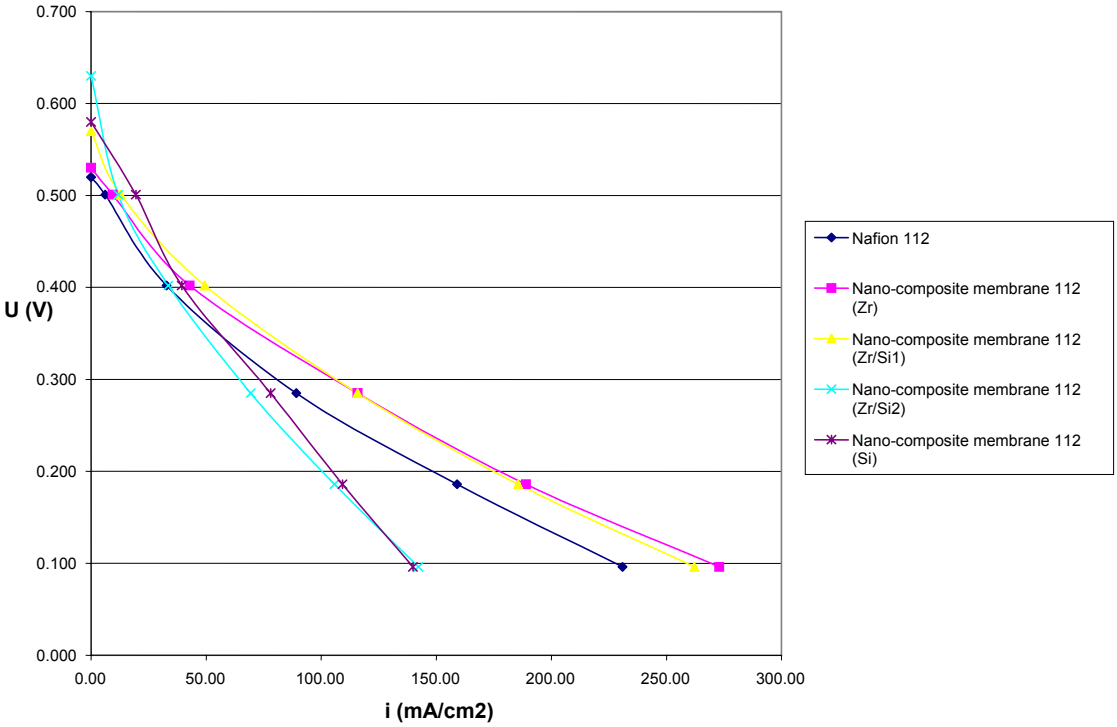

Figure 43: Effect of various 112 Nano-composite membranes at 80ºC

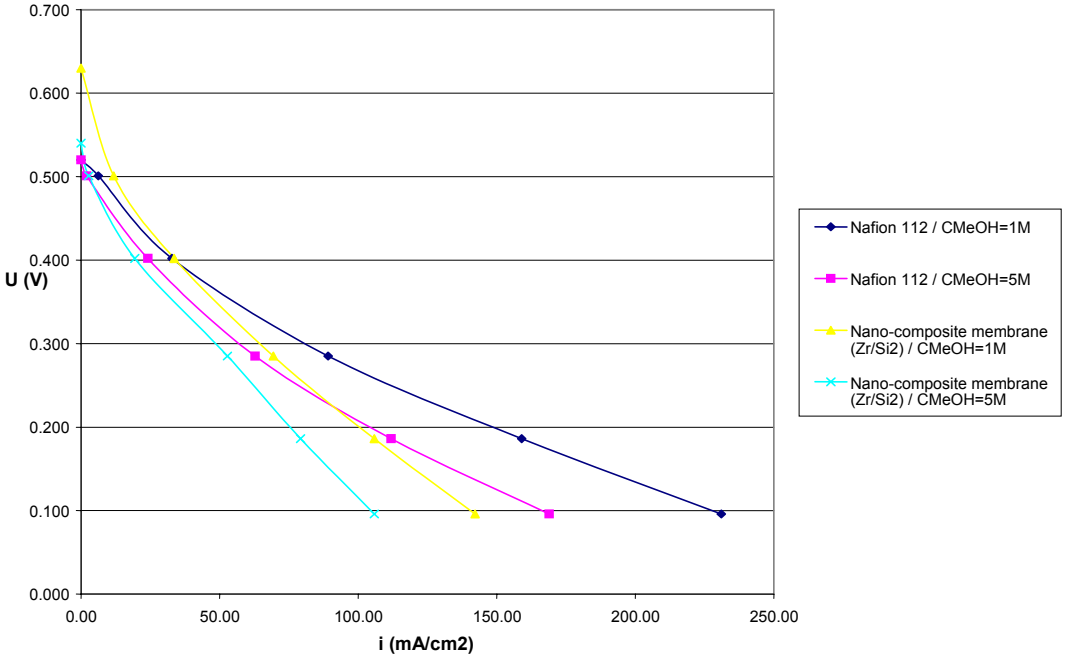

Figure 44: Effect of methanol concentration on the Zr/Si2 112 Nano-composite membrane on the cell performance at 80ºC

(Anode catalyst: 4mg/cm^2 Pt/Ru black, Cathode catalyst: 1mg/cm^2 20wt% Pt/C, Cathode flow rate = 75sccm, $T_{humidifier}$ = 25ºC)

The mixed Zr/Si membrane showed better performance than Nafion at 60ºC (Figure 41) whereas the pure Zr membranes had similar performance. At 80ºC, things have changed, however. Both Zr and Zr/Si membranes showed better performance (Figure 42).

Both proton conductivity and crossover becomes higher than in 112 membranes than in 117 membranes. In this case, proton conductivity becomes sufficient and crossover reduction becomes significant. That must be the reason for higher performance. Besides, the loading of inorganics affects the performance.

An increased silica loading has an undesirable effect on performance (Figure 43). Zirconia seems to be more suitable for low methanol permeation membranes than silica.

A higher methanol concentration had a negative effect on performance (Figure 44). Even if crossover is reduced at 1mol/L, the resistance to diffusion is not high enough.

6. Overall conclusions

Best performance was obtained for anode and cathode made respectively of 4mg/cm^2 Pt/Ru black and 4mg/cm^2 Pt black. The improvement due to other parameters depend on the operating conditions. It has been seen that Nafion and PTFE loading can enhance performance either at low or high current densities. However, it was not possible to optimize both at the same time.

The most important conclusion that can be drawn is that carbon dioxide formation is a great issue in Direct Methanol Fuel Cells. Even though it is possible to get rid of the oscillations by increasing the flow rate, CO_2 still has a dramatic effect on the performance. That is why both electrode and bipolar plates should be designed for effective carbon dioxide removal.

- Electrode optimization:

According to Lindermeir et al [7], catalyst particle size should be as small as possible to optimize the active area. Agglomeration was reduced by sonication to keep a small particle size and a narrow size distribution.

The hardest part is to control Nafion and PTFE structure in the catalytic layer. The effect of loading was studied but it seems that structure was not optimized. Always,

according to Lindermeir et al [7], a homogenous distribution of both hydrophilic and hydrophobic pores is desirable. Small and homogeneously spread hydrophilic pores will help to increase the number of efficient catalytic sites.

Hydrophobic pores will have an effect on CO_2 bubble formation and removal. Wide pores will remove a large amount of carbon dioxide but also form large bubbles. These bubbles will form slugs in the feed channel and lower performance. Thus, small pores may be more efficient in the sense that they may form many small bubbles and hopefully create a bubble flow instead of slug flow in bipolar plate feed channel. Escribano and Aldebert [17] used with success a sintering treatment to enhance PTFE structure in the catalytic layer. They heated the electrode at 335ºC for 2h (melting point of PTFE: 327ºC). PTFE melts and distributes to create a uniform distribution of hydrophobic pores. This treatment was applied to a 10wt% PTFE Pt/Ru black anode and was found to have no effect. However, it does not mean that this treatment is not working. The mesh of carbon fibers in the carbon cloth is not fine enough and creates macro pores. It is suspected that those pores concentrate carbon dioxide into large diameter bubbles. Consequently, the beneficial effect of the sintering treatment may not be seen in carbon cloth.

The structure of the electrode backing used has an important role to play. A different type of carbon cloth may have a beneficial effect, especially if it has no macro pores. The previous ideas about the effect of PTFE should also be used to investigate more the utilization of a resistance layer. Investigating the effect of such parameters as NAFION and PTFE loading and layer thickness may be useful to understand where and under which operating conditions the resistance layer could be efficient.

- Bipolar plates optimization:

The goal is to keep a uniform methanol flow in the feed channel. The drawback of the single serpentine flow-field used is that CO_2 accumulates along the channel. It was compared to parallel flow-field by Yang and Zhao [10], in which removal of bubbles by buoyancy is too slow. A solution consists either of pin flow bipolar plates (bubbles are immediately dragged to the outlet by the flow) or a new design. This is nevertheless an important factor in improving performance.

- Nano-composite membranes:

The nano-composite membranes showed they are able to reduce crossover and thus improve perfromance. This reduction is nevertheless effective only with 112 membranes. It means that nano-composite membranes would be suitable for DMFC only if the resistance to methanol diffusion can be increased without decreasing proton conductivity. Investigation can be done on the preparation mode and other inorganics should also be tested. According to James M. Fenton [20], such membranes can also be combined with Nafion membranes to form a trilayer membrane. It would help to reduce the thickness of the nano-composite membrane while the mechanic properties are kept constant. This would nevertheless be efficient only if the resistance of nano-composite membranes to methanol diffusion is increased.

V. Dynamic modeling of the DMFC

A dynamic model was developed to model the evolution of the cell performance with time (anode and cathode potential, adsorbed species coverage and cell current) for a fixed cell voltage. This model was subsequently used to calculate the cell current density at steady state for various cell voltages to obtain the polarization curve.

1. Reaction mechanism for methanol oxidation

This model was mainly based on the one used by Sundmacher et al [11].

The methanol oxidation mechanism used is the following:

(1): $CH_3OH + 3Pt \leftrightarrows Pt_3\text{-}COH + 3H^+ + 3e^-$

(2): $H_2O + Ru \leftrightarrows Ru\text{-}OH + H^+ + e^-$

(3): $Pt_3\text{-}COH + 2Ru\text{-}OH \leftrightarrows Pt\text{-}COOH + H_2O + 2Pt + 2Ru$

(4): $Pt\text{-}COOH + Ru\text{-}OH \leftrightarrows CO_2 + H_2O + Pt + Ru$

The overall oxygen reduction reaction used is the following:

The assumption is made that water is only adsorbed on ruthenium sites whereas methanol and its oxidation products can only be found on platinum sites.

(c): $3/2\ O_2 + 6H^+ + 6e^- \leftrightarrows 3H2O$

- Reaction rates:

$$r_1 = k_1 \exp\left(\frac{\alpha_1 F}{RT}\eta_A\right)\left(\theta_{Pt}^3 C_{CH_3OH} - \frac{1}{K_1}\exp\left(-\frac{F}{R.T}\eta_A\right)\theta_{Pt_3-COH}\right)$$

$$r_2 = k_2 \exp\left(\frac{\alpha_2 F}{RT}\eta_A\right)\left(\theta_{Ru} - \frac{1}{K_1}\exp\left(-\frac{F}{R.T}\eta_A\right)\theta_{Ru-OH}\right)$$

$$r_3 = k_3\left(\theta_{Pt_3-COH}\theta_{Ru-OH}^2 - \frac{1}{K_3}\theta_{Pt-COOH}\theta_{Pt}^2.\theta_{Ru}^2\right)$$

$$r_4 = k_4\left(\theta_{Pt-COOH}\theta_{RuOH}\right)$$

Both reaction 4 and the oxygen reduction reaction were considered as irreversible.

$$r_C = k_C \exp\left(\frac{\alpha_C F}{RT}\eta_C\right)\left(1 - \exp\left(-\frac{F}{RT}\eta_C\right)\left(\frac{P_{O_2}}{P_\theta}\right)^{\frac{3}{2}}\right)$$

2. Material balance on anode side

Six differential equations are needed to describe the system. The first one gives the rate of variation of methanol concentration in the anode compartment assumed to be well mixed. Three more equations are needed for the coverage of adsorbed species and two for the anodic and the cathodic over potentials.

The methanol solution in the feed channel was considered to be in direct contact with the catalytic layer although we know that at high current density this is not so due to back diffusion of CO_2. It is necessary to consider losses of methanol due to crossover. The flux of methanol through the membrane is written: N_{CH3OH}.

(a) $$\frac{dC_{CH3OH}}{dt} = \frac{1}{\tau}\left(C_{CH3OH}^F - C_{CH3OH}\right) - \frac{A_S}{V}N_{CH3OH} - \frac{A_S}{V}r_1$$

(b) $$\frac{d\theta_{Pt_3-COH}}{dt} = \frac{1}{\gamma C_t^*}\left(r_1 - r_3\right)$$

(c) $$\frac{d\theta_{Ru-OH}}{dt} = \frac{1}{\gamma C_t^*}\left(3r_2 - 2r_3 - r_4\right)$$

(d) $$\frac{d\theta_{Pt-COOH}}{dt} = \frac{1}{\gamma C_t^*}\left(r_3 - r_4\right)$$

(e) $$\frac{d\eta_A}{dt} = \frac{1}{C_a}\left(i_{Cell} - F\left(3r_1 + 3r_2\right)\right)$$

(f) $$\frac{d\eta_c}{dt} = \frac{1}{C_c}\left(-i_{Cell} - 6F\left(r_5 + N_{CH3OH}\right)\right)$$

Where: $\tau = \frac{V}{Q}$

This system can be solved if we have an expression for the methanol crossover flux. Methanol is transported through the membrane by convection and diffusion.

$N_{CH3OH} = -D^{M}_{CH3OH} \frac{dC^{M}_{CH3OH}}{dz} + C^{M}_{CH3OH} v$ where v is the convective flow velocity.

Sundmacher et al [1] gives an expression for v. It was deduced from Schlogl's expression for v and the Nernst-Plank equation for proton transport through the membrane:

$$v = \frac{k_\phi}{\mu} \cdot \left[\frac{\frac{i_{Cell}}{F} + C^{M}_{H^+} \cdot \frac{k_P}{\mu} \cdot \frac{dP}{dz}}{\frac{D^{M}_{H^+}}{R.T} + C^{M}_{H^+} \cdot \frac{k_\phi}{\mu}} \right] - \frac{k_P}{\mu} \cdot \frac{dP}{dz} \qquad \text{where} \quad \frac{dP}{dz} = \frac{P_A - P_C}{d^M}$$

Knowing an expression for v, the previous equation can be solved analytically.

$$N_{CH3OH} = \frac{D^{M}_{CH3OH}}{d^M} . C_{CH3OH} \cdot \frac{Pe . \exp(Pe)}{\exp(Pe) - 1} \qquad \text{where} \quad Pe = \frac{v . d^M}{D^{M}_{CH3OH}} \text{ is the Peclet number}$$

A code was written on Matlab (See Appendix) to solve these equations in which operating conditions were given. To be consistent with experimental data, this code computes the cell current density for a given cell voltage. In order to do this, the current density should be expressed as a function of the cell voltage and anode and cathode over potential.

$$i_{Cell} = -\frac{\kappa^M}{d^M} \left(U - U^0 + \eta_A - \eta_C \right)$$

3. Simulation

a. Initial conditions and parameters

The code was used the model the cell current density for a cell working under the following conditions:

T = 353K $\qquad$ Q = 1ccm = 1.67.10-8 m3/s

C_{CH3OH} = 1000 mol/m3 $\qquad$ P_A = 101325 Pa

P_C = 101325 Pa

Rate constants are unknown as well as double layer capacitance. They were guessed by trial and error. First, calculations were done with values provided by Sundmacher et al. These parameters are valid at 80ºC. Consequently this model can only be used at this temperature or else new fitted parameters need to be found.

$V = 2.10^{-7}$ m^3	Q = 1ccm = 1.67.10-8 m3/s
T = 353K	$A_S = 5.10^{-4}$m^2
γ = 100	$C_t^* = 2.2.10^{-5}$ mol/m^2
$C_A = 4.10^5$ F/ m^2	$C_C = 8.10^5$ F/ m^2
α_1 = 0.5	α_2 = 0.5
α_C = 0.5	F = 96485
R = 8.314 J/mol.K	$C^{M}{}_{H^+}$ = 1200 mol/m^3
$D^{M}{}_{H^+} = 5.4.10^{-9}$ m^2/s	$k_P = 1.57.10^{-18}$ m^2
$k\Phi = 1.13.10^{-19}$ m^2	$\mu = 3.353.10^{-4}$ kg/m.s
U^0 = 1.21V	κ^M = 17 Ω^{-1}.m^{-1}

Table 1: Parameter values employed in the model

The following initial conditions have been used:

C_{CH3OH} = 1000 mol/m3 $\qquad$ $\Theta_{Pt3\text{-}COH}$ = 0

$\Theta_{Ru\text{-}OH}$ = 0 $\qquad$ $\Theta_{Pt\text{-}COOH}$ = 0

η_A = 0 V $\qquad$ η_C = 0 V

$C_A = 4.10^5$ F/ m^2	$C_C = 8.10^5$ F/ m^2
$K_1 = 1$ mol/m^2.s	$K_2 = 1.10^{-5}$. mol/m^2.s
$K_3 = 1$ mol/m^2.s	$k_1 = 4.10^{-9}$ mol/m^2.s
$k_2 = 1$ mol/m^2.s	$k_3 = 1.10^{-2}$ mol/m^2.s
$k_4 = 1$ mol/m^2.s	$k_C = 1.10^{-2}$ mol/m^2.s

Table 2: Fitted parameter values

b. Search of fitting parameters

At a given potential, the calculated current density didn't fit experimental data. Thus, the code was modified to draw the polarization curve and find the fitted constants. In order to do that, the current density was calculated for fixed potential between 0.1V and 0.5V with a step of 0.1V.

The MEA used to do the comparison with experimental was made with 4mg/cm^2 Pt/Ru and 4mg/cm^2 Pt black electrodes and a 117 Nafion membrane. It was tested at 80ºC and an anode feed flow rate of 5ccm. As the model does not take count on the formation of CO_2, results should be more meaningful at high flow rate. It had no effect on the model in which calculations are done for a feed flow rate of 1ccm. It was indeed shown that small changes in feed flow rate do not affect the results. Besides, current density was taken at t = 100s as dynamic evolution showed that steady state is reached after about 60s (Figure 45, 46, 47).

The fitted rate constants are:

$k_1 = 6.10^{-12}$ mol/m^2.s
$k_2 = 1.10^{-2}$ mol/m^2.s
$k_3 = 1.6.10^{-2}$ mol/m^2.s
$k_4 = 4.10^{-2}$ mol/m^2.s

Only rate constants had to be modified. They are all smaller by two orders of magnitude.

The shape of the polarization curve depends almost only on the rate constant of methanol decomposition (k_1). It confirms the assumption made by Sundmacher et al [11] that decomposition was the rate limiting step.

Knowing acceptable rate constants, the code was run in dynamic mode.

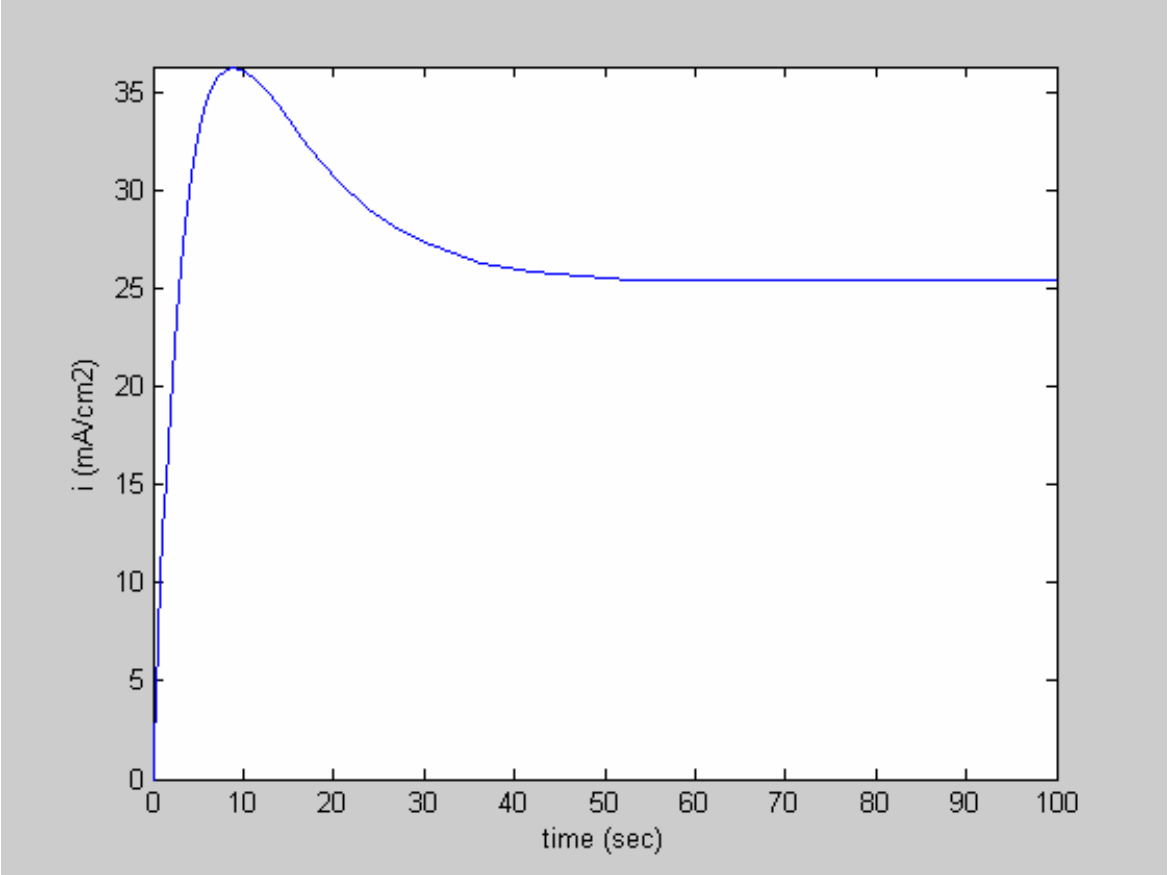

Figure 45: Current density as a function of time at U = 0.5V for a 117 Nafion membrane at 80ºC with F_{anode} = 1ccm, C_{CH3OH} = 1M and P_C = 0atm (rel.)

These results show that using current density at t = 100s was a good assumption. Whatever the cell voltage is, steady state is always reached after about 1 min.

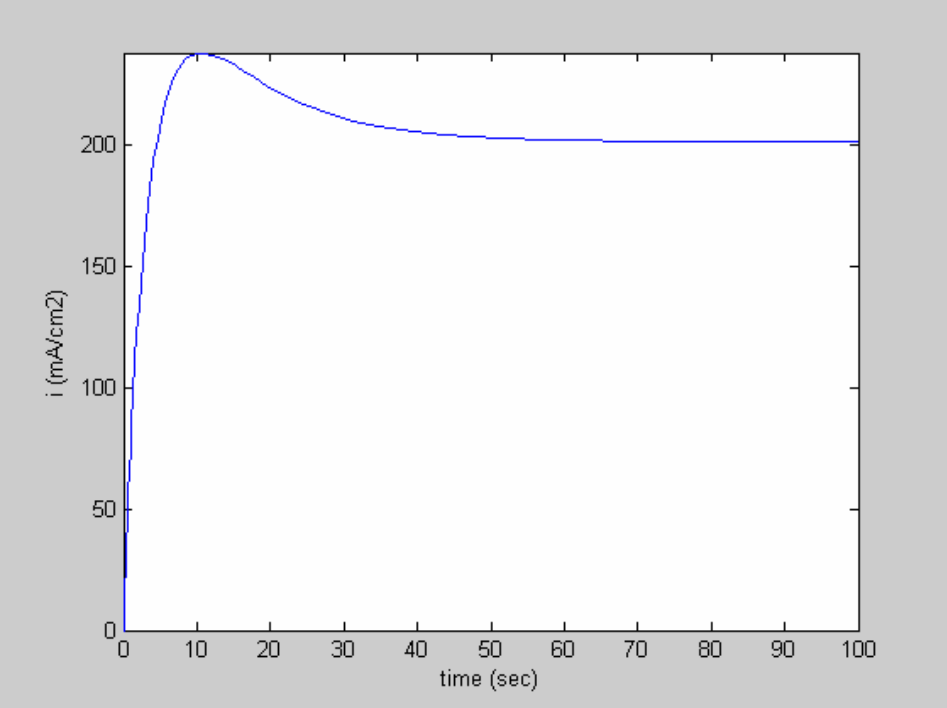

Figure 46: Current density as a function of time at U = 0.3V for a 117 Nafion membrane at 80ºC with F_{anode} = 1ccm, C_{CH3OH} = 1M and P_C = 0atm (rel.)

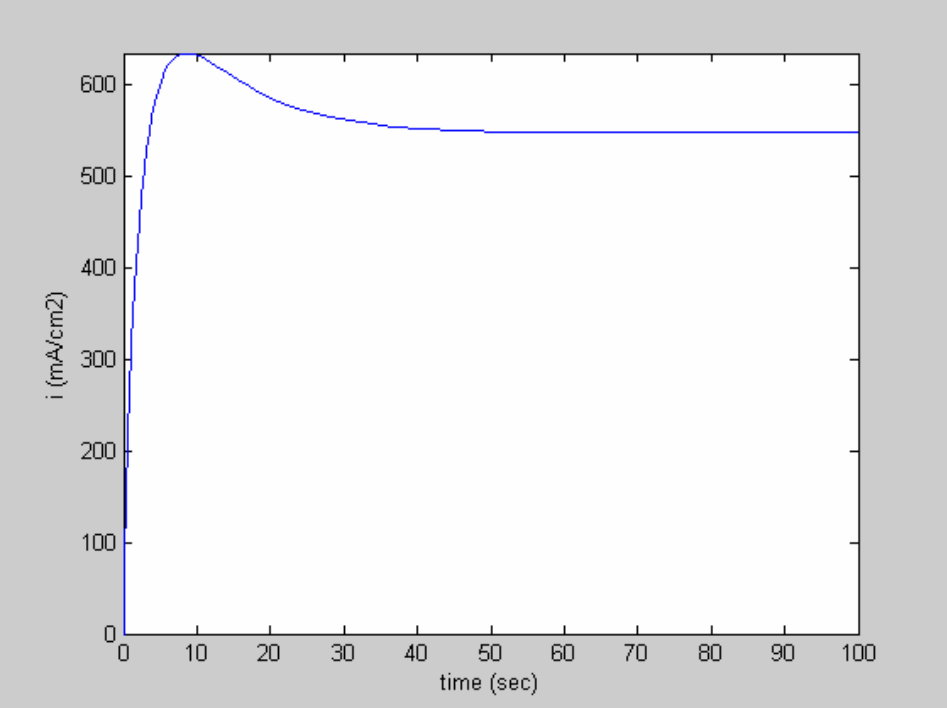

Figure 47: Current density as a function of time at U = 0.1V for a 117 Nafion membrane at 80ºC with F_{anode} = 1ccm, C_{CH3OH} = 1M and P_C = 0atm (rel.)

c. Discussion of the dynamic simulation

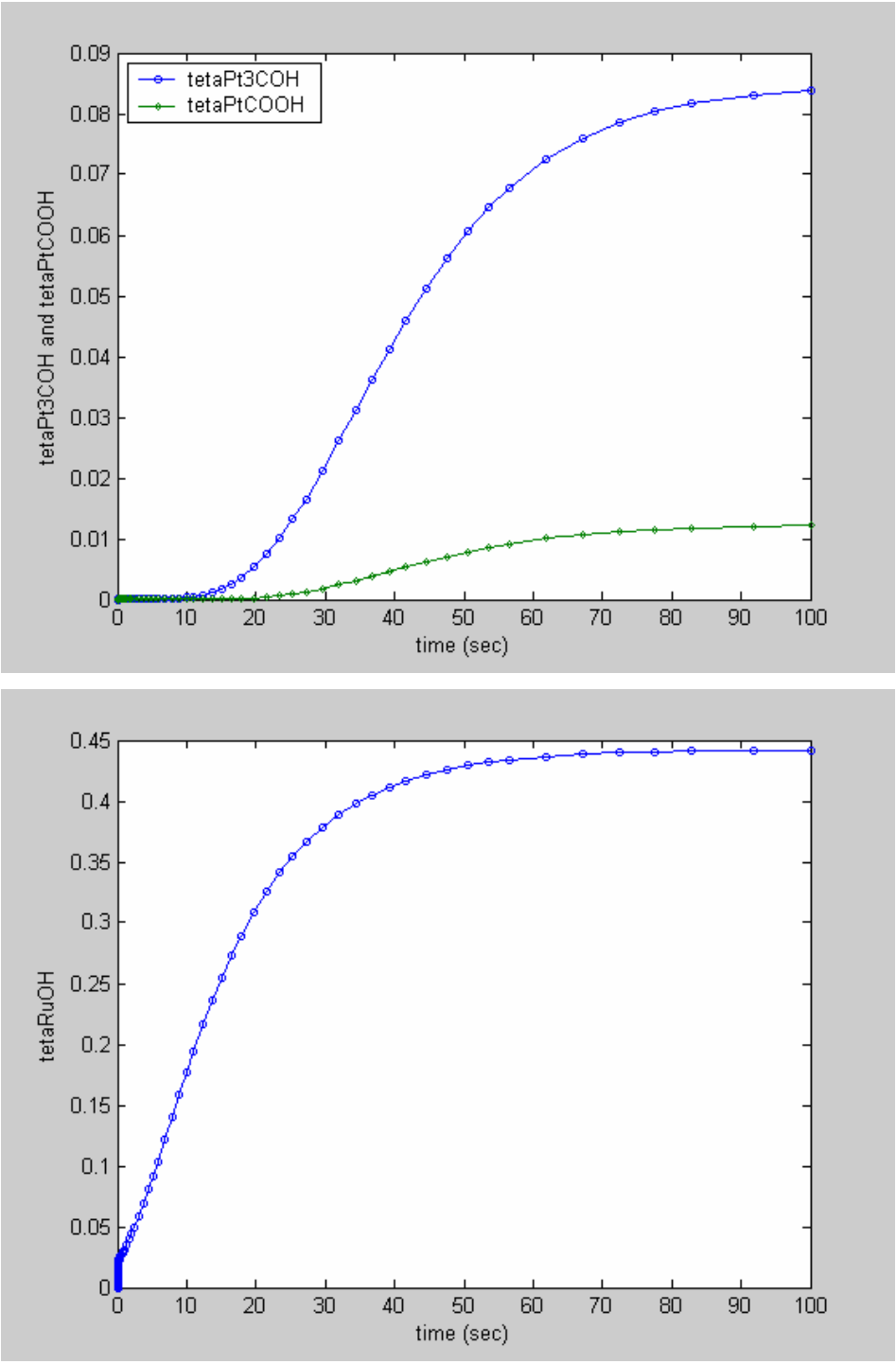

Figure 48: Surface coverage as a function of time at U = 0.5V for a 117 Nafion membrane at 80ºC with F_{anode} = 1ccm, C_{CH3OH} = 1M and P_C = 0atm (rel.)

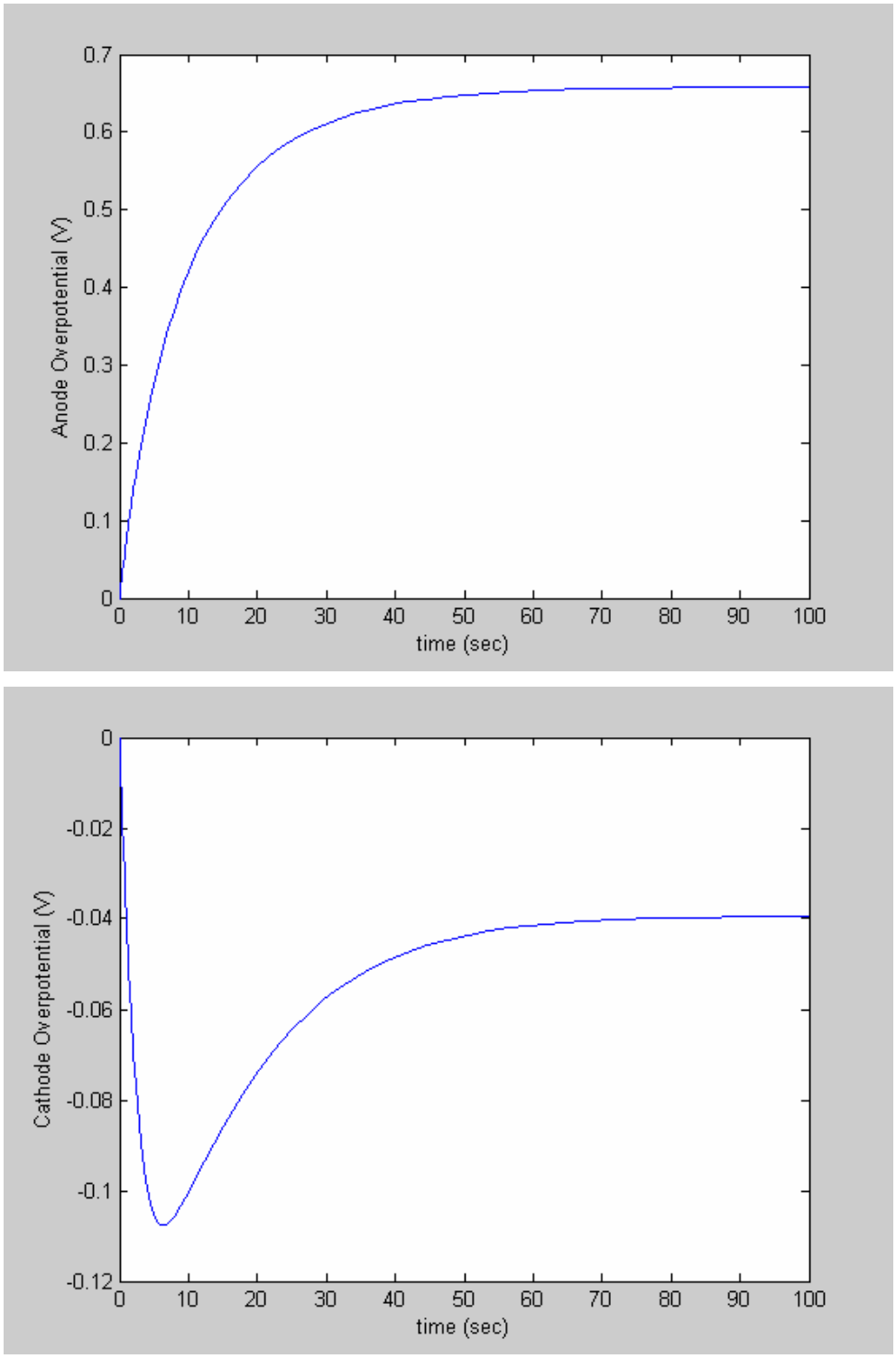

Figure 49: Anode and cathode over potentials as a function of time at U = 0.5V for a 117 Nafion membrane at 80ºC with F_{anode} = 1ccm, C_{CH3OH} = 1M and P_C = 0atm (rel.)

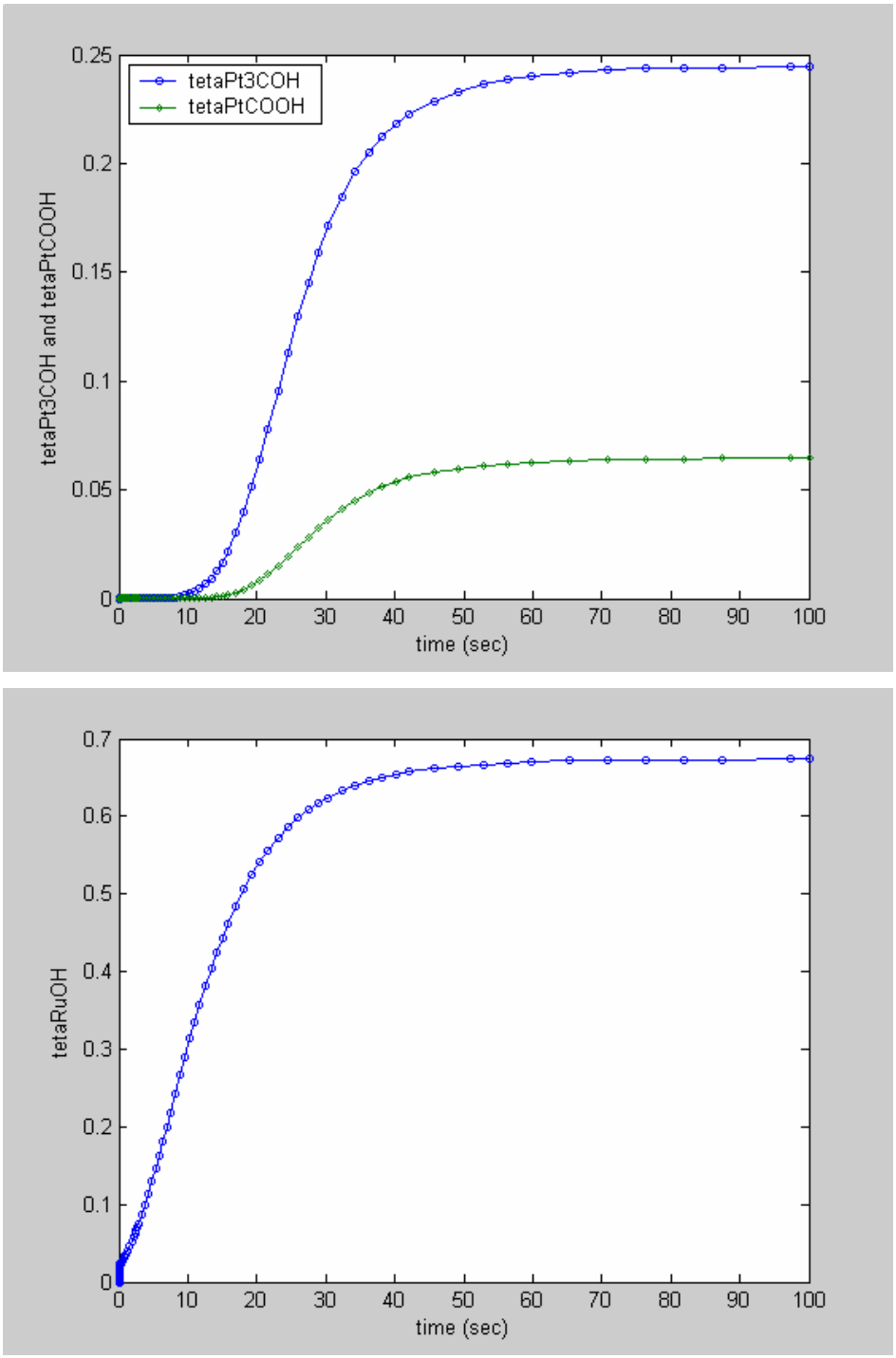

Figure 50: Surface coverage as a function of time at U = 0.3V for a 117 Nafion membrane at 80ºC with F_{anode} = 1ccm, C_{CH3OH} = 1M and P_C = 0atm (rel.)

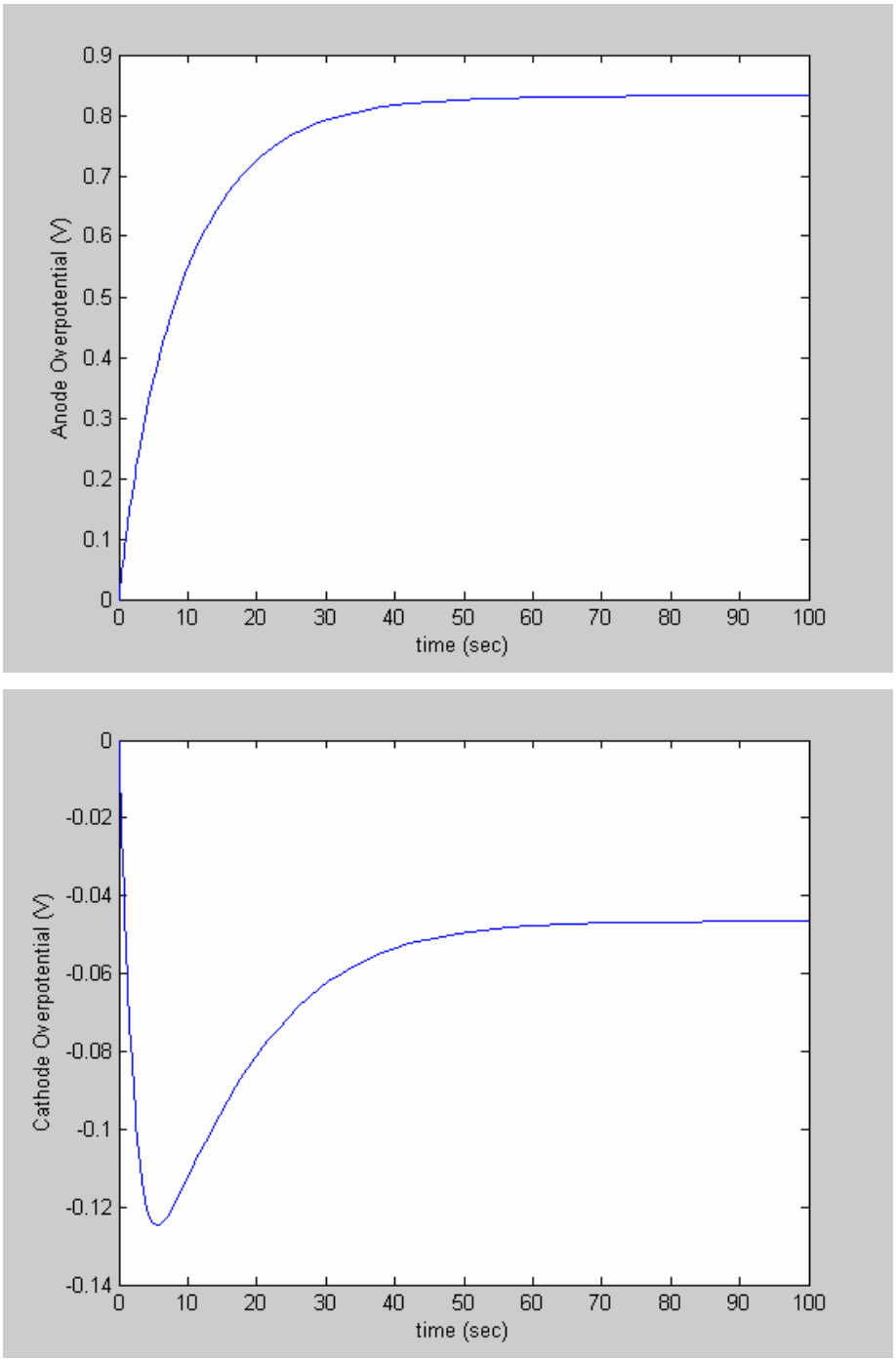

Figure 51: Anode and cathode over potentials as a function of time at U = 0.3V for a 117 Nafion membrane at 80ºC with F_{anode} = 1ccm, C_{CH3OH} = 1M and P_C = 0atm (rel.)

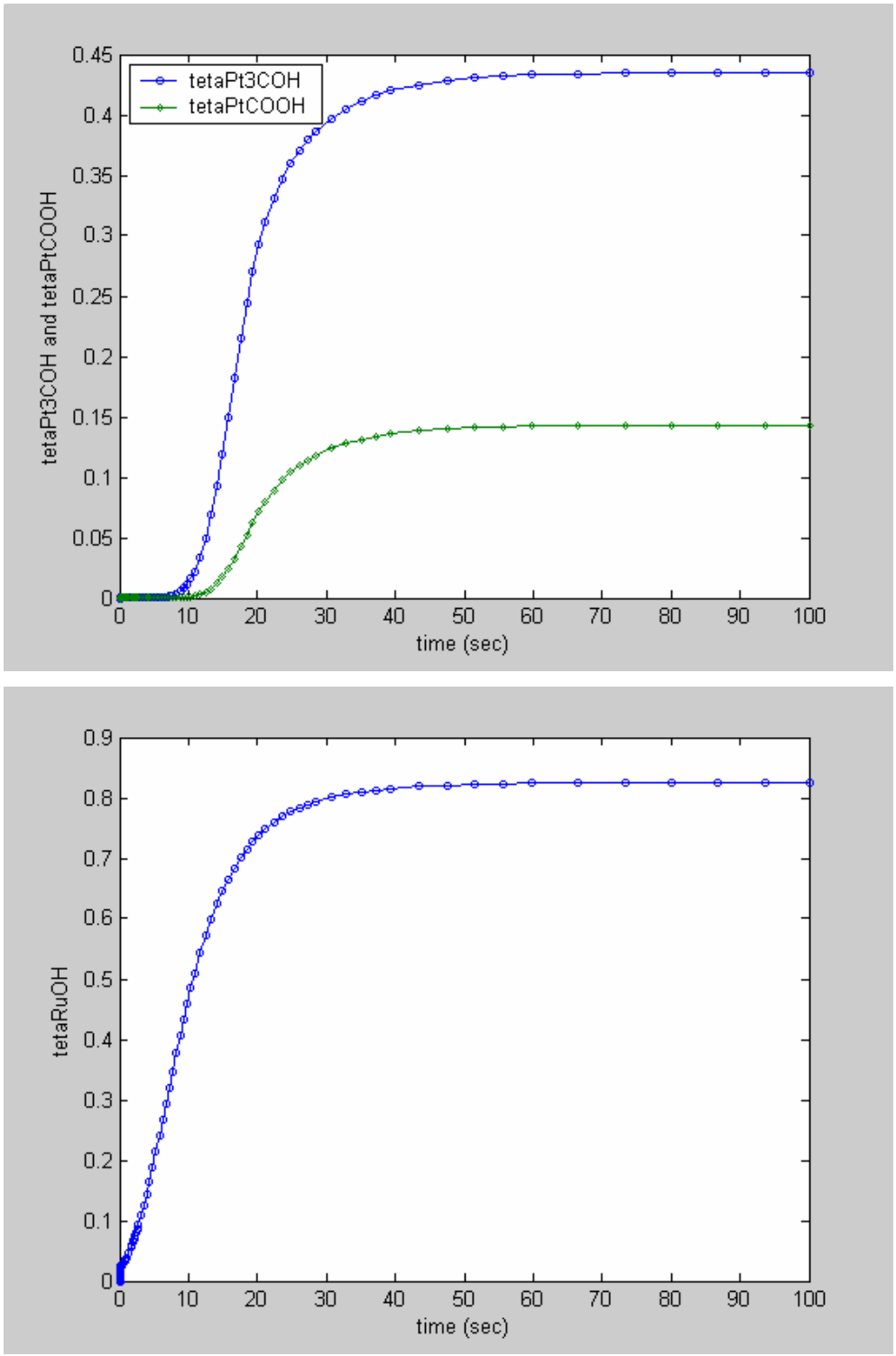

Figure 52: Surface coverage as a function of time at U = 0.1V for a 117 Nafion membrane at 80ºC with F_{anode} = 1ccm, C_{CH3OH} = 1M and P_C = 0atm (rel.)

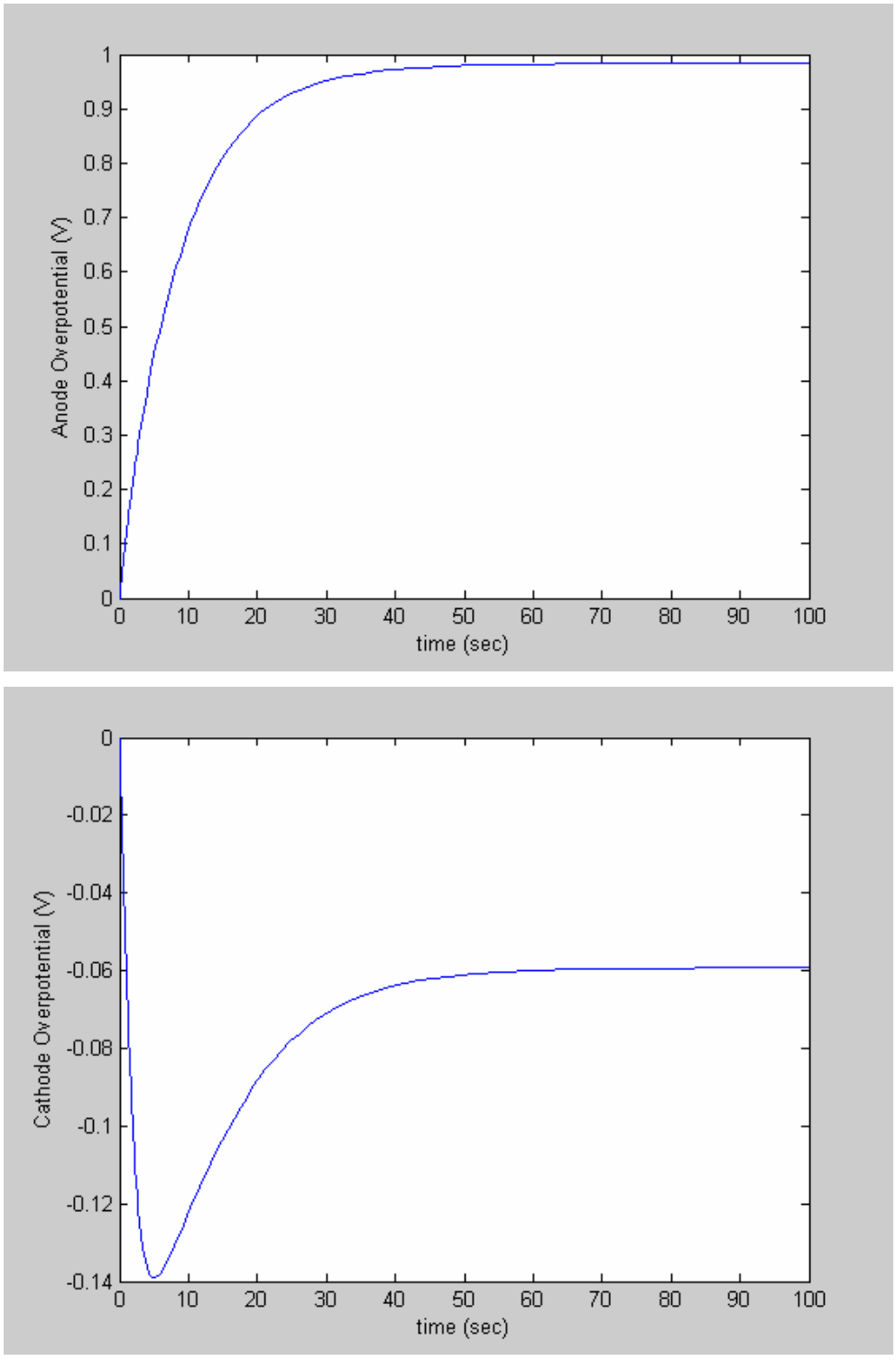

Figure 53: Anode and cathode over potentials as a function of time at U = 0.1V for a 117 Nafion membrane at 80ºC with F_{anode} = 1ccm, C_{CH3OH} = 1M and P_C = 0atm (rel.)

There is a small current overshoot before stabilization. It was also observed experimentally is some cases but the stabilization time is longer (some minutes).

It can be explained by the fact that the catalyst is covered by some kind of poisoning species that are not easily and quickly oxidized (Pt_3-COH and Pt-COOH in this case). When the cell is started, the coverage of these species will increase and reduce available catalyst for methanol adsorption. Consequently, less protons can be formed and the cell current decrease.

When the cell is started, the anode overpotential increases while the cathode overpotential decreases when the cell voltage increases to keep a constant current density (Figures 49, 51, 53).

A negative overshoot can be seen for cathodic over potential. It is related to the current density overshoot. When it occurs, more protons are formed at anode than at the steady state. Consequently, the cathodic over potential has to be decreased to improve oxygen reduction.

The coverage of the catalytic surface decreases with the cell voltage (Figures 48, 50, 52). A higher cell voltage, of course means a higher anode potential. It helps oxidation of the methanol decomposition products. Consequently their poisoning effect is lowered. However, the coverage of Pt_3-COH (which is higher than Pt-COOH) never exceeds 0.435. It is another proof that methanol decomposition is the rate limiting step. This is a surprising result as the poisoning species coverage (Pt-COH and Pt-COOH) close to one is expected for reaction 1 to be the rate limiting step.

d. Modeling of the polarization curve

In dynamic mode, the evolution of the different parameters with time matched what was expected theoretically. The fitted rate constants seem to give acceptable results.

The code was forced to give a polarization curve close to the experimental one in specific conditions (117 Nafion membrane, 80ºC, F_{anode} = 1ccm, C_{CH3OH} = 1M and P_C = 0atm rel.), however by fitting rate constants. In order to be trusted and used to predict the cell behavior it has to match the experiments when working conditions are changed. The

model was thus tested with a thinner (112) membrane, a higher cathode pressure and a higher concentration.

The new model was tested for the previous conditions (117 Nafion membrane, P_C = 0atm (rel.), C_{MeOH} = 1M):

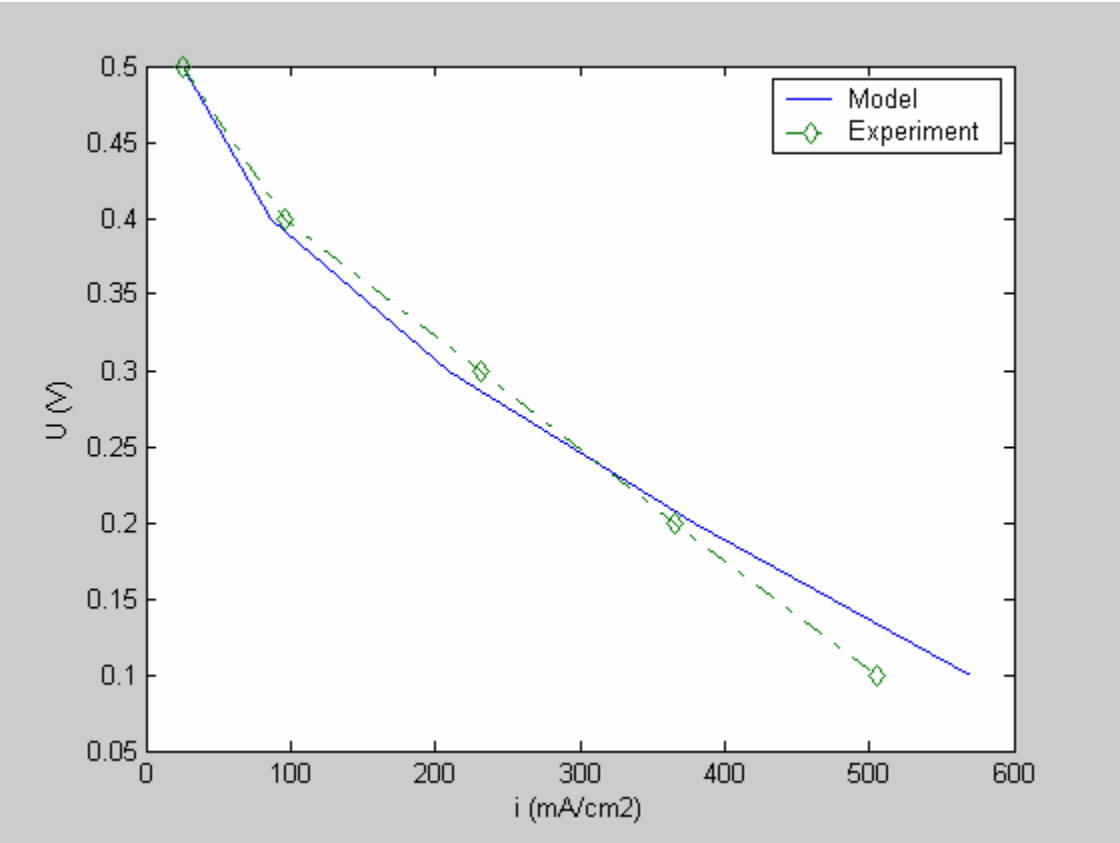

Figure 54: Theoretical polarization curve for a 117 Nafion membrane at 80ºC with F_{anode} = 1ccm, C_{CH3OH} = 1M and P_C = 0atm (rel.)

The model is close to the experiment except when the cell voltage is below 0.2mV (Figure 54). Even if the CO_2 effect was minimized by the high feed flow rate, it still exists. The model does not take count on it. That is why it exhibits higher performance. In other words we do not account for limiting current density limitation by diffusion.

For the model to be valid, it must remain reliable when operating conditions are changed.

Thus it was tested for 112 Nafion membrane, P_C = 0atm (rel.), C_{MeOH} = 1M:

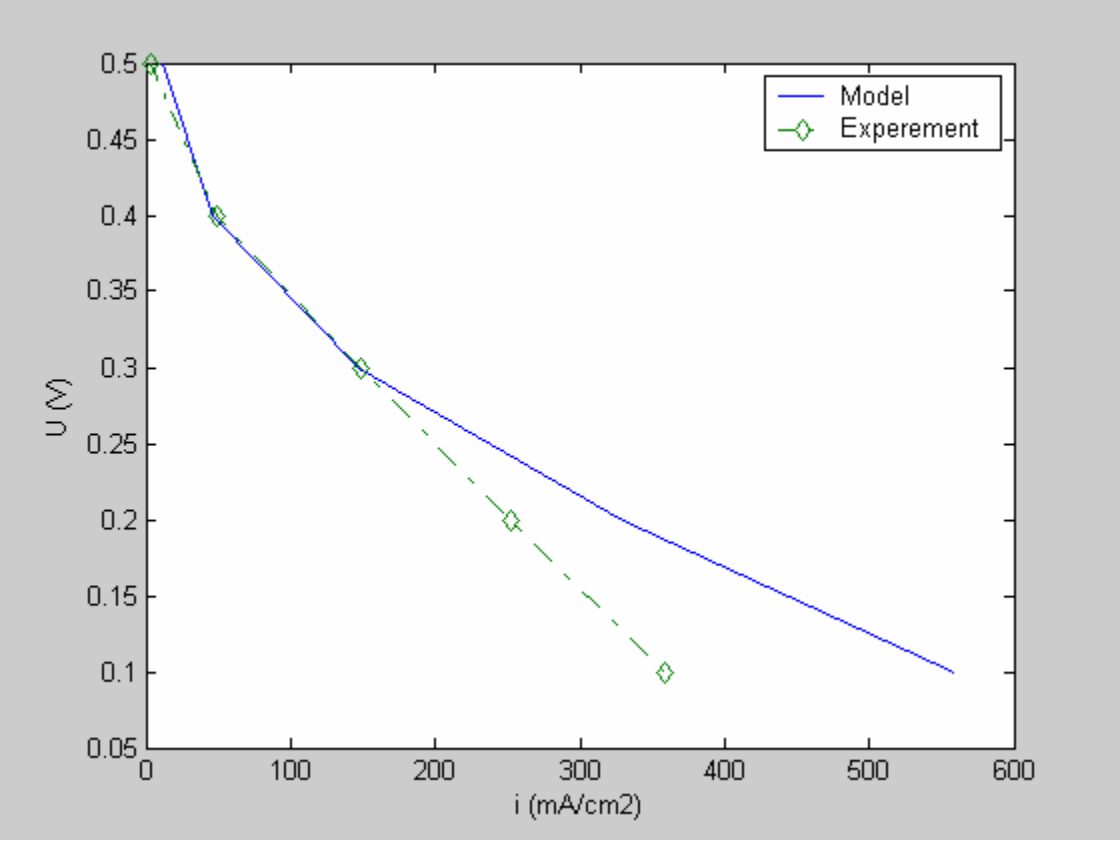

Figure 55: Theoretical polarization curve for a 112 Nafion membrane at 80ºC with F_{anode} = 5ccm, C_{CH3OH} = 1M and P_C = 0atm (rel.)

For a 112 Nafion membrane, theory and experiment fit well above 0.3V (Figure 55). Again this may be due to CO_2 formation. Such a difference at low cell voltage can be completely due to the low methanol diffusion due to CO_2 evolution. In addition we were not accounted for fouling of the cathode by the methanol that is crossing over to the cathode. The original code was modified to account for fouling of the cathode. Differential equations (a) to (e) appeared two times in the system, one time to describe methanol oxidation at the anode and a second time to describe methanol oxidation at the cathode side. It had nevertheless no effect on the final results. This may be due to an underestimation of methanol crossover by the model. Another reason may be that

methanol oxidation by oxygen at cathode is a surface reaction and, thus, does not depend on cathode potential.

Actually, crossover is promoted with a 112 membrane and the flux probably underestimated by the model in the concerned range of cell voltage.

The simulation was done for 117 Nafion membrane, P_C = 1atm (rel.), C_{MeOH} = 1M:

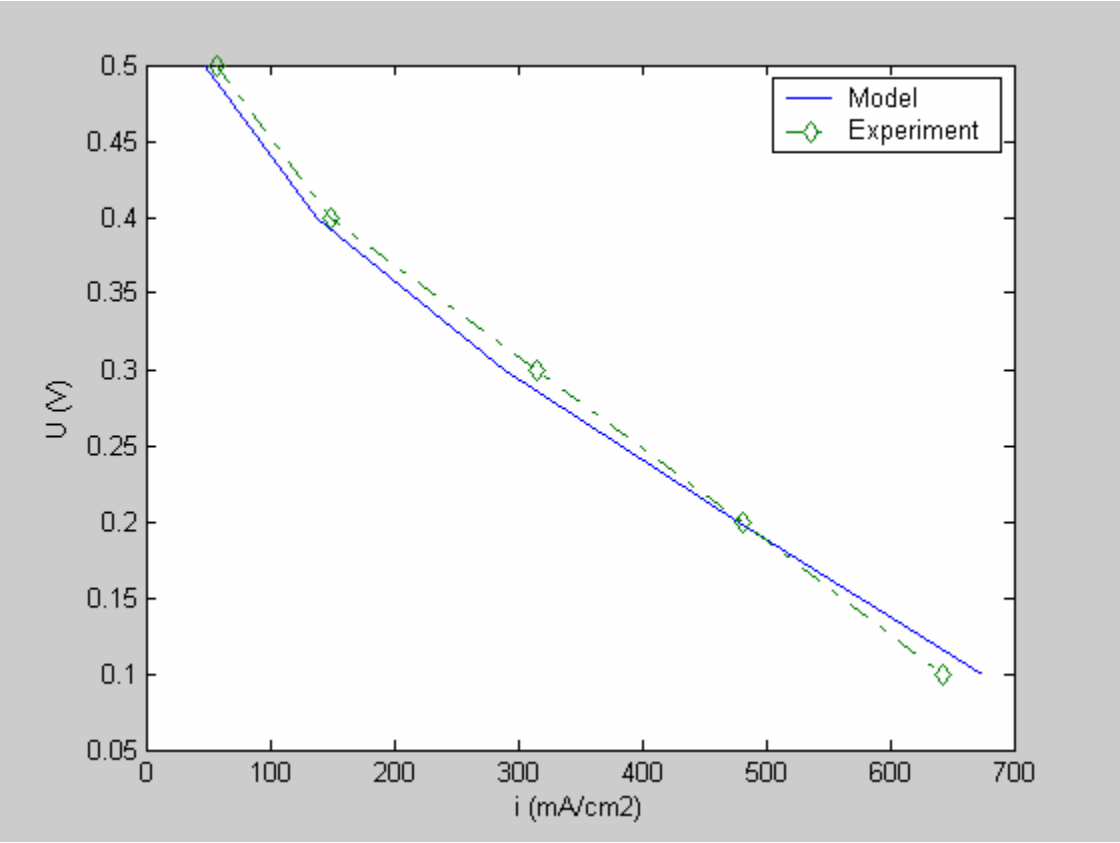

Figure 56: Theoretical polarization curve for a 117 Nafion membrane at 80ºC with F_{anode} = 5ccm, C_{CH3OH} = 1M and P_C = 1atm (rel.)

The model, thus, predicts well the performance when cathode pressure is changed (Figure 56).

The effect of higher methanol concentration was investigated for 117 Nafion membrane, P_C = 0atm (rel.), C_{MeOH} = 5M:

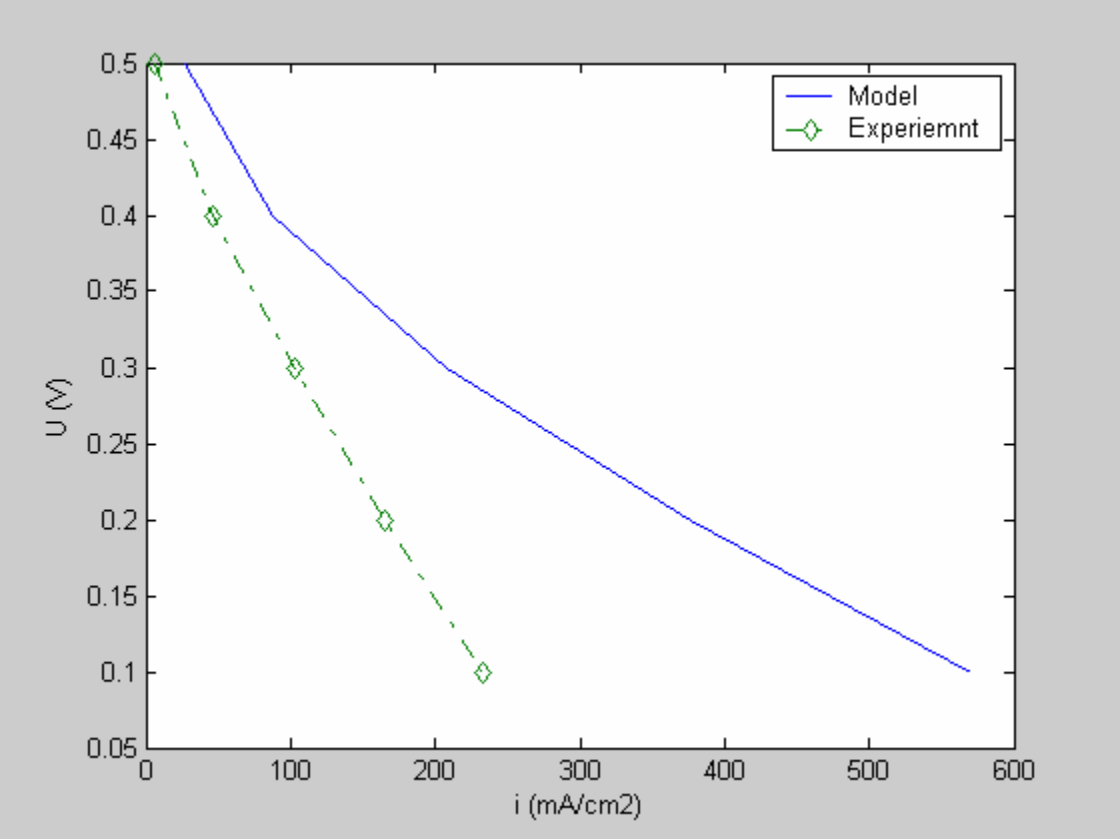

Figure 57: Theoretical polarization curve for a 117 Nafion membrane at 80ºC with F_{anode} = 5ccm, C_{CH3OH} = 5M and P_C = 0atm (rel.)

When a 5M methanol solution is fed to the anode, the model completely disagrees with the experiment (Figure 57). At high concentration, crossover becomes so important that performance drops quickly. It confirms that the effect of methanol crossover and fouling of cathode not accounted for by the model is very important in lowering performance.

4. Overall conclusions on dynamic model

It seems possible to rely on the model to predict the cell performance under a limited set of conditions. However, it can only be trusted above a cell voltage of 0.3V. Besides, if the range of cell voltage studied is reduced, it is possible to get more accurate fitting parameters.

The model does not accurately account for the cathode overpotential which it underestimates substantially. Further, the model does not take into consideration the inhibition of cathode kinetics as a result of methanol crossover. Finally, the diffusion limitations of methanol through gas-diffusion layer, especially at higher current densities and CO_2 evolution, are not included in the model and account for variation at low voltage. Sundmacher et al [11] accounted for the diffusion through the diffusion layer by considering a mass balance for Methanol and carbon dioxide both for the anode compartment and the catalytic layer. A code similar to the code studied previously was written including these two mass balances. It resulted in a modification in the fitted parameters but the shape of the coverage, potentials, and current evolution with time remained the same. This code still not account for methanol diffusion limitation due to carbon dioxide removal.

VI. Reaction Network Theory applied to the electro-chemical oxidation of methanol

Several mathematical models have been developed for methanol electro-oxidation. They use an oversimplified mechanism for the reaction considering only one or two intermediate species. However, the real mechanism is much more complicated and most steps remain unknown.

1. Reaction Network Theory

The new graph-theoretical approach developed by Fishtik et al [21] was used in an effort to improve our understanding of methanol electro-oxidation reaction and its mechanism. This approach is based on Reaction Route Graphs which depict all possible succession of reactions (Reaction Route) that lead to the studied overall reaction. It should be noted that in this case, the nodes do not represent a particular species. The drawing of this type of graph implies the knowledge of the complete mechanism or at least an assumption since every branch corresponds to a step in the mechanism.

An analogy can be made between these graphs and electrical networks. Besides, the concept of reaction resistance was introduced [22]. This allows the use of both Kirchhoff's and Ohm's law in order to analyze and reduce the network. The reaction resistance is defined as the mean value of the reciprocal rate (similar to a conductance) between the reverse and forward rate.

$$R_P = \left\langle \frac{1}{r_P} \right\rangle = \frac{\ln\left(\vec{r}_P \Big/ \overleftarrow{r}_P \right)}{\vec{r}_P - \overleftarrow{r}_P}$$

To calculate the resistance one needs an expression for the forward and reverse reaction rate of elementary step. Assuming that rate constants follow Arrhenius law, activation energies and pre-exponential factors can be calculated from a thermodynamic transition state model. By evaluating and comparing the resistances along parallel

pathways between two nodes, some of them can be neglected. Consequently, a clearer but still representative mechanism is obtained.

Besides, the overall reaction rate (r_{OR}) is easy to determine knowing the possible Reaction Routes. In analogy to Ohm's law it is a function of the overall reaction resistance and affinity.

$$r_{OR} = \frac{A_{OR}}{R_{OR}}$$

Such an approach seems to be an efficient one to simplify the complicated methanol oxidation mechanism and come up with a significant overall rate expression. However, Reaction Network Theory has been studied for surface reaction in gas phase. There are two challenges to face to adapt the method to methanol electro-oxidation in fuel cells.

The mechanism contains some electrochemical steps. For these, activation energy is potential dependant. Consequently, a fundamental model should be found to express them. Besides, the unity bond index-quadratic exponential potential method (UBI-QEP) developed by Shustorovitch [23], valid in gas phase needs to be adapted to liquid phase or be replaced by another ab initio model.

2. Methanol oxidation mechanism

The methanol oxidation overall reaction (OR) can be divided into two consecutive overall reactions. The first one is methanol decomposition into carbon monoxide. The second one is the water-gas shift reaction (WGSR).

OR1: $CH_3OH + 4H_2O \leftrightarrows CO + 4H_3O^+ + 4e^-$ (MeOH decomposition)

OR2: $CO + 3H_2O \leftrightarrows CO_2 + 2H_3O^+ + 2e^-$ (WGSR)

$CH_3OH + 7H_2O \leftrightarrows CO_2 + 6H_3O^+ + 6e^-$ (MeOH electro-oxidation)

In order to draw an overall of graph for methanol oxidation it seems easier to draw a graph for each of the consecutive reactions and then try to connect them together.

Even if a bimetallic catalyst is used in electro-oxidation of methanol the assumption was made that all adsorbates diffuse quickly to the interface between both catalysts. It can thus be considered that all reactions occur on the site kind of site.

The methanol decomposition was investigated by Gokhale et al [24] who reported a mechanism for decomposition of methanol on copper.

The mechanism needed to be adapted to the electro-chemical reaction that was studied. Original steps which form adsorbed hydrogen were considered as electrochemical. Consequently, they form a hydronium ion and an electron. The assumption that all these steps become electrochemical is certainly not true. However, it makes a good starting point.

The mechanism contains twelve steps for OR1:

s_1: $CH_3OH \leftrightarrows CH_3OHS$

s_2: $CH_3OHS + H_2O \leftrightarrows CH_3OS + H_3O^+ + e^-$

s_3: $CH_3OS + H_2O \leftrightarrows CH_2OS + H_3O^+ + e^-$

s_4: $CH_2O + H_2O \leftrightarrows HCOS + H_3O^+ + e^-$

s_5: $HCOS + H_2O \leftrightarrows COS + H_3O^+ + e^-$

s_6: $CH_3OHS + H_2O \leftrightarrows H_2COHS + H_3O^+ + e^-$

s_7: $H_2COHS + H_2O \leftrightarrows HCOHS + H_3O^+ + e^-$

s_8: $HCOHS + H_2O \leftrightarrows COHS + H_3O^+ + e^-$

s_9: $COHS + H_2O \leftrightarrows COS + H_3O^+ + e^-$

s_{10}: $HCOHS + H_2O \leftrightarrows COS + 2H_3O^+ + e^-$

s_{11}: $H_2COHS + H_2O \leftrightarrows CH_2OS + H_3O^+ + e^-$

s_{12}: $COS \leftrightarrows CO + S$

Methanol is dehydrogenated to form different intermediates. For the same chemical formula, adsorbates can have different structures. All those steps are considered to occur on platinum.

Fishtik et al [22] reported a mechanism for the Water-Gas Shift Reaction on copper. It was slightly changed to be adapted to the electro-oxidation that occurs in a methanol fuel cell. Steps which form adsorbed hydrogen were again considered as electrochemical.

Besides, this assumption prevents dihydrogen formation. Consequently, steps including this adsorbate were not considered.

Thus, twelve reactions remain:

S_{12}: $COS \leftrightarrows CO + S$

s_{13}: $H_2O + S \leftrightarrows H_2OS$

s_{14}: $H_2OS + OS \leftrightarrows 2OHS$

s_{15}: $2H_2O + S \leftrightarrows OHS + H_3O^+ + e^-$

s_{16}: $OHS + H_2O \leftrightarrows OS + H_3O^+ + e^-$

s_{17}: $COS + OS \leftrightarrows CO_2S + S$

s_{18}: $COS + OHS \leftrightarrows HCOOS + S$

s_{19}: $COS + OHS + H_2O \leftrightarrows CO_2S + S + H_3O^+ + e^-$

s_{20}: $HCOOS + OS \leftrightarrows CO_2S + OHS$

s_{21}: $HCOOS + H_2O \leftrightarrows CO_2S + H_3O^+ + e^-$

s_{22}: $HCOOS + OHS \leftrightarrows CO_2S + H_2OS$

s_{23}: $CO_2S \leftrightarrows CO_2 + S$

Steps 14 to 17 occur on ruthenium and correspond to water adsorption. This mechanism show such adsorbates as carbon monoxide and formic acid are intermediates in methanol electro-oxidation. However, according to Gojković et al [25], formic acid is formed during methanol electro-oxidation. Other intermediates like HCOHS and COHS appear in the reaction. COHS can react to form either CO or formaldehyde and formic acid. This intermediate seems to have an important role in the overall reaction.

Reactions including COHS were taken from the Fuel Cell handbook [26]:

S_{24}: $COHS + OS \leftrightarrows HCOOS + S$

S_{25}: $COHS + OS \leftrightarrows COS + OHS$

S_{26}: $COHS + OHS \leftrightarrows HCOOS + S + H_3O^+ + e^-$

The previous reactions are a link between the decomposition and WGSR graphs and may appear on an overall graph. However, for right now, we consider graphs for methanol decomposition (Figure 58) and WGS reaction separately (Figure 59).

3. Reaction Route graphs for methanol decomposition and WGS Reaction

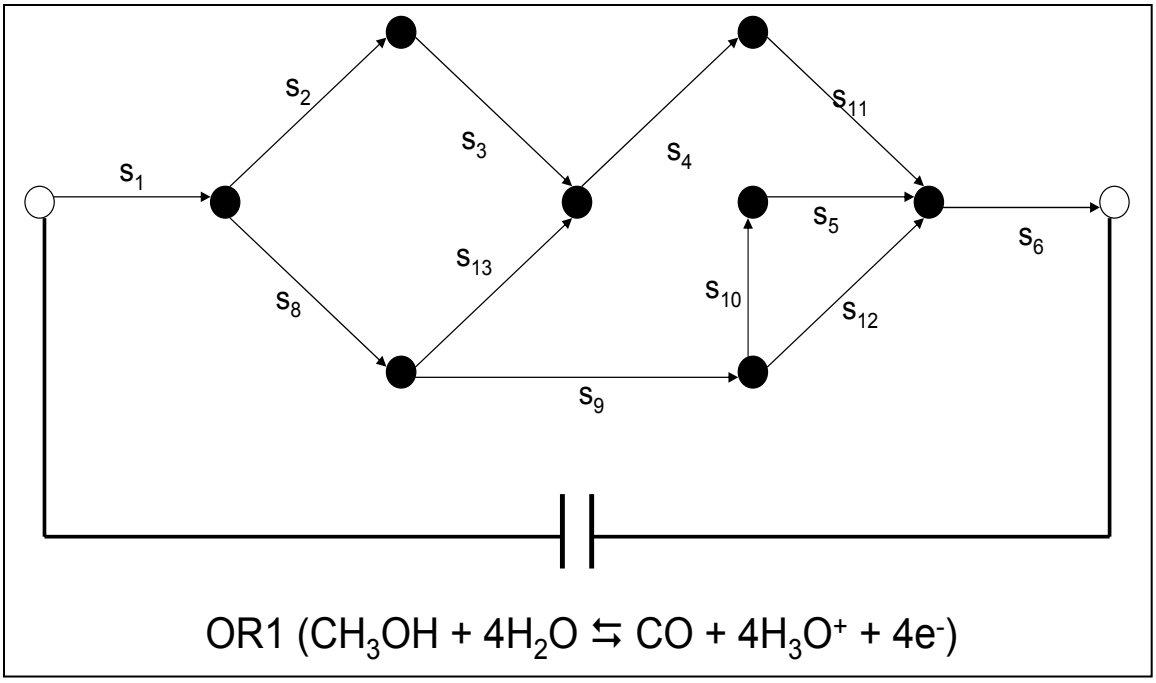

Figure 58: Methanol decomposition Reaction Route Graph

The first step of drawing a graph is finding one of the possible reaction routes for the overall reaction. All possible empty routes, which are a set of reaction that cancel each other, are added on this reaction route. It is preferable to start with small empty routes of 3 or 4 reactions. As a consequence, a lot of other reaction routes will appear on the graph. A Matlab program was developed to compute the sets of possible reaction routes and empty routes. All possible routes need to appear on the graph for it to be correct. Once all empty routes were added, the shape of the graph was modified in order to be more understandable. Another reason for having separated methanol electro-oxidation into two overall reaction is that a graph can become very complicated and confusing if there are too much reaction in the mechanism.

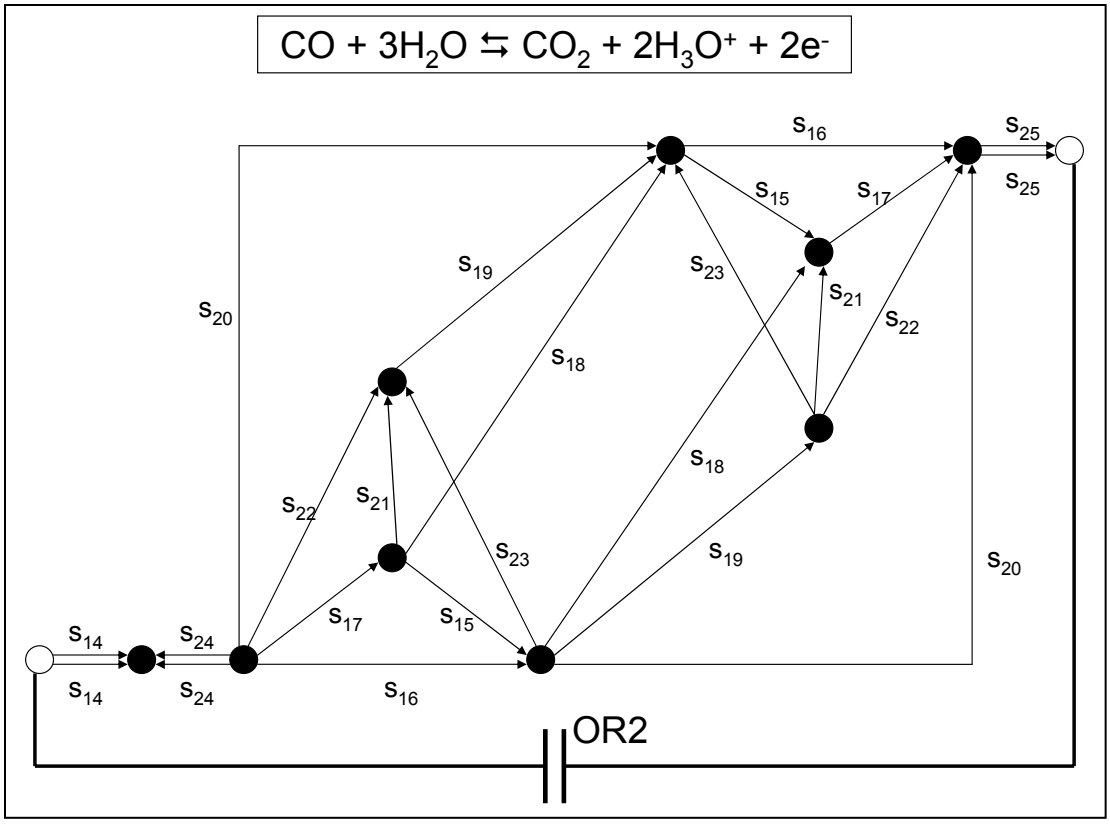

Figure 59: Water-Gas Shift Reaction Reaction Route Graph

○ : Terminal Node

● : Intermediate Node

4. Overall graph

It can be seen that step 12 is the same for both overall reactions. It appears in each mechanism to balance the overall reaction. If the two reactions are linked together in an overall graph for methanol electro-oxidation, adsorbed CO reacts directly and thus no desorption can occur. Consequently CO adsorption steps cancel each and the end of the methanol decomposition graph correspond to the beginning of the WGSR graph. However, three steps containing COHS as an intermediate remain (S_{24}, S_{25}, S_{26}). They

belong to the overall graph and need to be added to it. The easiest way to add the three remaining steps is to find empty routes that include all of them.
The two following empty routes contain all three steps:

- $S_{26} - S_{27} + S_{19} = 0$
- $S_{26} - S_{28} + S_{17} = 0$

These empty routes have to be added on the WGSR graph. Both of them contain S_{26}. Unfortunately, the sequence of the reaction makes those empty routes impossible to fit in the graph. Thus, either a new graph need to be draw using the overall methanol oxidation reaction or COHS can be omitted. The latter solution was adopted here. Actually, according to the state of the art in Reaction Route Graph theory, such a graph would be too difficult to draw.

5. Overall conclusions

The two graphs that are drawn here are a starting point for a detailed study of the electro-oxidation of methanol. Even tough, it is not complete it would make possible to identify the important steps and those which are limiting the reaction provided reaction kinetics of the steps are available.

Unfortunately, it was not possible to find a way to calculate the activation energy of electro-chemical steps as a function of the electrode potential. A method based on calculations of the energy of the complex formed during the reaction has been developed by Anderson [27]. It needs a program which can calculate this energy right before and after the reaction. It was not possible to investigate this further in this study because of a lack of time.

VII. Conclusions and recommendations for future work

According to experimental investigations, home-made electrodes were found to be much more efficient than commercial electrodes for the Direct Methanol Fuel Cells. Besides, these investigations permitted us to understand the role played by various MEA components on the cell performance.

Methanol diffusion through the membrane is of course well known, but its diffusion through the electrode backing was also revealed to be an important issue limiting performance. It was found to be difficult to control the balance between the flux of methanol and the flux of carbon dioxide which escapes the catalytic layer. This balance depends up on the Nafion and PTFE loading in the anode catalytic layer and the structure of the hydrophilic and hydrophobic pores created. PTFE loading may also have to be adjusted in the carbon cloth or in the resistance layer if it is used. The balance depends however on the operating point. Best performance were obtained with a $4mg/cm^2$ Pt/Ru black anode and $4mg/cm^2$ Pt black cathode on a 117 membrane. No PTFE was used and the optimum Nafion loading at cathode was 10wt%. However, the optimum Nafion loading at anode changed with the cell voltage. At high cell voltage and low current densities it was 10wt%, but below 0.25V, it the optimum Nafion loading became 5wt%.

The two-phase flow was not only posing problems in the diffusion layer but also in the feed channel. A slug flow reduces liquid phase diffusion area. This kind of flow is a great limitation to the cell performance and need to be avoided. Both methanol and carbon dioxide diffusion are strongly dependent on the diffusion layer, which was a piece of carbon cloth in this study. The carbon cloth remained the same and was already Teflon treated. It would be interesting to test non-treated carbon cloth. As seen during the study on PTFE content at anode and the resistance layer, PTFE can have a great effect on both methanol and CO_2 diffusion. The behavior of the diffusion layer toward diffusion may be drastically different with non-treated carbon cloth. A carbon cloth with another density may also be tested.

Conclusions were drawn for our cell station and some of them may not be true more frequently for other equipment. The stack itself might change some of the results that were obtained. For example, working with new bipolar plates or with $25cm^2$ electrodes

could change CO_2 management and lead to other observations. It could also possibly promote some solution considered to improve performance.

The dynamic DMFC modeling was focused on the effect of the two-phase flow at the anode but rather on the reaction mechanism. Even though it is highly simplified, this mechanism is somewhat consistent with reality as it contains two intermediate poisoning species. Their rate of reaction represents nevertheless a simplified global rate for a set of reaction coming from a more complicated mechanism. It was however sufficient to give reasonable predictions when operating conditions were changed. Rate constant in the model were fitted. However, better predictions could be made if the model could make a better estimate of the flux of methanol that diffuses to the cathode. The equation derived by Sundmacher et al [11] for N_{CH3OH} underestimate the flux. Fitting tests for the diffusion coefficient of methanol could solve the problem. It needs to be replaced by a more accurate expression.

Reaction route theory could give us a more precise idea on the importance of adsorbed CO and COOH based on the two graphs developed in the study. It is a powerful tool to study the mechanism. Unfortunately, at this point, computation of potential-dependant activation energies is still an issue.

References

1. A.S. Arico, S. Srinivasan and V. Antonucci
   "DMFCs: From Fundamental Aspects to Technology Development"
   FUEL CELLS 2001, 1, No.2

2. Anna Monis Shipley and R. Neal Elliott
   "Stationary Fuel Cells: Future Promise, Current Hype"
   American Council for a Energy-Efficient Economy, 2004, Report No. IE041

3. R. Dillon , S. Srinivasan , A. S. Aricò and V. Antonucci
   "International activities in DMFC R&D: status of technologies and potential applications"
   Journal of Power Sources, Volume 127, Issues 1-2, 10 March 2004, Pages 112-126

4. Michel Broussely and Graham Archdale
   "Li-ion batteries and portable power source prospects for the next 5–10 years"
   Journal of Power Sources, Volume 136, Issue 2, 1 October 2004, Pages 386-394

5. Gogel , T. Frey , Zhu Yongsheng , K. A. Friedrich , L. Jörissen and J. Garche
   "Performance and methanol permeation of direct methanol fuel cells: dependence on operating conditions and on electrode structure"
   Journal of Power Sources, Volume 127, Issues 1-2, 10 March 2004, Pages 172-180

6. G. Q. Lu and C. Y. Wang
   "Electrochemical and flow characterization of a direct methanol fuel cell"
   Journal of Power Sources, Volume 134, Issue 1, 12 July 2004, Pages 33-40

7. Lindermeir , G. Rosenthal , U. Kunz and U. Hoffmann
   "On the question of MEA preparation for DMFCs"
   Journal of Power Sources, Volume 129, Issue 2, 22 April 2004, Pages 180-187

8. Harry Hoster, Teresa Iwasita, Hermann Baumgärtner and Wolf Vielstich
   "Pt-Ru model catalysts for anodic methanol oxidation: Influence of structure and composition on the reactivity"
   Phys. Chem. Chem. Phys., 2001, 3, 337-346

9. Zhaobin Wei, Suli Wang, Baolian Yi, Jianguo Liu, Likang Chen, WeiJiang Zhou, Wenzheng Li and Qin Xin

"Influence of electrode structure on the performance of a direct methanol fuel cell"
Journal of Power Sources, Volume 106, Issues 1-2, 1 April 2002, Pages 364-369

10. H. Yang and T.S. Zhao
    "Effect of anode flow field design on the performance of liquid feed direct methanol fuel cells"
    Electrochimica Acta, In Press, Corrected Proof, Available online 12 January 2005,

11. K. Sundmacher, T. Schultz, S. Zhou, K. Scott, M. Ginkel and E. D. Gilles
"Dynamics of the direct methanol fuel cell (DMFC): experiments and model-based analysis"
Chemical Engineering Science, Volume 56, Issue 2, January 2001, Pages 333-341

12. Lindermeir, G. Rosenthal , U. Kunz and U. Hoffmann
"On the question of MEA preparation for DMFCs"
Journal of Power Sources, Volume 129, Issue 2, 22 April 2004, Pages 180-187

13. G. Q. Lu and C. Y. Wang
"Electrochemical and flow characterization of a direct methanol fuel cell"
Journal of Power Sources, Volume 134, Issue 1, 12 July 2004, Pages 33-40

14. Gaby J.M. Janssan, Michel P. de Heer, Dimitrios C. Papageorgopoulos
"Development of Bilayer Anodes for Improved reformate Tolerance of PEM Fuel Cells"
Energy research Centre of the Netherlands ECN, Fuel CellTechnology, P.O. Box1, 1755 ZG Petten / The Netherlands

15. Gogel , T. Frey , Zhu Yongsheng , K. A. Friedrich , L. Jörissen and J. Garche
"Performance and methanol permeation of direct methanol fuel cells: dependence on operating conditions and on electrode structure"
Journal of Power Sources, Volume 127, Issues 1-2, 10 March 2004, Pages 172-180

16. Nordlund, J.; Roessler, A.; Lindbergh, G.
"The influence of electrode morphology on the performance of a DMFC anode"
Journal of Applied Electrochemistry, Volume *32, Issue 3, 2002 March, Pages 259-265*

17. Sylvie Escribano and Pierre Aldebert
"Electrodes for hydrogen/oxygen polymer electrolyte membrane fuel cells"
Solid State Ionics, Volume 77, April 1995, Pages 318-323

18. S. P. Nunes, B. Ruffmann, E. Rikowski, S. Vetter and K. Richau
"Inorganic modification of proton conductive polymer membranes for direct methanol fuel cells"
Journal of Membrane Science, Volume 203, Issues 1-2, 30 June 2002, Pages 215-225

19. Weilin Xu, Tianhong Lu, Changpeng Liu and Wei Xing
"Low methanol permeable composite Nafion/silica/PWA membranes for low temperature direct methanol fuel cells"
Electrochimica Acta, In Press, Corrected Proof, Available online 20 January 2005,

20. Youngcho Si, Jung-chou Lin, H. Russel Kunz and James M. Fenton
"Trilayer membranes with a Methanol-Barrier Layer for DMFCs"
Journal of the Electrochemical Society, 151 (3) A463-A469 (2004)

21. Ilie Fishtik, Caitlin A. Callaghan, and Ravindra Datta
"Reaction Route Graphs. I. Theory and Algorithm"
J. Phys. Chem. B 2004, 108, 5671-5682

22. Ilie Fishtik, Caitlin A. Callaghan, and Ravindra Datta
"Reaction Route Graphs. II. Examples of Enzyme- and surface-Catalyzed Single Overall Reactions"
J. Phys. Chem. B 2004, 108, 5683-5697

23. Harrell Sellers and Evgeny Shustorovich
"Intrinsic activation barriers and coadsorption effects for reactions on metal surfaces: unified formalism within the UBI-QEP approach"
Surface Science, 504, 2002, 167-182

24. Amit A. Gokhale, Shampa Kandoi, Jeffrey P. Greeley, Manos Mavrikakis and James A. Dumesic
"Molecular-level descriptions of surface chemistry in kinetic models using density functional theory"
Chemical Engineering Science, Volume 59, Issues 22-23, November-December 2004, Pages 4679-4691

25. Snezana Lj. Gojković
"Mass transfer effect in electrochemical oxidation of methanol at platinum electrocatalysts"
Journal of Electroanalytical Chemistry, Volume 573, Issue 2, 1 December 2004, Pages 271-276

26. A.J. Appleby, F.R. Foulkes
"Fuel Cell Handbook (Sixth Edition)"
CRC Press, ISBN: 0849308771 August, 2002

27. Alfred B. Anderson
"Theory at the electrochemical interface: reversible potentials and potential-dependent activation energies"
Electrochimica Acta, Volume 48, Issues 25-26, 15 November 2003, Pages 3743-3749

Appendix

Main program for dynamic calculations at fixed cell voltage

```
clear all;
format long;
global U
global Q
global CCH3OHF
global Pa
global Pc
global icell
global K1
global K2
global K3
global K4
global R
global F
global T
global k1
global kc
global k2
global k3
global k4
global alpha1
global alphaC
global alpha2
global Ucell0
global kphi
global mu
global CprotM
global kp
global dM
global DprotM
global DCH3OHM
global PO2
global Pteta
global VA
global kLS
global AS
global VACL
global kappa
global CA
global CC
global gamma
global Ctstar
```

```
global tau

global C0A
global C1A
global C0C
global C1C
global sigma
global Czeta
global Cteta
global Const
global KC

global A
global B
global C
global D
global P


%Kinetic parameters
K1=1*10^-0; K2=1*10^-5; K3=1*10^0;
k1=0.6*10^-11; k2=1.0*10^-2; k3=0.16*10^-1; k4=0.4*10^-1; kc=1*10^-2;

alpha1=0.5; alphaC=0.5; alpha2=0.5;
Ucell0=1.2;
R=8.314; F=96500;
kphi=1.13*10^-9; mu=3.353*10^-4; CprotM=1200; kp=1.57*10^-18;
dM=1.778*10^-4;
DprotM=5.359*10^-4; DCH3OHM=4.9*10^-6;
PO2=Pc; Pteta=10^5;
VA=0.2*10^-6; kLS=8*10^-6; AS=5*10^-4; VACL=9*10^-9; kappa=17*10^-0;
CA=4*10^2; CC=8*10^2; gamma=100; Ctstar=20*2.2*10^-5; C0A=CA; C1A=CA/100;
C0C=CC; C1C=CA/10; sigma=1; Czeta=55556; Cteta=32.68;

%Operating parameters of the cell
Q=1.67*10^-8; CCH3OHF=1000;
Pa=101325; Pc=101325;
tau=VA/Q;
T=353;

A=kphi/mu;
B=CprotM*kp/mu*(Pc-Pa)/dM;
C=(DprotM/(R*T)+CprotM*kphi/mu);
D=kp/mu*(Pc-Pa)/dM;
```

```
%Given value of the cell voltage
U=0.1;


t=[0 100];
   [t,X,s]=ode15s('ODEfixedU',t,[1000;0;0;0;0;0]);

  for j=1:length(t)
     icell(j)=kappa/dM*(Ucell0-U-X(j,5)+X(j,6))/10;
     time(j)=j;
  end

%Plot :
figure(1)
plot(t,icell(:))
xlabel('time (sec)');
ylabel('i (mA/cm2)');

figure(2);
plot(t,X(:,2),t,X(:,4));
xlabel('time (sec)');
ylabel('tetaPt3COH and tetaPtCOOH');

figure(3);
plot(t,X(:,3));
xlabel('time (sec)');
ylabel('tetaRuOH');

figure(4);
plot(t,X(:,5));
xlabel('time (sec)');
ylabel('Anode Overpotential (V)');

figure(5);
plot(t,X(:,6));
xlabel('time (sec)');
ylabel('Cathode Overpotential (V)');

figure(6);
plot(t,X(:,1));
xlabel('time (sec)');
ylabel('CCH3OH');
```

Solving function for dynamic calculations at fixed cell voltage

```
function dXdt=ODEfixedU(t,X)
global U
global Q
global CCH3OHF
global Pa
global Pc
global icell
global K1
global K2
global K3
global K4
global R
global F
global T
global k1
global kc
global k2
global k3
global k4
global alpha1
global alphaC
global alpha2
global Ucell0
global kphi
global mu
global CprotM
global kp
global dM
global DprotM
global DCH3OHM
global PO2
global Pteta
global VA
global kLS
global AS
global VACL
global kappa
global CA
global CC
global gamma
global Ctstar
global tau

global C0A
```

```
global C1A
global C0C
global C1C
global sigma
global Czeta
global Cteta
global Const
global KC

global A
global B
global C
global D
global P

dXdt=[1/tau*(CCH3OHF-X(1))-AS*X(1)*P*(DCH3OHM/dM*((-kphi/mu*CprotM*F*-
((((Ucell0-U-X(5)+X(6))*kappa/dM)/F+CprotM*kp/mu*(Pc-Pa)/dM)...
      /(CprotM*F*(DprotM/R/T+CprotM*kphi/mu)))-kp/mu*(Pc-
Pa)/dM)*dM/DCH3OHM)*exp((-kphi/mu*CprotM*F*-...
      ((((Ucell0-U-X(5)+X(6))*kappa/dM)/F+CprotM*kp/mu*(Pc-
Pa)/dM)/(CprotM*F*(DprotM/R/T+CprotM*kphi/mu)))-kp/mu*(Pc-Pa)/dM)...
      *dM/DCH3OHM)/(exp((-kphi/mu*CprotM*F*-((((Ucell0-U-
X(5)+X(6))*kappa/dM)/F+CprotM*kp/mu*(Pc-
Pa)/dM)/(CprotM*F*(DprotM/R/T+CprotM*kphi/mu)))-kp/mu*(Pc-
Pa)/dM)*dM/DCH3OHM)-1))-AS*(k1*exp(alpha1*F*X(5)/(R*T))*((1-X(2)-
X(4))^3*X(1)-1/K1*exp(-alpha1*F/(R*T)*X(5))*X(2)^3))
   1/(gamma*Ctstar)*((k1*exp(alpha1*F*X(5)/(R*T))*((1-X(2)-X(4))^3*X(1)-
1/K1*exp(-alpha1*F/(R*T)*X(5))*X(2)^3))-(...
      k3*(X(2)*X(3)^2-1/K3*X(4)*(1-X(2)-X(4))^3*(1-X(3))^2)))
   1/(gamma*Ctstar)*((k2*exp(alpha2*F*X(5)/(R*T))*((1-X(3))^3-1/K2*exp(-
alpha2*F/(R*T)*X(5))*X(3)^3))-2*(k3*(X(2)*X(3)^2-...
      1/K3*X(4)*(1-X(2)-X(4))^3*(1-X(3))^2))-(k4*(X(4)*X(3))))
   1/(gamma*Ctstar)*((k3*(X(2)*X(3)^2-1/K3*X(4)*(1-X(2)-X(4))^3*(1-X(3))^2))-
(k4*(X(4)*X(3))))
   (AS/CA)*(((Ucell0-U-X(5)+X(6))*kappa/dM)-
F*(3*(k1*exp(alpha1*F*X(5)/(R*T))*((1-X(2)-X(4))^3*X(1)-1/K1*exp(-
alpha1*F/(R*T)*X(5))...
      *X(2)^3))+3*(k2*exp(alpha2*F*X(5)/(R*T))*((1-X(3))^3-1/K2*exp(-
alpha2*F/(R*T)*X(5))*X(3)^3))))
   (AS/CC)*(-((Ucell0-U-X(5)+X(6))*kappa/dM)-
6*F*(P*X(1)*AS*(DCH3OHM/dM*((-kphi/mu*CprotM*F*-((((Ucell0-U-
X(5)+X(6))*kappa/dM)...
      /F+CprotM*kp/mu*(Pc-Pa)/dM)/(CprotM*F*(DprotM/R/T+CprotM*kphi/mu)))-
kp/mu*(Pc-Pa)/dM)*dM/DCH3OHM)*exp((-kphi/mu*CprotM*F*-...
      ((((Ucell0-U-X(5)+X(6))*kappa/dM)/F+CprotM*kp/mu*(Pc-
Pa)/dM)/(CprotM*F*(DprotM/R/T+CprotM*kphi/mu)))-kp/mu*...
```

```
        (Pc-Pa)/dM)*dM/DCH3OHM)/(exp((-kphi/mu*CprotM*F*-((((Ucell0-U-
X(5)+X(6))*kappa/dM)/F+CprotM*kp/mu*(Pc-Pa)/dM)/...
        (CprotM*F*(DprotM/R/T+CprotM*kphi/mu)))-kp/mu*(Pc-
Pa)/dM)*dM/DCH3OHM)-1))+(kc*exp(alphaC*F*X(6)/(R*T))*...
        (1-exp(-F*X(6)/(R*T))*(PO2/Pteta)^(3/2)))))];
```

Main program for the polarization curve modeling

```
clear all;
format long;
global U
global Q
global CCH3OHF
global Pa
global Pc
global icell
global K1
global K2
global K3
global K4
global R
global F
global T
global k1
global kc
global k2
global k3
global k4
global alpha1
global alphaC
global alpha2
global Ucell0
global kphi
global mu
global CprotM
global kp
global dM
global DprotM
global DCH3OHM
global PO2
global Pteta
global VA
global kLS
global AS
global VACL
global kappa
global CA
global CC
global gamma
global Ctstar
global tau
```

```
global C0A
global C1A
global C0C
global C1C
global sigma
global Czeta
global Cteta
global Const
global KC

global A
global B
global C
global D
global P

%Operating parameters of the cell
Q=1.67*10^-8; CCH3OHF=1000; T=353;
Pa=101325; Pc=101325;
tau=VA/Q;

%Kinetic parameters
K1=1*10^-0; K2=1*10^-5; K3=1*10^0;
k1=0.80*10^-7; k2=1.0*10^-2; k3=0.3*10^-1; k4=0.15*10^-1; kc=1*10^-2;


alpha1=0.5; alphaC=0.5; alpha2=0.5;
Ucell0=1.2;
R=8.314; F=96500;
kphi=1.13*10^-9; mu=3.353*10^-4; CprotM=1200; kp=1.57*10^-18;
dM=5.08*10^-5;
DprotM=5.359*10^-3; DCH3OHM=5.359*10^-4;
PO2=Pc; Pteta=10^5;
VA=0.2*10^-6; kLS=8*10^-6; AS=5*10^-4; VACL=9*10^-9; kappa=17*10^-0;
CA=4*10^2; CC=8*10^2; gamma=100; Ctstar=20*2.2*10^-5; C0A=CA; C1A=CA/100;
C0C=CC; C1C=CA/10; sigma=1; Czeta=55556; Cteta=32.68;

A=kphi/mu;
B=CprotM*kp/mu*(Pc-Pa)/dM;
C=(DprotM/(R*T)+CprotM*kphi/mu);
D=kp/mu*(Pc-Pa)/dM;

for i=1:5
   voltage(i)=0.6-i/10;
   U=voltage(i);
   t=[0 600];
```

```
   [t,X,s]=ode15s('ODEpolarization',t,[1000;0;0;0;0;0]);

  for j=1:length(t)
     icell(j)=kappa/dM*(Ucell0-U-X(j,5)+X(j,6));
  end
  currentdensity(i)=icell(length(t))/10;
end

%Plot :

%C=5M
exp4(5)=233.6;
exp4(4)=165.8;
exp4(3)=102.6;
exp4(2)=46;
exp4(1)=6.2;

%Pc=1atm rel
exp3(5)=642;
exp3(4)=480.9;
exp3(3)=315.7;
exp3(2)=149;
exp3(1)=57.6;

%N112
exp2(5)=358.6;
exp2(4)=252.2;
exp2(3)=149.2;
exp2(2)=49.4;
exp2(1)=2.8;

%normal
exp(5)=505;
exp(4)=365;
exp(3)=232;
exp(2)=96;
exp(1)=26;

figure(1)
plot(currentdensity(:),voltage(:),exp2(:),voltage(:));0.1);
xlabel('i (mA/cm2)');
ylabel('U (V)');
```

Solving function for the polarization curve modeling

```
function dXdt=ODEpolarization(t,X)
global U
global Q
global CCH3OHF
global Pa
global Pc
global icell
global K1
global K2
global K3
global K4
global R
global F
global T
global k1
global kc
global k2
global k3
global k4
global alpha1
global alphaC
global alpha2
global Ucell0
global kphi
global mu
global CprotM
global kp
global dM
global DprotM
global DCH3OHM
global PO2
global Pteta
global VA
global kLS
global AS
global VACL
global kappa
global CA
global CC
global gamma
global Ctstar
global tau

global C0A
```

```
global C1A
global C0C
global C1C
global sigma
global Czeta
global Cteta
global Const
global KC

global A
global B
global C
global D
global P

dXdt=[1/tau*(CCH3OHF-X(1))-AS*X(1)*P*(DCH3OHM/dM*((-kphi/mu*CprotM*F*-
((((Ucell0-U-X(5)+X(6))*kappa/dM)/F+CprotM*kp/mu*(Pc-Pa)/dM)...
      /(CprotM*F*(DprotM/R/T+CprotM*kphi/mu)))-kp/mu*(Pc-
Pa)/dM)*dM/DCH3OHM)*exp((-kphi/mu*CprotM*F*-((((Ucell0-U-X(5)+X(6))...
      *kappa/dM)/F+CprotM*kp/mu*(Pc-
Pa)/dM)/(CprotM*F*(DprotM/R/T+CprotM*kphi/mu)))-kp/mu*(Pc-
Pa)/dM)*dM/DCH3OHM)/...
      (exp((-kphi/mu*CprotM*F*-((((Ucell0-U-
X(5)+X(6))*kappa/dM)/F+CprotM*kp/mu*(Pc-Pa)/dM)/(CprotM*F*...
      (DprotM/R/T+CprotM*kphi/mu)))-kp/mu*(Pc-Pa)/dM)*dM/DCH3OHM)-1))-
AS*(k1*exp(alpha1*F*X(5)/(R*T))*((1-X(2)-X(4))^3*X(1)...
      -1/K1*exp(-alpha1*F/(R*T)*X(5))*X(2)^3))
   1/(gamma*Ctstar)*((k1*exp(alpha1*F*X(5)/(R*T))*((1-X(2)-X(4))^3*X(1)-
1/K1*exp(-alpha1*F/(R*T)*X(5))*X(2)^3))-(k3*(X(2)*X(3)^2-...
      1/K3*X(4)*(1-X(2)-X(4))^3*(1-X(3))^2)))
   1/(gamma*Ctstar)*((k2*exp(alpha2*F*X(5)/(R*T))*((1-X(3))^3-1/K2*exp(-
alpha2*F/(R*T)*X(5))*X(3)^3))-2*(k3*(X(2)*X(3)^2...
   -1/K3*X(4)*(1-X(2)-X(4))^3*(1-X(3))^2))-(k4*(X(4)*X(3))))
   1/(gamma*Ctstar)*((k3*(X(2)*X(3)^2-1/K3*X(4)*(1-X(2)-X(4))^3*(1-X(3))^2))-
(k4*(X(4)*X(3))))
   (AS/CA)*(((Ucell0-U-X(5)+X(6))*kappa/dM)-
F*(3*(k1*exp(alpha1*F*X(5)/(R*T))*((1-X(2)-X(4))^3*X(1)-1/K1*exp...
      (-alpha1*F/(R*T)*X(5))*X(2)^3))+3*(k2*exp(alpha2*F*X(5)/(R*T))*((1-X(3))^3-
1/K2*exp(-alpha2*F/(R*T)*X(5))*X(3)^3))))
   (AS/CC)*(-((Ucell0-U-X(5)+X(6))*kappa/dM)-
6*F*(P*X(1)*AS*(DCH3OHM/dM*((-kphi/mu*CprotM*F*-((((Ucell0-U-X(5)+X(6))...
      *kappa/dM)/F+CprotM*kp/mu*(Pc-
Pa)/dM)/(CprotM*F*(DprotM/R/T+CprotM*kphi/mu)))-kp/mu*(Pc-
Pa)/dM)*dM/DCH3OHM)*...
      exp((-kphi/mu*CprotM*F*-((((Ucell0-U-
X(5)+X(6))*kappa/dM)/F+CprotM*kp/mu*(Pc-Pa)/dM)/(CprotM*F*...
```

```
(DprotM/R/T+CprotM*kphi/mu)))-kp/mu*(Pc-Pa)/dM)*dM/DCH3OHM)/(exp((-
kphi/mu*CprotM*F*-((((Ucell0-U-X(5)+X(6))*kappa/dM)...
/F+CprotM*kp/mu*(Pc-Pa)/dM)/(CprotM*F*(DprotM/R/T+CprotM*kphi/mu)))-
kp/mu*(Pc-Pa)/dM)*dM/DCH3OHM)-1))+...
(kc*exp(alphaC*F*X(6)/(R*T))*(1-exp(-F*X(6)/(R*T))*(PO2/Pteta)^(3/2)))))];
```